Using Silicon Nanomembranes to Evaluate Stress in Deposited Thin Films

By

Anna M Clausen

A dissertation submitted in partial fulfillment of the requirements for the degree of

Doctor of Philosophy
(Materials Science)

at the

University of Wisconsin-Madison

2012

Date of final oral examination: 08/20/2012

The dissertation is approved by the following members of the Final Oral Committee:

Max G. Lagally, Professor, Materials Science
Susan E. Babcock, Professor, Materials Science
Donald S. Stone, Professor, Materials Science
Mark A. Eriksson, Professor, Physics
Robert H. Blick, Professor, Electrical and Computer Engineering

Acknowledgements

This work would not be possible without the help and support of so many people. I would first like to thank my advisor, Professor Max Lagally, who has given me so many opportunities that have helped me grow professionally. I would also like to thank the many people whom I have gotten to know through Max's group; many fellow graduate students, post docs, researchers, undergraduate students, and visitors have been helpful throughout this work. The staffs at the Wisconsin Center for Applied Microelectronics, the Materials Science Center, and the Wisconsin Institutes for Discovery have taught me so much, and I appreciate their support and time. I am grateful to my committee members for taking the time to give me important feedback, which has made my work stronger.

This work has been supported with material, time, and resources from many people outside the university. I would like to acknowledge everyone who helped me in the beginning of this project at Oakridge National Laboratory, especially Dr. Ivan Kravchenko. About half of my years have been spent working at the Synchrotron Radiation Center learning and working with Dr. Narayan Appathurai. He was extremely supportive in teaching me to become independent on the XPEEM and how to interpret my data. Dr. Katherine Saenger at IBM was very generous in providing material resources for my XPEEM work. In addition, Dr. Joseph Jakes contributed to this work with many useful nanoindentation measurements and mechanics discussions.

Most importantly, I would not have made it through this process if it were not for the support of my family: Matt Howards, Carol Clausen, and Roger Clausen. These people helped me believe I could do this even throughout the times that I struggled.

Abstract

Using Silicon Nanomembranes to Evaluate Stress in Deposited Thin Films

Anna M Clausen

Under the supervision of Professor Max G. Lagally

At the University of Wisconsin-Madison

Thin-film deposition is widely used and has been well studied on thick substrates. The stress that forms in these systems can be characterized by the physical effect it has on the substrate. Ultra-thin substrates are unique because of their potential for a dynamic response to the film stress during deposition. While theoretical studies have looked at the effect that ultra-thin substrates have on the physical changes in the substrate, little has been done to learn what happens to the film itself.

Si and Ge nanomembranes, extremely thin sheets of single-crystalline material, were used as a tethered substrate with SiN_x as the stressor film. Nanomembranes are released from a handle wafer with wet etching and transferred to a hole etched into a Si wafer. The nanomembrane window provides a platform for SiN_x deposition and strain measurements on the nanomembrane. By measuring the strain in the nanomembrane, the film's stress could be inferred from force balancing. In a similar fashion, the film's stress can be compared on bulk substrates. My observations demonstrate that the strain in the tethered nanomembranes increases as the nanomembrane is made thinner while the stress in the deposited film surprisingly appears to remain constant. A physically realistic model to explain this behavior is suggested. These findings can be used as a way to

increase the strain in materials that are difficult to strain and as a demonstration of tethered nanomembranes as a potential strain gauge.

Contents

Chapter 1

Introduction

The application of different material layers is common for uses such as coatings, contacts, and barrier layers. The deposition of a material onto a dissimilar substrate generally leads to stress, but mechanisms creating this stress are complicated and not well understood at the atomic level, although much work exists.[Thompson, 2000]

One aspect that has not been considered in these studies is the influence of a thin substrate on the development or relaxation of stress in a deposited thin film. The mechanics of a thin film on a thick substrate are well understood, as described later, and are derived from measuring bending in the film/substrate system in response to the film stress.

Deposition of a stressed layer on nanoscale substrates may alter the total strain in the system relative to what it is for deposition on a bulk substrate. The reason is that nanoscale substrates are more flexible and are able to share strain more effectively than thicker, more rigid substrates.[Roberts, 2006] If as a consequence the morphology or microstructure of the deposited film were to change, significant consequences may occur in the application of films in modern technology, where dimensions such as we are considering here are becoming commonplace.

It will not matter whether a continuous film or local stressors are deposited: as the stress relaxes, it deforms the substrate. Local stressors, such as individual, separate grains or nanocrystals, will deform the substrate locally.[Huang, 2009][Huang, 2005] As

local stressors begin to populate a substrate more densely, one expects the mechanics to become similar to those of a continuous film.[Liu, 2002]

Nanomembranes, because they are flexible and thus highly responsive to applied stress, should be an ideal substrate platform to study the mechanics of thin film stress evolution. Because of its thinness a nanomembrane may, in fact, react dynamically to an evolving stress. This effect has been observed in the size development and ordering of local, epitaxial Ge quantum dot stressors deposited on Si(001). [Ritz, 2010] We would like to explore whether and how we can observe the influence of a thin substrate on the stress evolution of a global stressor film during deposition. Single-crystal Si nanomembranes are ideal for this purpose, because strain in Si can be measured very sensitively with Raman spectroscopy.

Conversely, there is also intense interest in understanding how much stress one can impart to a thin crystalline sheet, and how the properties of this sheet can change. A film deposited on a crystalline nanomembrane enables such studies, if one knows the stress evolution in the deposited film.

The goal, therefore, of this work is to use single-crystal Si and Ge nanomembranes as substrates to measure the stress in a growing film as observed through the response of the substrate. Because deposition on a freestanding, nanoscale substrate is extremely difficult, two sample setups are employed. In the first, the Si nanomembrane is attached to an underlying oxide layer, which is less stiff than bulk Si. I apply local stressors and observe the stress relaxation at a free edge. In the second, a nanomembrane covers a hole made in a Si wafer and is bonded at the edges of the hole, in the way one might apply a piece of plastic as a storm window. The edges are far enough away that

measurements made in the middle of the membrane should not be influenced by any strain gradients at the edges. A continuous stressor film is applied over the freestanding region.

SiN_x is used as the stressor film because it has been widely integrated into silicon microelectronics fabrication. It can offer a wide range of stress states, from tensile to compressive, depending on the deposition technique and composition of the film. The deposition parameters and the precursors that are used control the microstructure and composition of the deposited film. The films used in this thesis are amorphous, but, in retrospect, a polycrystalline film may have yielded more information about the film and would be a great choice for further exploration of the stress evolution mechanisms during deposition on nanomembrane substrates.

1.1 Structure of dissertation

The outline of the rest of the dissertation is as follows. Chapter 2 will cover the mechanics of stress and strain in bilayer (and trilayer) systems. The causes of stress build-up in thin films as well as the effect that the substrate has during deposition will also be explored.

In Chapter 3, I describe the fabrication of and measurement methods for global stressor films on tethered, freestanding nanomembrane substrates. Processing of the rigid frame, nanomembrane fabrication, window formation, and the SiN_x deposition will be discussed.

In Chapter 4, I describe results from the measurements of stress or strain, both for SiN_x deposited on bulk substrates and on the freestanding tethered Si nanomembranes for varying thicknesses of the Si nanomembrane and the deposited SiN_x film. Measurements

were partially repeated with Ge nanomembranes. Efforts to interpret the results in terms of a physically realistic picture are presented as well in this chapter.

In Chapter 5, I provide a brief summary along with some ideas for future work. It is quite clear that my work serves as only an introduction to this very interesting research area. It is hoped that others will use it to continue investigations of this nature.

An appendix will cover local stressors on bonded nanomembranes substrates. Using patterned SiN_x, stress relaxation at the edges of the pattern can be observed. With bonded nanomembranes, less strain is imparted and measurements require high strain and spatial sensitivity. The strain imparted to the bonded Si nanomembrane can be observed through changes in the atomic bonding and Si electronic band structure, but the sample fabrication may need to be altered to include a higher stress in the SiN_x. While I have spent about half of my time working on this project, the work strays from the main topic of this dissertation, which is why it is set aside from the rest.

1.2 References

Huang, M. et al. (2005). Bending of nanoscale ultrathin substrates by growth of strained thin films and islands. *Physical Review B, 72*, p.085450.

Huang, M. et al. (2009). Mechano-electronic superlattices in silicon nanoribbons. *ACS Nano, 3*, p.721-7.

Liu, F. et al. (2002). Response of a strained semiconductor structure. *Nature, 416*, p.498.

Roberts, M. et al. (2006). Elastically relaxed free-standing strained-silicon nanomembranes. *Nature Materials, 5*, p.388-393.

Ritz, C. et al. (2010). Ordering of nanostressors on free-standing silicon nanomembranes and nanoribbons. *New Journal of Physics, 12*, p.103011.

Thompson, C. (2000). Structure evolution during processing of polycrystalline films. *Annual Review of Materials Science, 30*, p.159-90.

Chapter 2

Thin-film mechanics

Generally with the deposition of thin films, stresses may develop that can affect the properties of both the deposited film and the substrate. [Freund, 2004] Stress can arise from differences in bond lengths and bond strengths, from thermal expansion differences, from grain coarsening and boundary motion with time or added mass, to name a few, or more generally from thermodynamic and kinetic limitations. There is an extensive literature on film growth modes and failure mechanisms, as well as distortions of the substrate.[Abermann, 1985][Thompson, 2000] Specialized tools exist for the investigation of such properties.[Ogura, 2009][Cuthrell, 1989] In this chapter, I will review in general terms the stress evolution in thin-film deposition and the role of the substrate during stress relaxation.

In classical thin-film technology, the deposited film is always much thinner than the substrate, and effectively all of the literature reflects that combination. In this dissertation, we take a new approach: making the substrate ultrathin. I expect that this nanoscale substrate will result in different system strain than if the film was deposited on a thick substrate. In this chapter, I therefore also review the existing status of film/substrate mechanical properties for deposition on thick substrates, briefly discuss thin substrates (nanomembranes), and review prior work from our group of the behavior of a local stressor deposited on a nanoscale substrate.

Strain in a materials system can induce changes in the electronic, magnetic, and optical properties,[Chu, 2009] as well as "macroscopic" mechanical properties (hardness, toughness, etc.) and even chemical properties (corrosion resistance, etc.) As atomic bonds are stretched, compressed, or distorted, the energetics of the electrons in a solid material may also change. For example, in semiconductors or semimetals, strain can lead to the creation of a band gap where there was none, can change the magnitude of the band gap or the band offset in a heterojunction, or cause a solid to change from having an indirect band gap to having a direct band gap.[Euaruksakul, 2009][Liu, 2009] [Sánchez-Pérez, 2011][Huang, 2009]

2.1 Stress and strain

Stress is the force per unit area experienced by a materials system. Strain is the response to the stress and is defined as the percentage change of a material's equilibrium dimension, L,

$$\varepsilon = \frac{\Delta L}{L}. \qquad \textbf{Equation 1}$$

For a crystalline material, strain can be written as the change in the lattice constant, $\frac{\Delta a}{a}$.

Strain can be the result of an external stress applied to the system or an internal stress created by microstructure changes and/or growth conditions. External stress can arise, among other sources, from the difference in the coefficients of thermal expansion between two bonded layers, from chemical reactions, or from a reaction to electrostatic or magnetic forces, or simply from applied forces. Internal stresses can arise, for example,

during film deposition from lattice mismatch, grain agglomeration and boundary motion, or impurity inclusions.

When a stress is exerted on a bar of material, other dimensions perpendicular to the stress direction respond with a change in length opposite in sign to the applied stress. Thus, if a stress elongates a material in one direction, the two perpendicular directions typically contract in response. The ratio of the contraction to the elongation (or vice versa depending on the direction of the force) is called the Poisson ratio, υ, and is defined as

$$\upsilon = -\frac{\varepsilon_{\perp}}{\varepsilon_{//}}, \qquad \textbf{Equation 2}$$

the ratio of the perpendicular strain, $\varepsilon_{\perp}$, to the parallel strain, $\varepsilon_{//}$, where parallel refers to the direction of the applied stress. Typical Poisson ratios for metals lie between 0.25 and 0.35 while ceramics tend to be lower and polymers are higher.[Callister, 2005]

If the material's response to a stress is elastic, its dimensions return to their original values when the stress is removed. In this regime, the relationship between a uniaxial stress and the resulting strain is linear and characterized by Hooke's law,

$$\sigma = E\varepsilon, \qquad \textbf{Equation 3}$$

where the proportionality constant, *E*, is called the Young's modulus. A large value for *E* implies the material is stiffer compared to a material with a small value. With sufficiently large applied stress, the system's response can be inelastic, where the relationship between stress and strain is no longer linear and the change in dimensions is permanent. The extent of the linear region in the stress-strain curve depends on many factors, including the nature of the material, the temperature, and the dimensions.

Although not all materials have a linear relationship between stress and strain, a majority of systems do, including the ones explored in this dissertation. A schematic one-dimensional stress versus strain plot is shown in Figure 1, where the Young's modulus, *E*, is the slope in the elastic regime.

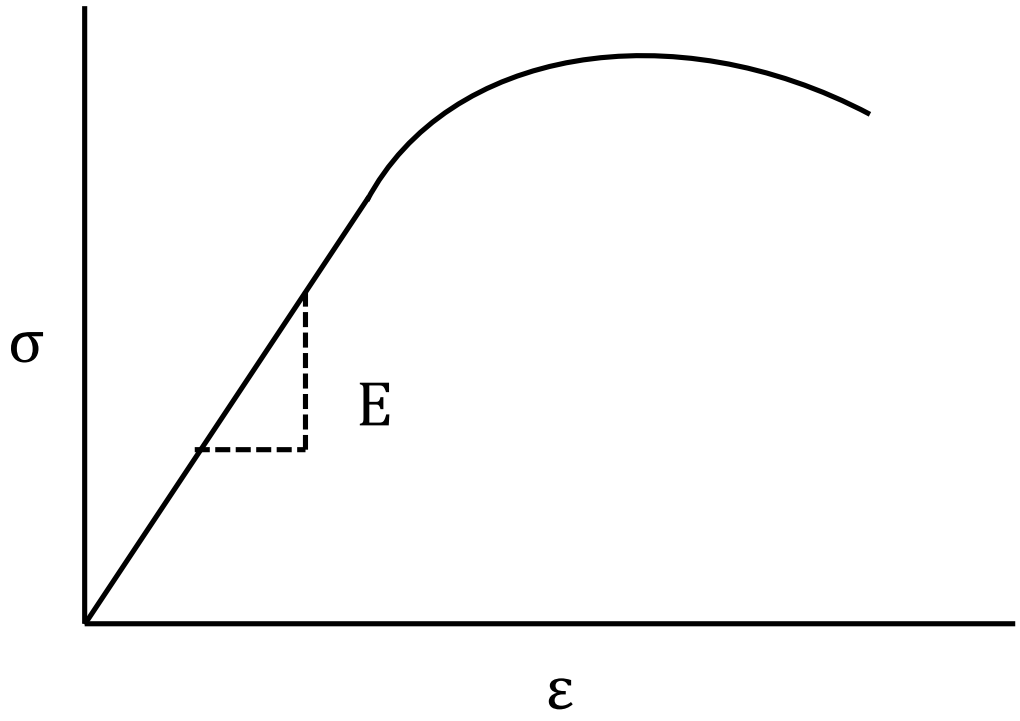

Figure 1: Schematic diagram of the measured strain as a function of applied stress. The Young's modulus can be found using the slope of the linear regime. When the slope is no longer a constant, the material is plastically deformed.

When stress is biaxial, applied in two orthogonal directions in the plane, the proportionality constant, *M*, is called the biaxial modulus. The biaxial modulus and the Young's modulus, *E*, are related by

$$M = \frac{E}{1-\upsilon}, \qquad \textbf{Equation 4}$$

where υ is the Poisson's ratio.

The work done by a stressed film on a substrate, W, is defined generally as

$$W = \int F\,dx, \qquad \textbf{Equation 5}$$

where the F is force of the film and x is the elongation of the bilayer after relaxation. For a uniaxial stress applied to a substrate, similar to Hooke's law with a spring, the work done by the strain energy density, U, is

$$U = \int \sigma\,d\varepsilon = \int E\varepsilon\ d\varepsilon = \frac{1}{2}E\varepsilon^2, \qquad \textbf{Equation 6}$$

where the Young's modulus, E, is analogous to the spring constant and the strain, ε, is the elongation. The strain energy density is then the area under the plot in Figure 1.

In isotropic materials, the material response is independent of the orientation and the strain is isotropic. In anisotropic materials, the strain response is dependent on the orientation of the material. Therefore, the equations that are used to characterize the response to an applied stress must take into account the orientation of the stress and the direction-dependence of the resulting strain. The generalized stress-strain relations for a three-dimensional system are then expressed as

$$\sigma_{ij} = c_{ijkl}\varepsilon_{kl} \qquad \textbf{Equation 7}$$

$$\varepsilon_{ij} = s_{ijkl}\sigma_{kl}, \qquad \textbf{Equation 8}$$

where c_{ijkl} are the stiffness constants, s_{ijkl} are the compliance constants, and i,j,k, and l can be 1, 2, or 3. The stress and strain are second-order tensors, while the stiffness and compliance constants are fourth-order tensors. The ij indicates the crystal face on which

the stress is applied and direction for the applied stress, respectively, and the *kl* indicates the crystal face and direction for the measured strain response, respectively, as seen in Figure 2.[Ting, 1996][Tamulevicius, 1998] For example, σ_{11} is the normal stress applied to the x_1 face in the x_1 direction and ε_{23} is the shear strain response of the x_2 face in the x_3 direction. If the strain is measured in the same plane as the applied stress, *ij* and *kl* are the same. The fact that in c_{ijkl} or s_{ijkl}, $ij = ji$ and $kl=lk$ reduces the number of independent elastic constants from 81 to 36. In a cubic crystal, like Si, symmetry further reduces the number of independent constants to just three.

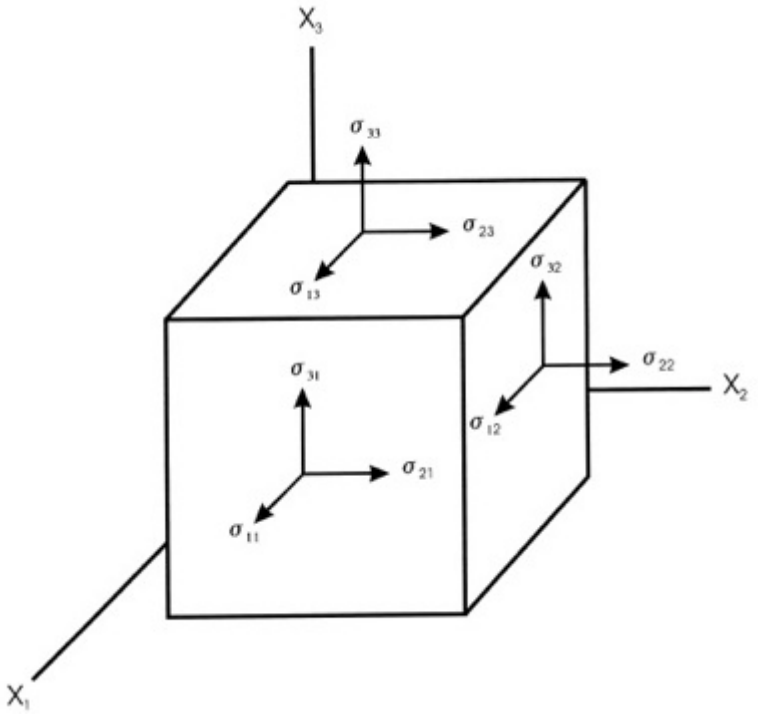

Figure 2: Diagram indicating the meaning of each component in the stress tensor in Equation 7 and Equation 8.[Tamulevicius, 1998]

2.2 Thermodynamics in film formation: Growth modes

Both thermodynamics and kinetics can influence the formation and magnitude of stress in a deposited film. If the film deposition is limited by thermodynamics, the minimization of free energy in the film and substrate drives microstructure formation. If the film deposition is limited kinetically, the atomic mobility controls film growth.

Thermodynamic limits assume very slow deposition and very rapid accommodation of atoms to their equilibrium positions. In this limit, assuming a perfect single-crystal substrate, the way a film grows can be classified into three growth modes: Frank-van der Merwe, Stranski-Krastanov, and Volmer-Weber.[Venables, 2003] For the continuous layer-by-layer (Frank-van der Merwe) growth mode (Figure 3a) the film and

substrate must have the same lattice parameters. This relatively rare case occurs in homoepitaxial growth or for some heteroepitaxial alloys. Ideally, the strain in this system is negligible.

The Stranski-Krastanov growth mode, Figure 3b, is a combination of an initial continuous layer that wets the surface, followed by three-dimensional island formation, as the film gets thicker. In this case, the adatoms desire chemically to bond with the substrate, but the strain energy that builds up in the film with the addition of more layers can relax through the growth of islands or clusters. This growth mode is prevalent and seen during heteroepitaxy where the lattice constants of the film and substrate are different but close.

In the Volmer-Weber growth mode, Figure 3c, incoherent (not lattice matched) three-dimensional-island formation begins already at the submonolayer level. The growth mode is driven both by large lattice mismatch and by chemical differences that imply that adatoms desire to bond with each other instead of the substrate. This mode occurs when the film and the substrate have very different lattice constants. The large chemical-energy differential and the strain energy that resists layer formation mean the film quickly forms three-dimensional islands, leaving some of the substrate initially exposed. This type of growth commonly leads to a polycrystalline microstructure.

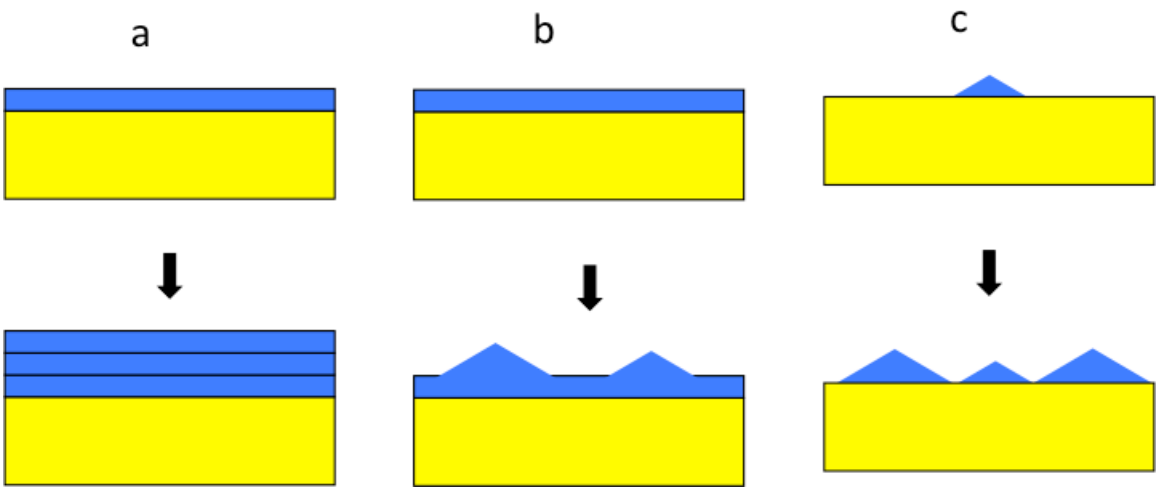

Figure 3: Schematic diagrams of the Frank-van der Merwe (a), Stranksi-Krastanov (b), and Volmer-Weber (c) thermodynamic-limit growth modes. Image by S. Scott.

The role of strain in epitaxy is well known for the conventional growth of a thin film on a bulk substrate. Heteroepitaxial growth of $Si_{1-x}Ge_x$ on a Si substrate provides an example for the growth modes shown in Figure 3a and b, depending on the concentration of Ge. The Ge lattice constant, a_{Ge}, is about 4% larger than that of Si, a_{Si}, with the $Si_{1-x}Ge_x$ lattice constant linearly related to the concentration of Ge in the film [Vegard, 1921],

$$(1-x)a_{Si} + xa_{Ge} = a_{Si_{1-x}Ge_x}. \qquad \textbf{Equation 9}$$

When there is no Ge or x = 0, the film is 100% Si and is deposited layer-by-layer as the Frank-van der Merwe model predicts. When $0 < x \leq 1$, the film is compressively strained from being forced to match the substrate's atomic lattice because of the strong chemical forces. As the film becomes thicker, the strain energy increases until the elastic limit is reached at the critical thickness (Figure 4) and the film relaxes plastically. A low Ge concentration results in small strain, and the film prefers to relax through dislocation formation. For a higher Ge concentration and thus larger strain, the film

prefers to relax initially via formation of coherent (i.e., lattice matched) three-dimensional islands after the two-dimensional critical thickness is exceeded. The islands can only be achieved if the temperature is high enough to allow the required diffusion and nucleation.[Tu, 2007]

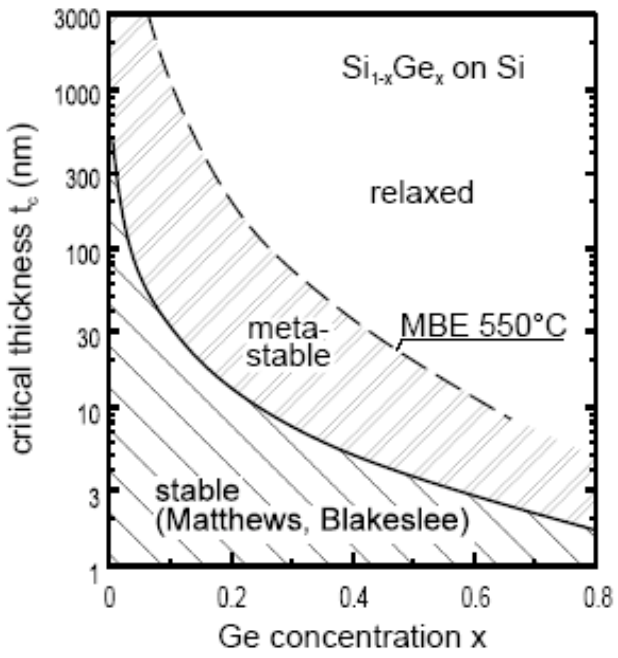

Figure 4: Graph of the $Si_{1-x}Ge_x$ critical thickness as a function of the Ge concentration. The "stable" region implies that the growth is still epitaxial. The metastable region is the same but kinetically limited to be an epitaxial film without dislocations. Past that point dislocations and incoherent 3D islands can form to relieve stress. [Schäffler, 1997]

2.3 Kinetics in film formation

One expects strain to be present in either of the latter two film growth modes, but it may also occur in epitaxial growth. Kinetic limitations can exacerbate the stress conditions. When adatom motion is restricted to sites near the initial impingement site or the rate of deposition is large relative to the diffusion rate of atoms at the growth front, film growth is limited kinetically. Restricted atomic mobility leads to poor long-range

order. Thus even films that thermodynamically would prefer to grow layer-by-layer may become polycrystalline (nucleating at various locations on the surface and then meeting at grain boundaries), amorphous, or nanocrystalline (in the regime of diffusion limited aggregation). Thus in Frank-van der Merwe growth, the substrate is heated to improve the surface mobility and the deposition rate is kept low to allow the deposited atoms to find a location that is most energetically favorable. Stress may otherwise develop even in epitaxial films.

Kinetically limited deposition can build up stress as the film is deposited. Through the nucleation of clusters, boundary movements, and random inclusions into the film, the film stress is a function of the thickness and its behavior is dependent on the deposition parameters. We consider one common scenario for Volmer-Weber growth. With the nucleation of initial clusters on the substrate, surface tension and adatom-substrate interactions create a small amount of compressive stress.[Cammarata, 2000] As the clusters grow and begin to impinge on each other, the overall surface (interface) free energy can be reduced as the grain edges stretch (to create tensile stress) to fill in any gaps and make a continuous film, as seen in Figure 5.[Friesen, 2002] Once in contact, atoms may move from one cluster to another, generally growing the larger cluster at the expense of the smaller, which relaxes stresses in the growing film.[Floro, 2001] It has been speculated that sufficiently slow growth rates or the addition of surface adatoms results in variations in the surface chemical potential, which drives adatoms into the grain boundary, and this creates a compressive stress.[Zepeda, 2009] In contrast, reducing the adatom mobility further and increasing the growth rate (while still in the kinetic regime) will lead to a tensilely strained film.[Tello, 2007] As the film is deposited, the stress

formation and annihilation mechanisms reach a steady-state where the film stress plateaus as a function of film thickness and the surface becomes smoother.[Tello, 2007]

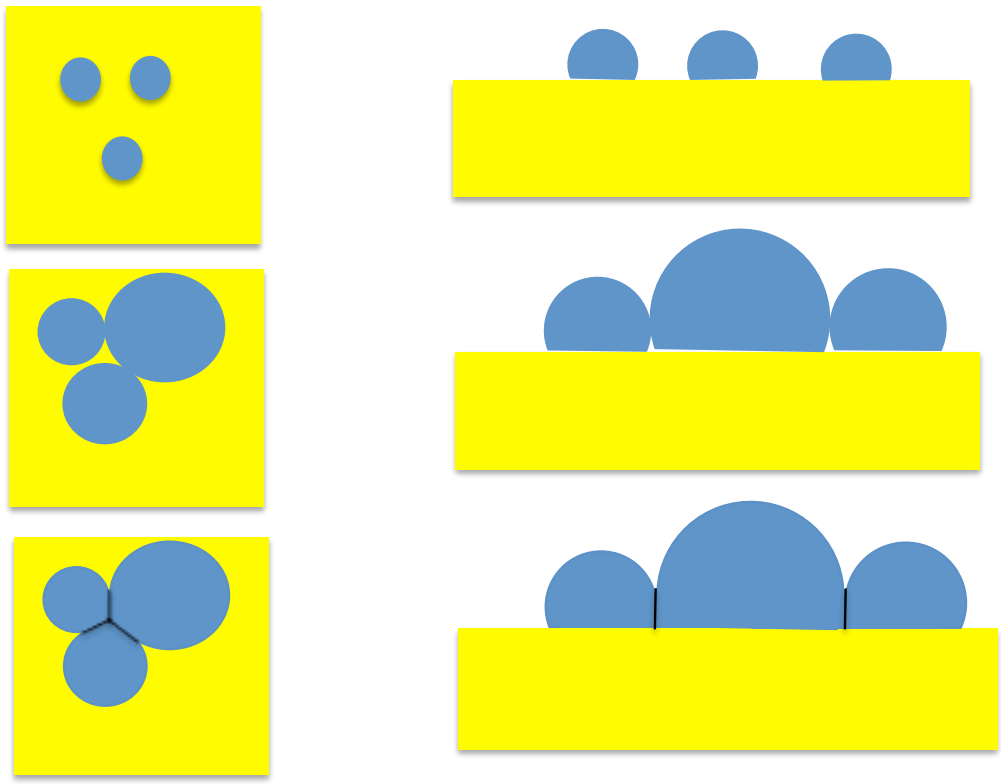

Figure 5: The coarsening and coalescence of clusters of film atoms as the film is initially deposited onto the surface. The clusters grow and the boundaries begin to merge. A continuous film is formed as the cluster boundaries are eliminated or reduced, in turn lowering the amount of surface/interface free energy.

As an example of the film stress evolution for Volmer-Weber growth, I have plotted schematic diagrams of the stress for a generally compressive film in Figure 6. The stress plotted is an average through the film; positive stress values are tensile, while negative values are compressive. The stress generally starts compressive as the clusters start to form, then becomes less compressive (and sometimes tensile) after the first dashed vertical line as the boundaries of the clusters impinge, and finally after the second

dashed vertical line, the stress plateaus (either tensile or compressive) as the film reaches a steady state. After the third vertical dashed line, inelastic stress relaxation and plastic deformation reduces the film's stress.

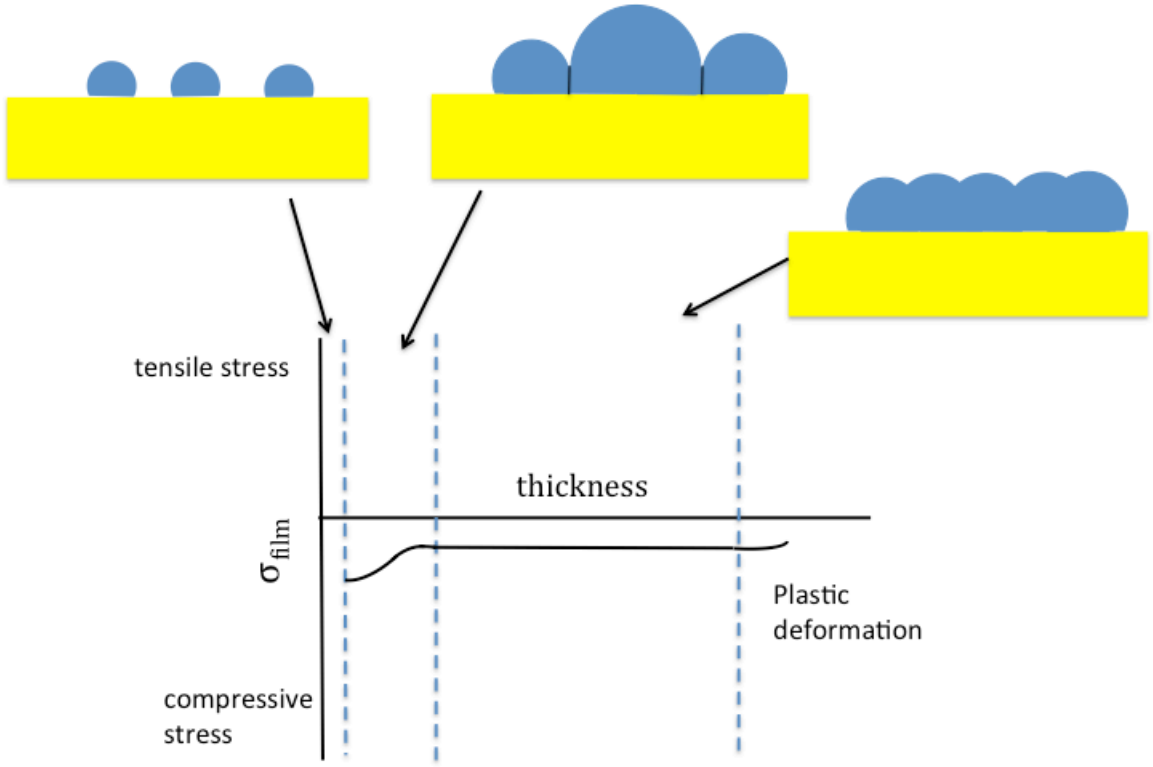

Figure 6: An example of stress evolution during Volmer-Weber growth on a bulk substrate, as a function of film thickness. Positive values denote tensile stress and negative values denote compressive stress. The vertical lines demark important microstructure changes in the film: from separate islands, to grain boundary formation, to continuous film thickening, and eventual plastic stress relaxation.

A zone model has been developed that shows the tradeoff between the two kinetic factors that control film microstructure during growth: flux arrival rate and atom diffusion rate. The model generalizes the gradual microstructure changes that occur as a

consequence in sputtered or evaporated films.[Movchan, 1969][Thornton, 1977] An example of the zone model for a constant evaporation rate, is plotted against the normalized temperature, which is based on the ratio of the substrate temperature to the melting temperature of the film material, $\frac{T_s}{T_m}$, in Figure 7. The zones, while actually continuous, are shown as separate for clarity. The first zone consists of mostly domed columnar grains that are porous due to shadowing effects and very low mobility. Because of increasing mobility, the second zone consists of larger, denser grain with faceted surfaces. In Zone 3, the crystallites are bulk-like, as diffusion becomes high. In this general model, the stress in each zone is a function of the deposition parameters, which includes the temperature.

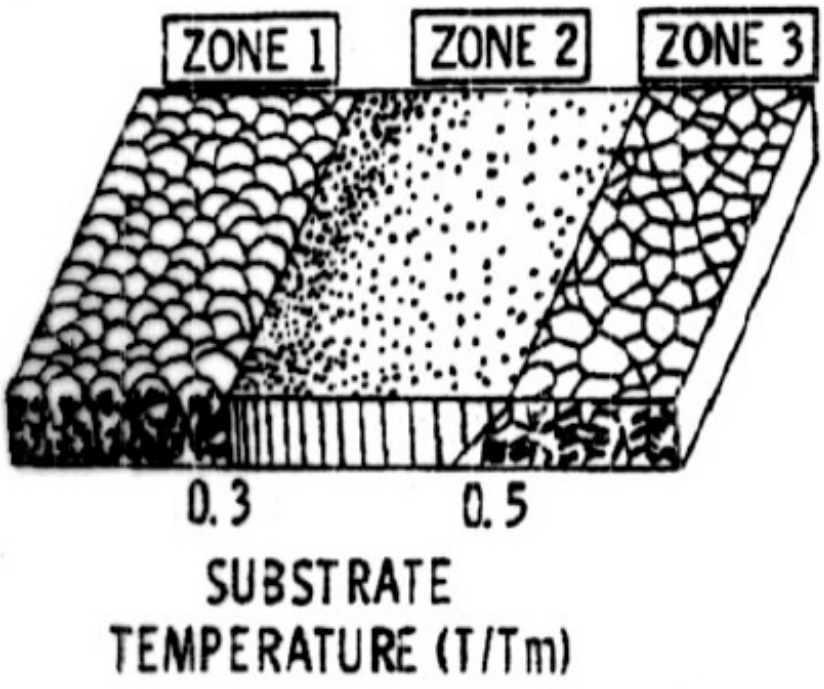

Figure 7: Structure evolution of polycrystalline film growth as a function of substrate temperature.[Movchan,1969]

In a different categorization, the dependence of the evolution of stress during thin-film growth on the mobility of the atoms being deposited can be classified into two types.[Thompson, 1996] For type I films, comprised of low-mobility atoms, the tensile stress reaches a maximum and plateaus as the film is grown thicker. For type II films, with high atom mobility, the stress quickly becomes compressive, then reverses to tensile, and eventually plateaus as compressive, as shown in Figure 8.

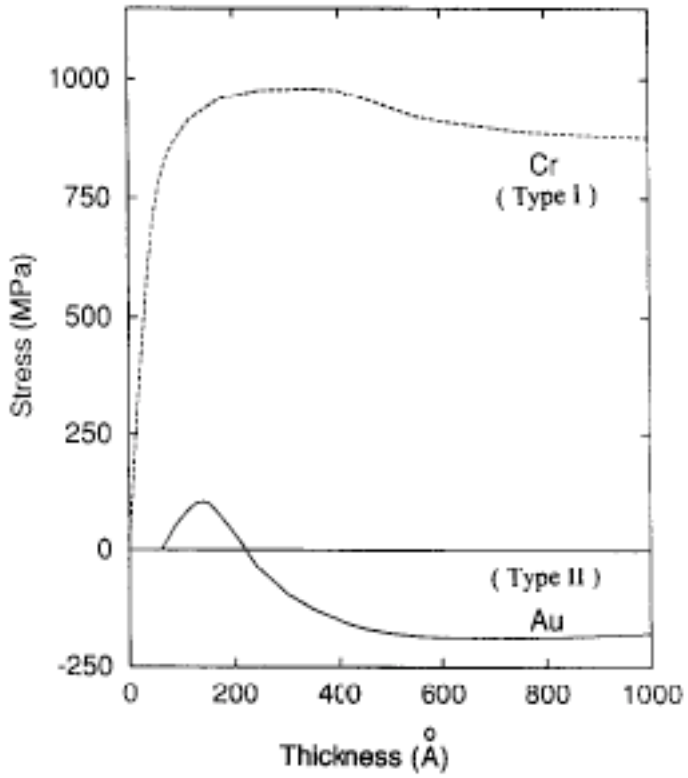

Figure 8: An example of polycrystalline-film stress evolution as a function of thickness due to the atomic mobility. Type I is for low-mobility atoms such as Cr and type II is for high-mobility atoms such as Au. In there cases, the stress plateaus around 60nm, but this can vary with different films and deposition conditions.[Thompson,1996]

Figure 7 and Figure 8 are presented here only to illustrate the complexity in understanding how stress develops in films and the multiplicity of causes for stress. The

actual variation of the stress as a function of film thickness is dependent not only on the composition of the thin film but also on the deposition conditions.

2.4 Extrinsic stress

The zone model and stress evolution described so far are due to intrinsic stresses. The addition of heat to the substrate during deposition is one form of extrinsic stress. Heating the substrate may improve the adatom mobility, but it can also cause strain due to different rates of expansion in the substrate and film. The strain produced is calculated as

$$\varepsilon = (\alpha_f - \alpha_s)\Delta T \,, \qquad \textbf{Equation 10}$$

where the thermal expansion coefficient, α, quantifies the extent of the material volume change and T is the temperature. One can also apply stress by external mechanical means, as is done in materials testing.

2.5 Response of the substrate to stress

As stress in the film relaxes elastically, it deforms the substrate through bending and stretching. By measuring the substrate deformation, we can determine the stress in the film. For a film deposited on a thick substrate, strain energy partitioning requires that most of the stress stays in the film and the redistribution of stress in equilibrium will bend the substrate.[Freund, 2004] As the substrate is made thinner, it is able stretch and bend as the thin film relaxes, and more strain is found in the substrate.[Huang, 2005]

2.5.1 Classic elastic stress relaxation

The mechanics of growth on thin sheets are rooted in early work done on macroscale systems, and are largely based on Stoney's and Timoshenko's theories of

metallic bilayers.[Stoney, 1909][Timoshenko, 1925] These models are based on force balancing between adherent layers of a bilayer that are elastically relaxing and sharing strain. If the system is then allowed to relax strain elastically, we know that the forces are conserved, such that

$$\varepsilon_f M_f h_f + \varepsilon_s M_s h_s = 0\,, \qquad \textbf{Equation 11}$$

where h_f and h_s are the thicknesses, M_f and M_s are the biaxial moduli, and ε_f and ε_s are the strains of the film and the substrate, respectively. The SI units of Equation 11 are Newtons per meter. The mismatch strain, ε_m, is generally defined as the difference between the average strain throughout the film and the strain in the substrate,

$$\varepsilon_m = \varepsilon_f - \varepsilon_s\,, \qquad \textbf{Equation 12}$$

for any bilayer system. If an epitaxial relationship exists between the two layers, we can define a quantity called the mismatch strain that is the difference in the elongation or contraction of the lattice parameters of the two materials at the interface. When the layers are adherent and the stress relaxation is elastic, the mismatch strain is conserved during relaxation, with the strain state before relaxation the same as the strain state after relaxation.

If Equation 11and Equation 12 are combined and solved for the strain in each layer, the value will be of opposite sign, as

$$\varepsilon_f = \frac{-\varepsilon_m M_s h_s}{M_f h_f + M_s h_s} \text{ and} \qquad \textbf{Equation 13}$$

$$\varepsilon_s = \frac{\varepsilon_m M_f h_f}{M_f h_f + M_s h_s}. \qquad \textbf{Equation 14}$$

When the substrate is much thicker than the film, Equation 13 and Equation 14 show that the strain is mostly in the film and the substrate's strain is very small in comparison. In the opposite situation, an extremely thin substrate with a thick film, the strain is mostly in the substrate. In the case where the film and substrate are of similar thickness, the strain is distributed more evenly between the layers. These cases can be seen in Figure 9.

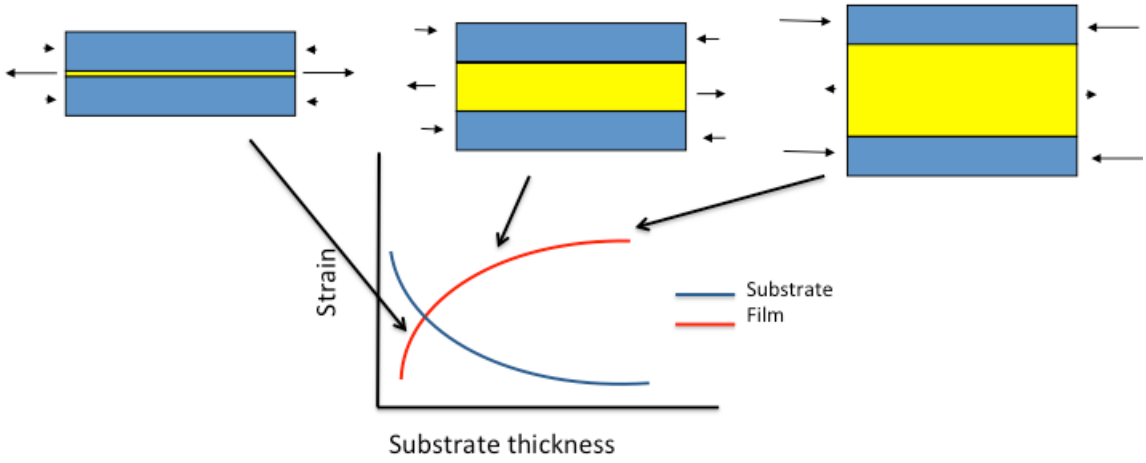

Figure 9: A example of how strain shares in a trilayer system, where the yellow layer is the substrate of changing thickness and the blue layer is the film with constant thickness. The plot is a representation of how the strain changes in the film and substrate as a function of substrate thickness. As a side note, this experiment cannot actually be done, as we cannot thin the middle layer of the trilayer.

For a trilayer, as in Figure 9, the system will remain flat because the symmetry will balance the bending moment. As a first case scenario, when a thin film is deposited onto a thick substrate, the strain is mostly in the film and therefore the mismatch strain is approximately the film strain. If the substrate could be thinned, it could accept more strain while the film strain would be lessened, and the mismatch strain would follow Equation 12. If the relaxation is elastic, the mismatch strain remains a constant value

even though the magnitude of strain in each layer is changing because the film and substrate have opposite signs of strain.

A second case is when a thin film is deposited directly onto an ultra-thin substrate. The mechanics may be different from the previous scenario because the ultra-thin substrate can dynamically react to the film strain during deposition. While the forces in the system must remain balanced, the mismatch strain does not have to remain constant if the film is inherently different from the one deposited in the previous case under similar deposition conditions. The example provided in Figure 10 uses a constant film stress, the reason that will be explained later, as the substrate thickness is allowed to change. I have set out to explore case two and will explain further in the next section.

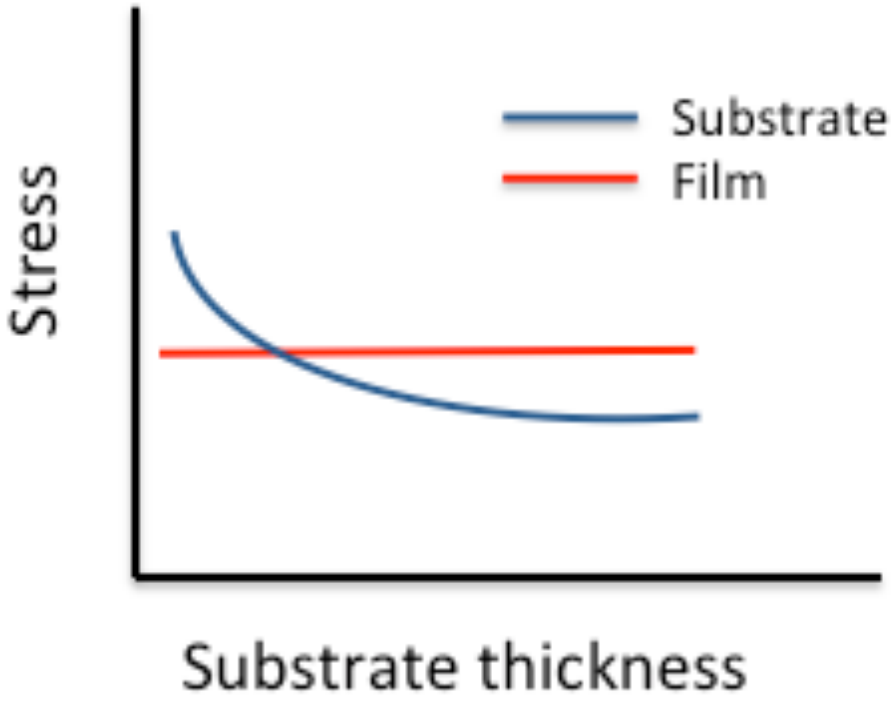

Figure 10: As a function of substrate thickness, the theoretical stress predicted by force balancing in the film and substrate are plotted when the film stres is held constant.

For a film grown on a bulk substrate that would be near its critical thickness for dislocation formation (see Figure 4), strain sharing with a thin substrate can increase the critical thickness. As Figure 11 shows, a thinner substrate can allow the film to grow thicker than it normally could before plastic relaxation occurs, which is denoted by a textured color in the lower images. After plastic relaxation, the strain in the film, and hence also in the substrate, will be lessened, as seen in Figure 12. The work in this dissertation happens to be in a thickness-independent stress range so that the stress (and therefore strain) in the film eventually reaches a constant value, but the strain in the substrate is still changing with strain sharing as the film is deposited.

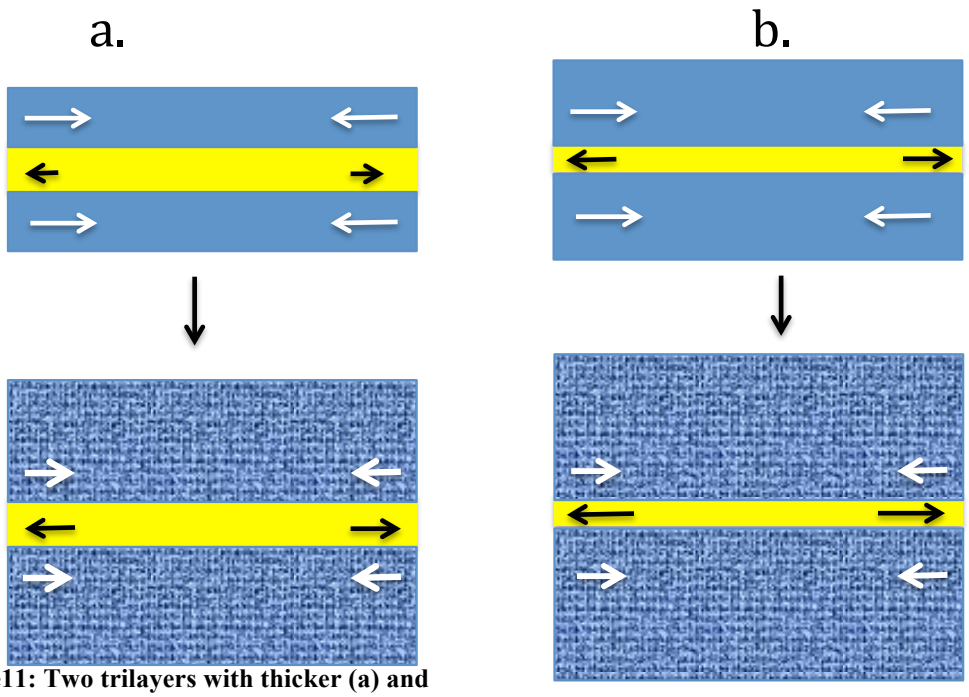

Figure11: Two trilayers with thicker (a) and thinner (b) substrates as the middle layer. A stressed film is deposited on both sides. The top images demonstrate that a thinner substrate should accept more strain than a thicker substrate before plastic relaxation occurs, which is depicted as a textured color on the bottom images. After plastic deformation, the strain in the film (and hence also the substrate) will decrease.

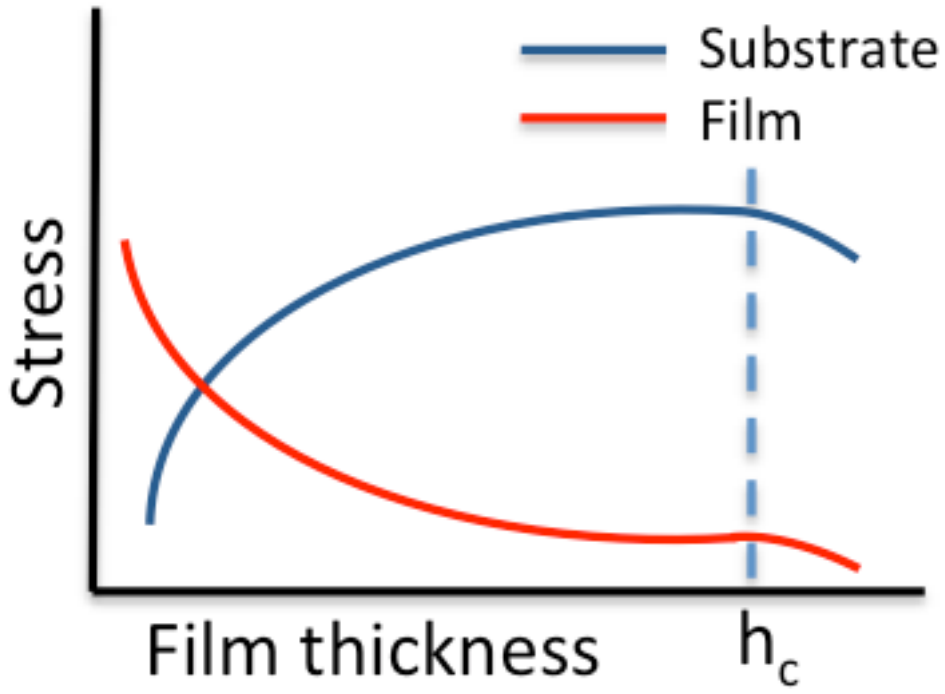

Figure 12: An example of how the stress may behave in a trilayer as a function of film thickness. While the substrate remains dislocation free, past the film's critical thickness, h_c, the film's stress decreases and that in turn applies less force to the substrate, decreasing its stress as well.

In a bilayer, an uneven distribution of stress between film and substrate creates a bending moment, which bends the system with a curvature, κ. To solve for the curvature, κ, of a strain sharing bilayer, I start by setting the midplane of the substrate to $z = 0$. The in-plane normal strain is

$$\varepsilon = \begin{cases} \varepsilon_0 + \varepsilon_s - \kappa z & \text{for } -\frac{1}{2}h_s < z < \frac{1}{2}h_s \\ \varepsilon_0 + \varepsilon_f - \kappa z & \text{for } \frac{1}{2}h_s < z < \frac{1}{2}h_s + h_f \end{cases} \qquad \textbf{Equation 15}$$

where ε_0 is the strain due to stretching, and κz is due to bending during stress relaxation. The potential energy, which is the strain energy density integrated throughout the volume in cylindrical coordinates (for a circular wafer substrate), is written as

$$V(\varepsilon_0,\kappa) = 2\pi \iint rM\varepsilon^2\, dz\, dr \ . \qquad \textbf{Equation 16}$$

To solve for the curvature independent of ε_0, set $\frac{\partial V}{\partial \varepsilon_0} = 0$ and the midplane curvature of the substrate is given as

$$\kappa = 6\varepsilon_m \frac{1}{h_s}\gamma\beta(1+\beta)[1+4\gamma\beta+6\gamma\beta^2+4\gamma\beta^3+\gamma^2\beta^4]^{-1} \qquad \textbf{Equation 17}$$

where γ is biaxial modulus ratio, $\frac{M_f}{M_s}$, and β is the thickness ratio, $\frac{h_f}{h_s}$. Equation 17 is modeled after Timoshenko's calculation of a bilayer that can bend and stretch. If we take $h_s >> h_f$, Equation 17 reduces to Stoney's equation

$$\kappa = \frac{6\varepsilon_m\gamma\beta}{h_s^2}. \qquad \textbf{Equation 18}$$

Figure 13 is a plot of the curvature predicted by Stoney's and Timoshenko's equations as a function of h_s. As h_s gets thicker, the two models converge to the same value, as predicted.

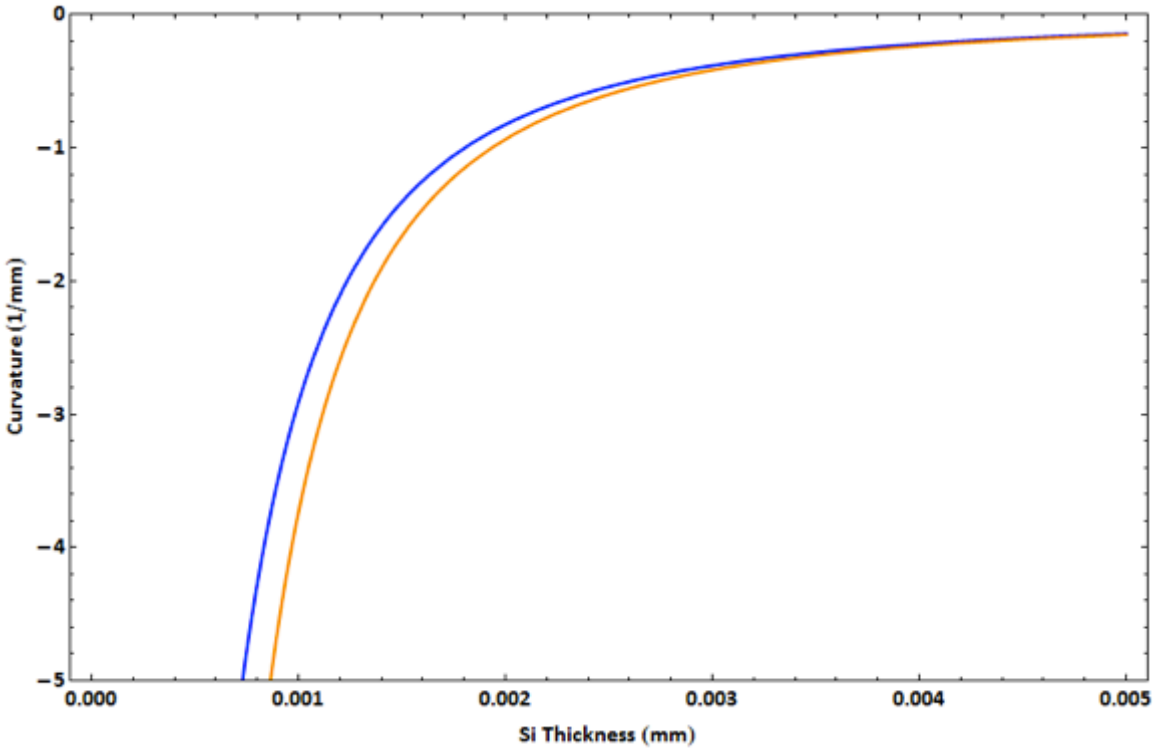

Figure 13: The curvature of a Si/SiN_x bilayer as a function of Si thickness with 100nm SiN_x. Stoney's model for this system is represented by the blue line while Timoshenko's model is in yellow. The two models converge towards 0 for an infinitely thick substrate, but as the substrate gets thinner the two models no longer agree.

The curvature, as predicted by Stoney's and Timoshenko's equations, can be plotted as a function of the ratio, β, of film and substrate thicknesses, h_f and h_s. Such a plot is shown in Figure 14. Stoney's formula is valid only at very small β where the curvature increases linearly with the thickness ratio. Now consider an identical deposited film on a increasingly thinner substrate. The strain in the deposited film would be lessened as the strain is shared more with the substrate. The curvature will eventually reach a maximum at a certain thickness ratio, and that maximum value depends on the biaxial moduli of the two materials. The curvature and mismatch as a function of increasing β is plotted below for a Si substrate and a Ge film.

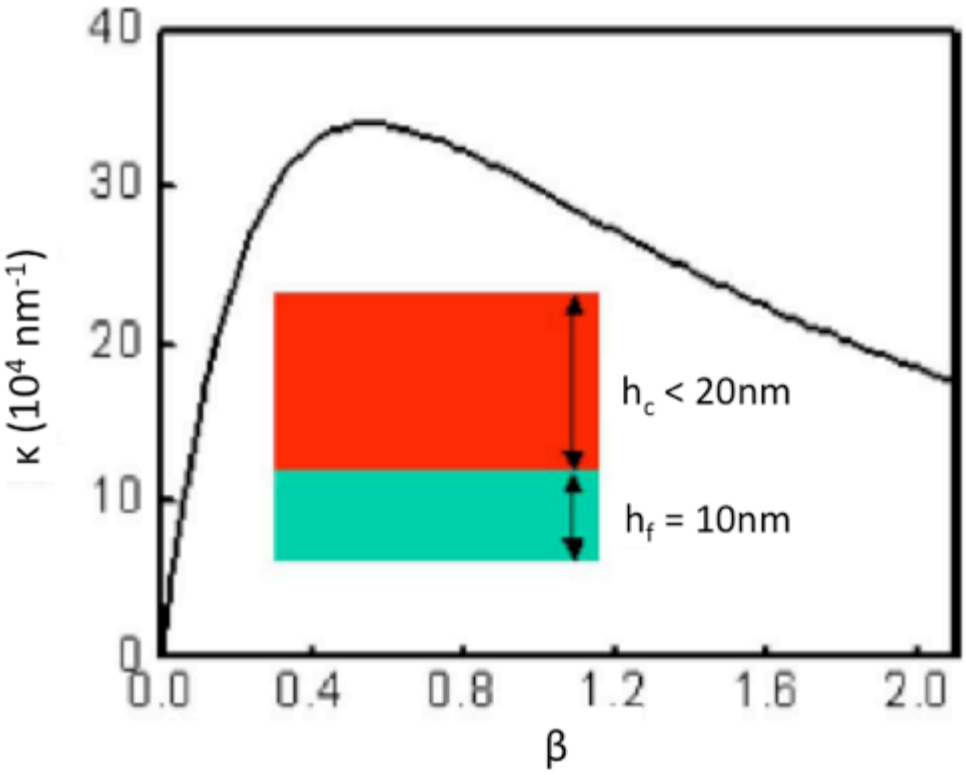

Figure 14: The curvature, κ, of a bilayer as a function of β, the thickness ratio. The model is based on a Si substrate with a epitaxial Ge film. [Huang, 2005] The inset shows conditions for β ≤ 2.0.

2.5.2 Nanoscale-thickness substrates

In the above section, we made the assumption that the film microstructure was always identical for deposition on substrates with decreasing thicknesses. That is a realistic model in the situation where the deposition is performed on a thick substrate and then the substrate is somehow thinned. When the film is directly deposited on a very thin substrate, the possibility arises that the film not only can deform the substrate as discussed above, but that there is a feedback where now the dynamic response of the substrate as it accepts strain from the growing film can influence the final strain state of the film.

There is evidence for this conjecture. It has been shown that $Si_{1-x}Ge_x$ quantum dots on a nanoscale substrate change their shape and ordering when compared to the same deposition on a thicker substrate.[Kim-Lee, 2008][Flack, 2007] With the increased flexibility of a nanoscale substrate, the growing nanostructure can produce large substrate deformations as it shares strain with the substrate, which in turn can lead to changes in the deposited-material distribution[Liu, 2002][Huang, 2005][Zang, 2007].

While both limited theoretical and experimental work has been done with local stressors on nanoscale substrates, global stressors on thin substrates appear to have been considered only theoretically, and then only to examine how stress can deform and alter properties of the nanomembrane. One of my goals in this research was, instead, to attempt to use the nanomembrane as a "strain gauge" to infer the strain in a growing film on a dynamic, ultra-thin substrate. Amorphous SiN_x films, although not the ideal choice for these studies, were used because of their universal application in the semiconductor industry. While I could not determine mechanisms for film stress evolution, I was able to show an increase in the substrate strain. This result will be demonstrated and explored later in the dissertation. A constant (or possibly nearly constant) stress in the deposited film, independent of the thickness, does, however, allow me to explore simply the effect of strain sharing on ever thinner substrates and will allow in the future the introduction of large amounts of strain in the substrate so that the structural and electronic properties of the semiconductor NM substrate can be fully explored.

My work may therefore also have implications for microelectronic and optoelectronic device fabrication. Lachut et al. noted, when looking at surface stress in

doubly-clamped beams, that “miniaturization to the nano/atomic scale can enable gigantic tunability of the mechanical properties.”[Lachut, 2012]

2.6 Summary

The microstructure and stress developed in thin films during growth is controlled by thermodynamic and kinetic limits. Internal stresses are due to a range of factors including diffusion and deposition rates. The relaxation of film stress can deform the substrate and the measurement of this deformation can be used to determine the film stress. For thick substrates, the amount of strain in the substrate is extremely small compared to the strain in the film. As the substrate is thinned, it becomes less rigid and more stress can be shared between the film and the substrate. A thin film on a thin substrate therefore provides a fascinating scenario for studies of mechanics of thin films. Because of their extreme thinness, nanomembranes therefore make a unique substrate to explore the evolution of stress in deposited thin films.

2.7 References

Abermann, R. et al. (1985). The internal stress in thin silver, copper, and gold films. *Thin Solid Films, 129*, p.71-78.

Callister, W. (2005). Fundamentals of Materials Science and Engineering. New York, NY: John Wiley and Sons Inc.

Cammarata, R. et al. (2000). Surface stress model for intrinsic stresses in thin films. *Journal of Materials Research, 15*, p.2468-74.

Chu, M. et al. (2009). Strain: A solution for higher carrier mobility in nanoscale MOSFETs. *Annual Review of Materials Science, 39*, p.203-29.

Cuthrell, R. E. (1989). Measurements of residual stresses in films of unknown elastic modulus. *Review of Scientific Instruments, 60*, p.1018-1020.

Euaruksakul, C. et al. (2009). Relationship between strain and band structure in Si(001) and Si(110) nanomembranes. *Physical Review B, 80*, p.115323.

Flack, F. (2007) Unpublished images of $Si_{1-x}Ge_x$ quantum dots on wrinkled Si nanomembranes taken in SEM.

Floro, J.A. et al. (2001). The dynamic competition between stress generation and relaxation mechanisms during coalescence of Volmer-Weber thin films. *Journal of Applied Physics, 89*, p.4886-4897.

Freund, L. and Suresh, S. (2004). Thin Film Materials. Cambridge, UK: Cambridge University Press.

Friesen, C. et al. (2002). Reversible stress during precoalescence interruptions of Volmer-Weber thin film growth. *Physical Review Letters. 89*, p. 126103.

Huang, M. et al. (2005). Bending of nanoscale ultrathin substrates by growth of strained thin films and islands. *Physical Review B, 72*, p. 085450.

Huang, M. et al. (2009). Mechano-electronic superlattices in silicon nanoribbons. *ACS Nano, 3*, p.721-7.

Kim-Lee, H. et al. (2008). Engineering SiGe growth using mechanically responsive ultrathin substrates. *ECS Transactions, 16*, p.299-305.

Lachut, M. et al. (2012). Effect of surface stress on the stiffness of thin elastic plates and beams. *Physical Review B, 85*, p.085440.

Liu, F. et al. (2002). Response of a strained semiconductor structure. *Nature, 416*, p.498.

Liu, J. et al. (2009). Direct-gap optical gain of Ge on Si at room temperature. *Optics Letters, 34*, p.1738-40.

Movchan, A. et al. (1969). Study of structure and properties of thick vacuum condensates of nickel, titanium, tungsten, aluminum oxide, and zirconium dioxide. *Physics of Metals and Metallography, 28*, p.83-90.

Ogura et al. (2009). Evaluation and control of strain in Si induced by patterned SiN stressor. *Electrochemical and Solid-State Letters, 12*, p.H117-119.

Sánchez-Pérez, J. et al. (2011). Direct-bandgap light-emitting germanium in tensilely strained nanomembranes. *Proceedings of the National Academy of Sciences of the United States of America, 108*, p.18893-18898.

Schäffler, F. (1997). High-mobility Si and Ge structures. *Semiconductor Science and Technology, 12*, p.1515-1549.

Stoney, G. (1909). The tension of metallic films deposited by electrolysis. *Proceedings of the Royal Society of London A, 82*, p.172-5.

Tamulevicius, S. (1998). Stress and strain in vacuum deposited thin films. *Vacuum, 51*, p.127-139.

Tello, J. et al. (2007). Kinetic model of stress evolution during coalescence and growth of polycrystalline thin films. *Physical Review Letters, 98*, p.216104.

Thompson, C. et al. (1996). Stress and strain growth in thin films. *Journal of Mechanics and Physics of Solids, 44*, p. 657-73.

Thompson, C. (2000). Structure evolution during processing of polycrystalline films. *Annual Review of Materials Science, 30*, p.159-90.

Thornton, J. (1977). High rate thick film growth. *Annual Review of Materials Science. 7*, p.239-60.

Timoshenko, S. (1925). Analysis of bi-metal thermostats. *Journal of Optical Society of America, 11*, p.233-255.

Ting, T. (1996). Anisotropic Elasticity. New York, NY: Oxford Science Publications.

Tu, Y. et al. (2007). Coarsening, mixing, and motion: the complex evolution of epitaxial islands. *Physical Review Letters, 98*, p.096103.

Vegard, L. et al. (1921). Die Konstitution der Mischkristalle und die Raumfüllung der Atome. *Zeitschrift für Physik, 5*, p.17-26.

Venables, J. (2003). Introduction to Surface and Thin Film Processes. Cambridge, UK: Cambridge University Press.

Zang, J. et al. (2008). Modified Timoshenko formula for bending of ultrathin strained bilayer films. *Applied Physics Letters, 92*, p. 021905.

Zepeda-Ruiz, L. et al. (2009). Understanding the relation between stress and surface morphology in sputtered films. *Applied Physics Letters, 95*, p.151910.

Chapter 3

Experimental: fabrication of tethered nanomembranes, film growth, and characterization

This chapter explains the fabrication and processing details for the tethered nanomembranes. I will begin with how the window frame that holds the nanomembrane (NM) is made from bulk Si. Following that, I describe the processing steps to make a NM starting with silicon-on-insulator or germanium-on-insulator and using chemical etching to get a freestanding NM, and then the transfer and bonding of that NM to the frame. I then discuss the deposition of the SiN_x onto the backside of the NM. I deposit compressively stressed SiN_x; the stress depends on the deposition parameters, which will be described.

The techniques I use to measure SiN_x properties, such as microstructure and elastic modulus, are explained. As a result of stress relaxation in the film, the NM becomes strained. I will explain the methods used to characterize the stress in the SiN_x and the resulting strain in the NM.

3.1 Fabrication methods

3.1.1 Approaches for fabricating thin-film/thin-substrate bilayers

There are three main methods for fabricating a bilayer from a thin film and an ultra-thin substrate. The first way is to deposit directly onto a thick substrate and then thin the substrate until it is nanometers thick. The film's microstructure will be the same during the substrate's thinning, but the strain will change due to strain sharing, and the bilayer will curl during thinning as in Figure 15. This method may be preferable because the thick substrate makes initial handling easy, but nothing new can be learned about the film microstructure. A second way is to deposit directly onto an ultra-thin substrate. The film stress can in principle dynamically respond to the flexibility of the substrate, and therefore it can end up with different properties than the film in the first case. Again the strain will share and the bilayer will curl. Because it is not possible to handle and deposit on this kind of sample, my sample is fabricated by depositing onto a thin, freestanding substrate whose edges are tethered very far away, as shown in Figure 16.

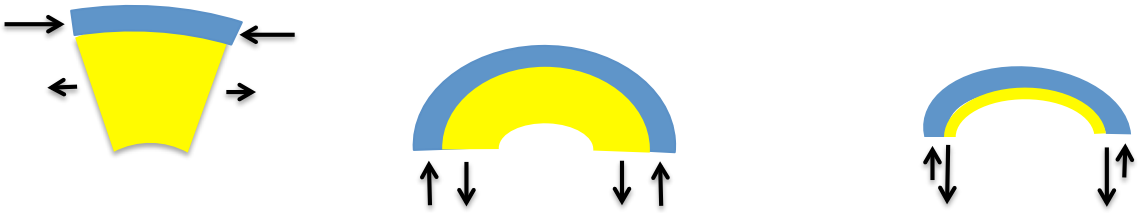

Figure 15: Schematic diagram of a thin compressively strained film deposited onto a thick substrate. The film wants to expand and thus bends the substrate. As the substrate is thinned, the strain is more and more shared between the two layers. The microstructure and interface are assumed not to change during this process

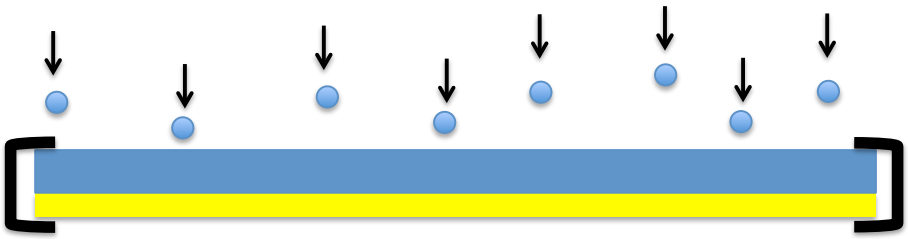

Figure 16: Schematic diagram of the sample setup used in this dissertation. A thin compressively strained film is deposited onto a thin substrate whose edges are tethered far away. The area that is not tethered is essentially freestanding and capable of bending and elongating during strain sharing.

3.1.2 Bulk-Si window frame

The frame for the tethered NM is essentially a hole over which the NM is bonded. The hole is made in a ~400μm thick Si wafer. A chemical etch removes material in a patterned region that results in a 600μm square hole after processing. To direct the etching to the hole and prevent etching over the whole Si piece, a 200nm hard SiN_x mask is deposited with low-pressure chemical vapor deposition (LPCVD) on the whole Si wafer. LPCVD SiN_x is used here because it is resistant to certain chemical etches.

A square hole is lithographically patterned with photoresist onto the SiN_x mask, which is then dry etched with a CF_4 gas, exposing the backside of the Si wafer. A stripe can also be scratched with a diamond scribe to remove some of the SiN_x mask but produces less consistent results. On pattered samples, the photoresist is removed with

acetone prior to wet etching the Si with tetramethylammonium hydroxide (TMAH), which is heated to 90°C to increase the etch rate and Si selectivity. TMAH etches the Si (110) planes faster than other Si orientations, leaving (111) facets defining the hole, as seen in Figure 17.[Gosálvez, 2003] After 8-10 hours in the heated TMAH bath, a hole is formed in the Si. If the Si piece is kept in the TMAH longer, the hole size increases slowly, and the lateral dimensions of the Si frame shrink where I have left exposed edges during dicing. An originally square piece can become very jagged when this happens. Any pinholes in the SiN_x mask allow the TMAH to etch the Si and this becomes more apparent the longer the piece is in the etchant. The SiN_x mask is then removed with hydrofluoric (HF) acid. To aid the NM bonding, the surface of the Si frame is usually left hydrogen-terminated and oxide free.

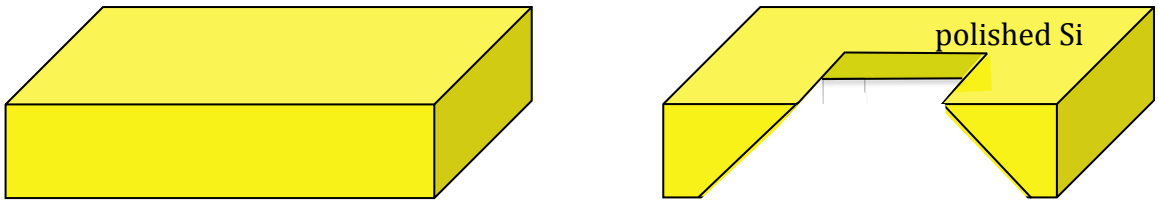

Figure 17: A diagram of a bulk Si substrate before and after TMAH etching. The angled (111) facets defining the hole are due to ease of etching of the Si (110) planes.

For my samples, the original pattern is a square with edge length ~462μm that leaves a 600μm square hole after etching. If the patterned area is smaller (≤200μm), the (111) planes intersect before the 400μm thick Si is etched through. The etching slows down and longer etching times do not improve the results.

3.1.3 Nanomembrane fabrication

To fabricate a NM, I start with a clean piece of silicon-on-insulator (SOI) or germanium-on-insulator (GOI) with an out-of-plane orientation of <001>. Both SOI and

GOI are made by SOITEC. As shipped, the outer-Si (template) layer of the SOI is usually >100nm thick, with a buried oxide (BOX) ≥ 1μm thick. The template layer is thinned with dry oxidation at 1000°C. This new top layer of oxide must be removed before proceeding to pattern the membrane. The GOI initially has a SiO_2 capping layer, a template layer around 400nm thick, and a similar thickness of BOX. Because of the way Ge oxide forms, dry oxidation can't be used as it is with Si. For GOI the oxide capping layer is removed with HF and the Ge template layer is thinned with a very dilute solution of H_2O_2 in H_2O.[Sánchez-Pérez, 2011]

Etch holes are made to facilitate a uniform release. As the BOX is etched underneath the NM, capillary forces draw the NM back down and this can cut off the etching front. Many etch holes are made so that there are multiple etch fronts that prevent the NM from being drawn back to the substrate.[Kelly, 2007] The hole size and spacing are dependent on the thickness of the template layer and the BOX. If the template layer or BOX is thick, the holes can be smaller and farther apart because the likelihood of the NM rebonding is lower.

For the best results, a NM that is much larger in lateral dimensions than the hole in the bulk Si frame will have more area to bond. The NMs that I made were 2-3mm square with square etch holes that ranged from 10-30μm laterally with 60-100μm spacing. The etch holes represent about 3-11% of the NM total surface area.

A reactive-ion etch is performed with SF_6 gas to remove parts of the silicon template layer to form the membrane and the etch holes. Keeping the photoresist intact, the whole piece of SOI or GOI is placed into 49% concentrated HF solution. The HF selectively etches the buried oxide (BOX) while leaving the Si or Ge template layer and

the PR virtually untouched. The small amount of stress from the photoresist, ~ -10MPa, improves the liftoff of the template layer.[S. Scott, personal communication]

After the BOX is etched, the NM lightly bonds through van der Waals forces onto the substrate. The whole piece is transferred at an angle into deionized (DI) water. The water helps to release the NM from the handle wafer, and it then floats on the surface. Using a wire loop that is slightly larger than the membrane, a drop of water can be picked up and held in the loop, similar to a soap film for blowing bubbles.[B. Tanto, personal communication] The nanomembrane can be scooped up from the water in this manner, transferred to a new substrate and aligned over the frame made in the Si wafer. A paper wipe is used to wick away excess water to help the NM lie flat.

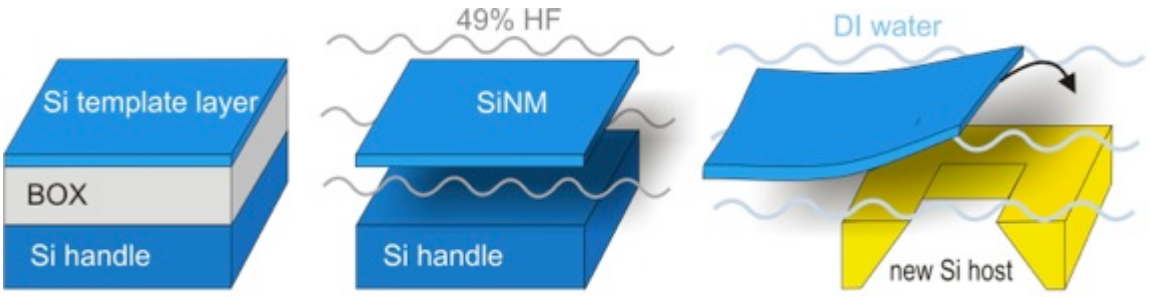

Figure 18: A step-by-step diagram of the nanomembrane fabrication and transfer process starting with SOI. Image by S. Scott.

The PR is kept on the nanomembrane during transfer. Removal of the PR can be done before or after the NM is bonded to the Si frame depending on the thickness of the NM. When the nanomembranes are around 50nm or thicker, acetone and isopropyl alcohol (IPA) can be use to remove PR before or after bonding occurs, but with thinner nanomembranes, the surface tension of the solvent can break the released NM. For any NM thickness, after the nanomembrane is bonded over the hole, the PR can be removed with an O_2 plasma etch. The plasma process imparts a small compressive strain to the

NM and, along with other strains from the PR and transfer process, contributes about 0.1% strain.

The NM is bonded in place in air overnight or longer. Bonding with heat was tested, and it was noted that if heated immediately after transfer, the NM will break. If the NM is bonded with PR still intact, the NM needs to be bonded in air for at least 8 hours prior to PR removal. The air helps evaporate the water, and time allows the Si bonds to start forming. Small amounts of heat can be applied to aid in the bonding, but too much will char the photoresist.

3.1.4 SiN_x film: materials specifics and deposition

SiN_x was chosen as a stressor material because it is relatively easy to deposit in a wide range of stress states. While it can be deposited in a variety of ways, I used plasma-enhanced chemical vapor deposition (PECVD). The resulting film has an amorphous microstructure, which is typical of PECVD-deposited films.

In PECVD, plasma breaks down precursor gases of SiH_4, NH_3, and N_2 to form the SiN_x film. A Plasma Therm (PT) 70 reactor is available in the Wisconsin Center for Applied Microelectronics. In this parallel plate reactor, the two plates act as conductive electrodes and bias the substrate to direct the deposition onto the sample. The plasma is used to keep the deposition temperature low and typically produces an amorphous film.

The gases come in a predetermined ratio of 2% SiH_4:N_2 and 5% NH_3:N_2 for safety reasons. The precursor gases affect the composition of the film; more N_2 gas can create a more nitrogen-rich film, which results in high tensile stress.[Ong, 2006] Hydrogen content also plays a role in stress formation in SiN_x. Studies have found that

an increase is H in the SiN_x film leads to more tensile stress and annealing can cause an out-diffusion of H, leading to a more compressive stress.[Ogura, 2009][Paduschek, 1983]

Studies have shown that the SiN_x film stress and deposition rate depend on the PECVD deposition parameters, such as the ratio of SiH_4 to NH_3 precursor gas mentioned previously. Other factors that affect the stress in the SiN_x are the chamber temperature, the plasma power, the gas pressure, and the plasma frequency. The chamber temperature is limited to 350°C for the PT 70, but studies have shown that an overall increase in temperature can lead to an increase in the compressive stress in the film.[Toivola, 2003] [Cotler, 1993] The plasma power and the chamber pressure are intimately linked because the reaction requires that there is enough pressure to ionize the plasma with a given RF power. It has been shown that an increase in RF power will lead to a more compressively stressed film, [Cotler, 1993] while an increase in chamber pressure will lead to a more tensilely stressed film.[Ong, 2006] The average ion momentum, p_{ion}, which is proportional to the pressure, P, and the power, W,

$$\bar{p}_{ion} \propto \left(\frac{W}{\nu P}\right)^{1/4} \qquad \textbf{Equation 19}$$

increases as more ions are implanted in the film, which results in a compressive stress.[Johlin, 2012] While the frequency, ν, has also been known to affect the film stress[Arghavani, 2006], the PT 70 chamber only has one fixed RF frequency setting, which is 13.56MHz. With chambers that allow for a lower RF frequency, cycling between the high and low frequencies can build up high compressive stress, which is due to an increase in the average ion momentum, as seen with Equation 19.

To prepare for growing SiN_x, the PECVD chamber is first conditioned by running it while empty at the settings that were used for the deposition. Conditioning ensures the recipe runs properly before inserting samples and also coats the walls with the film so that there is none of the previous user's film that could contaminate the deposition. After conditioning, the sample is put into the chamber, upside down, and supported on two edges by some spare pieces of Si wafer so that the NM does not come into immediate contact with the chamber. The SiN_x is deposited in a directional way so that the back of the Si nanomembrane is coated with SiN_x through the hole in the Si frame as in Figure 19. Simultaneous depositions on a bulk wafer and a masked piece of Si are usually done at the same time as the NM sample. The curvature due to the film on the bulk wafer can be used to calculate the stress in the SiN_x film with Stoney's equation while the masked piece of bulk Si can be used for thickness measurements.

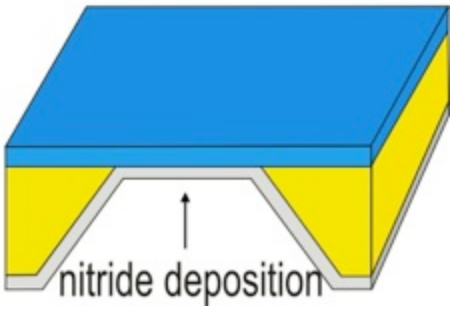

Figure 19: An upside down illustration of the SiN_x deposition from the back side of the bulk Si frame. Image by S. Scott.

It is clear that the NM bonded to the frame is not freestanding but tethered. Because of these edge constraints, I am limited to looking at SiN_x films under

compressive stress, and Figure 20 illustrates the reason why. If a compressive film is deposited onto the NM substrate, the compressive film wants to expand laterally, taking the NM with it. As the deposited film elongates the NM, the freestanding area is free to bulge or ripple to accommodate the elongation, as in Figure 20a. If a tensilely stressed film were deposited onto the NM, the film wants to relax by pulling material from the edge into the freestanding area as in Figure 20b. Because the edges are fixed, if tensile stress is high enough, it can lead to fracture of the freestanding window sooner than if the same magnitude but opposite sign of stress was applied.[Martyniuk, 2006]

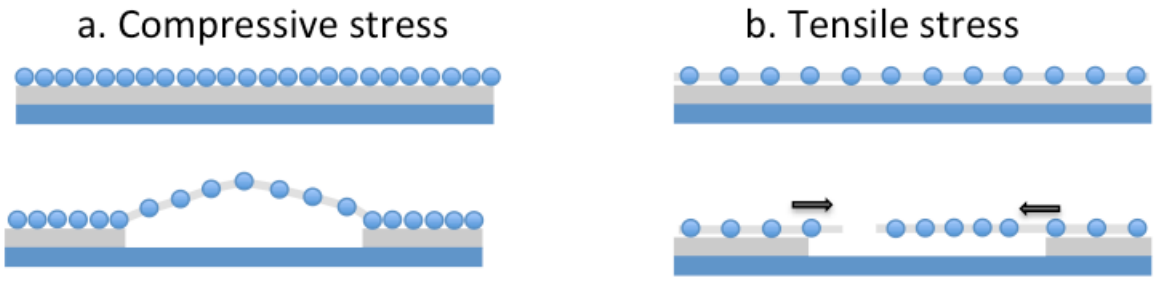

Figure 20: An illustration of elastic stress relaxation in a tethered thin film after the substrate was partially removed for a compressively stressed film (a) and a tensilely stressed film (b).

To reiterate, compressive strain in a film deposited on an initially unstrained nanomembrane creates an elongation that needs to be accommodated by bowing and wrinkling. A window with constraints provided by the frame may modify the behavior near the frame. For my purposes, I measure the degree of strain in the membrane very far from the window frame edges where the membrane is held rigid. I know from a separate measurement on a strained Si/SiGe superlattice NM that in the inverse situation, the strain field's extent near an etch hole, that the strain modification reaches out ~700nm. As explained below, the aspect ratio of the bilayer thickness to the size of the window frame is of the order of 3000.

As mentioned earlier, the photoresist can also induce a small amount of stress (-10 MPa) in the NM. If the PR remains on the NM during bonding, any strain in the NM remains after bonding and PR removal. A majority of time the NM is slightly bowed up after transfer and during bonding. After the PR is removed, the NM remains bowed in the same direction. After compressively stressed SiN_x is deposited, the bow in the NM increases and the NM either continues to stay bowed up or creates a large wave with parts bowed up and parts bowed down, thus confirming increased elongation. White-light interferometry confirms that the magnitude of the bow is greater after SiN_x deposition. Details of this measurement will be discussed in the following section.

3.2 Characterization methods

3.2.1 SiN_x film characterization

The characterization of the SiN_x film consists of thickness measurements with atomic force microscopy and stress measurements for growth on bulk Si with laser deflection. Using nanoindentation, the response of the SiN_x was used to calculate the Young's modulus. I use x-ray diffraction for structural characterization of the film.

The color of a SiN_x film depends on the thickness. Color chart references have been made that link the two. Along with the color charts, the film's thickness is verified by step height measurements of SiN_x on a piece of bulk Si with Kapton tape as a mask. The tape is removed with the help of solvents, although residue is sometimes left behind. In the regions without residue, a small, sharp tip is rastered across the step, and the height difference is measured by the deflection of the cantilever arm. I measured the thickness of the SiN_x film with either atomic force microscopy (AFM), on a Digital Instruments Nanoscope III, or by profilometry, on a Tencor AlphaStep 200. Ideally, the vertical

resolution of AFM is sub Angstrom and profilometry is on the range of 25-50 Angstroms. In my experience though, a sharp tip was needed to get these resolutions and for a multi-user instrument like profilometry, this was not always possible.

After a film is deposited on a bulk substrate, the substrate's deformation can give information about the film's stress. The bulk wafer curvature is commonly measured, and Stoney's equation is used to calculate the stress in a deposited film if the substrate modulus and thicknesses of both layers are known.[Freund, 2004] The difference in the curvature is measured by reflecting a laser off the sample surface. Using the interference pattern created, the sample's deflection can be calculated. This technique requires film uniformity over a large area, usually 10s of mms in diameter depending on the wafer size. Dual laser wavelengths are available at 670nm or 750nm to find the maximum intensity for materials that may be transparent at one wavelength. The surface must also be reflective. If the film does not reflect well, a double side polished wafer can be used to maintain a reflective side and the curvature of the opposite side is measured.

The Tencor FLX-2320 was used to measure the wafer curvature. It can only perform line scans across the wafer so measurements are typically done at two orientations, 0° and 90°. If the wafer's deformation is isotropic in that plane, the calculated stress at 0° and 90° will be similar. For SiN_x that is the expected result. While the optimal resolution of this measurement is typically $0.00003m^{-1}$, the actual limit is based on the ability to place the wafer repeatedly in the same azimuthal orientation. The film stress is based on the difference in the initial and final wafer curvatures, so if the measurements are not taken at the same location each time, the difference will have some error associated with it. For the highest-resolution measurements, the film should be

thick and the substrate thin (while still in the Stoney's formula regime) to amplify the curvature. For example, a thickness ratio (h_{SiN}/h_{Si}) of 1/37.5 will have a three orders of magnitude better stress resolution than a bilayer with a thickness ratio of 1/37500.[Tencor, 1995] The stress resolution for my measurements is ~5 MPa.[Tencor, 1995]

To calculate the elastic modulus of the SiN_x, I worked with Dr. Joseph Jakes at the Forest Products Laboratory, who did nanoindentation measurements for films of a thickness range of 95-155nm that I deposited on a Si wafer. The nanoindentation measurements were performed on a Hysitron TriboIndenter 900 with a pyramid-shaped Berkovich tip. When indented, if the film does not peel or delaminate with the applied force, the measured mechanical properties are reliable, which is the case for these measurements (Figure 21). The amount of force versus the tip displacement can be plotted and the slope of the unloading curve is indicative of the stiffness, S, of the material.[Oliver, 2004] The hardness, H, the reciprocal of the stiffness, can be calculated as the maximum load per area, A,

$$H = \frac{P_{\max}}{A}. \qquad \textbf{Equation 20}$$

The area of the indent, A, is measured with either AFM or scanning electron microscopy (SEM). The effective Young's modulus is then

$$E_{eff} = \frac{S}{\sqrt{A}}. \qquad \textbf{Equation 21}$$

On a bilayer, such as the SiN_x on bulk Si, the substrate's response will be part of the measurements. Removing the substrate's contribution is not trivial and has been studied and modeled extensively by Professor Donald S. Stone.[Stone] Using the models described above, the reduced Young's modulus was found to be about 120±20GPa. Assuming the Poisson ratio of SiN_x is similar to that of stoichiometric Si_3N_4, υ=0.22 [Freund, 2004], then the biaxial modulus of our deposited amorphous SiN_x is 160±25GPa. This value is about half of the reported modulus for crystalline, stoichiometric Si_3N_4, which lies in the range of 280-310GPa.[Freund, 2004] The measured value is acceptable for amorphous SiN_x because it should less dense and therefore less stiff than single-crystal Si_3N_4.

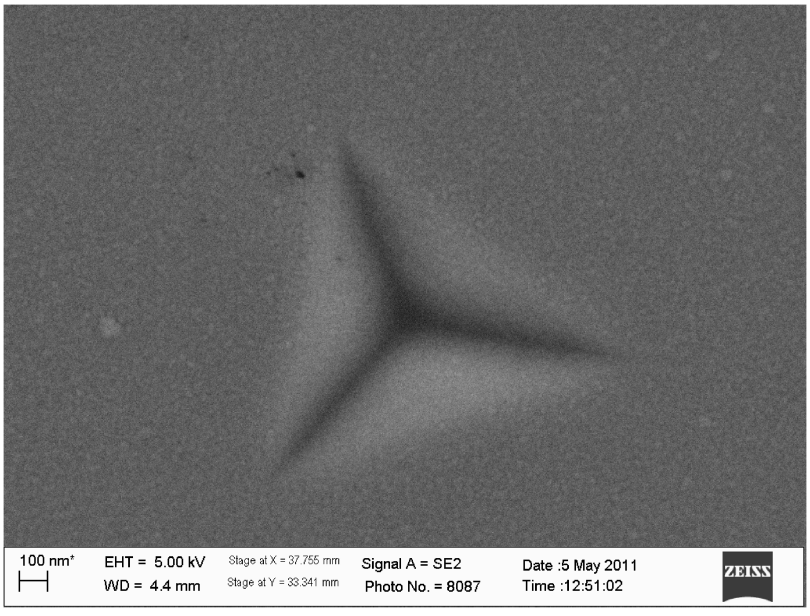

Figure 21: A SEM image of a nanoindent done on 100nm of SiN_x deposited on Si. The absence of pileups or film delamination will allow for accurate Young's modulus calculation.

X-ray diffraction can quickly and non-destructively assess the microstructure of a material. For x-rays of wavelength, λ, scanning through a range of angles, θ, will

produce peaks when the scattered x-rays constructively interfere according to Bragg's law,

$$n\lambda = 2d_{hkl}\sin\theta\,, \qquad \textbf{Equation 22}$$

where n is an integer and d_{hkl} is the spacing of the atomic planes (Figure 22). If the positions of a material's atoms are highly periodic, as in a single crystal, there are sharp and intense peaks at select angles. As the positions become less periodic, in polycrystalline and amorphous materials, the peaks broaden and the intensity decreases.

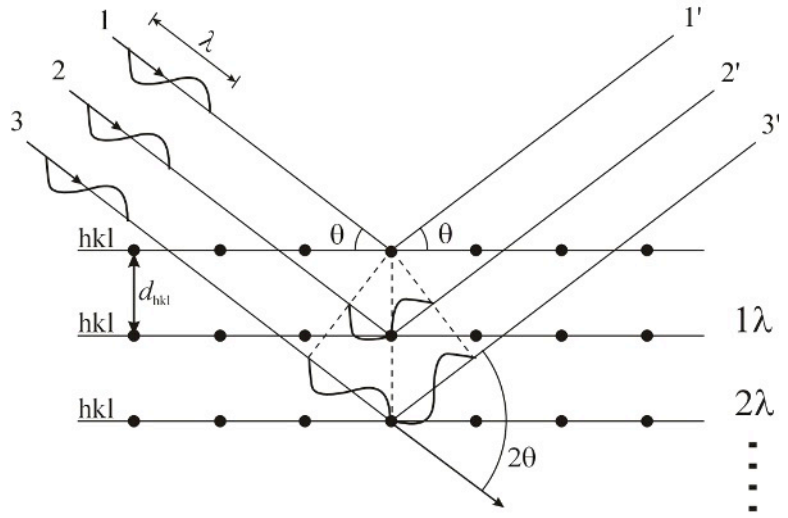

Figure 22: A schematic diagram of constructive interference of beams of wavelength, λ, incident at an angle, θ, on and exciting from a set of periodic rows of atoms with spacing d_{hkl}.[IVK]

X-ray diffraction (XRD) was done on 100nm of SiN_x deposited on a bulk Si wafer and the diffraction pattern in Figure 23 was acquired from a scan through 2θ. Both the underlying single-crystal Si structure ((113) and (220) peaks) as well as a broad amorphous peak from the SiN_x (at small 2θ values) are apparent. This is not surprising as PECVD-deposited SiN_x films are typically amorphous.

The microstructure was assumed to be amorphous on the NM window as well, because it couldn't be measured directly with XRD. Because of the small size of the freestanding area, alignment was extremely difficult. A larger freestanding area would make it easier to measure the microstructure on both the bulk and NM for comparison.

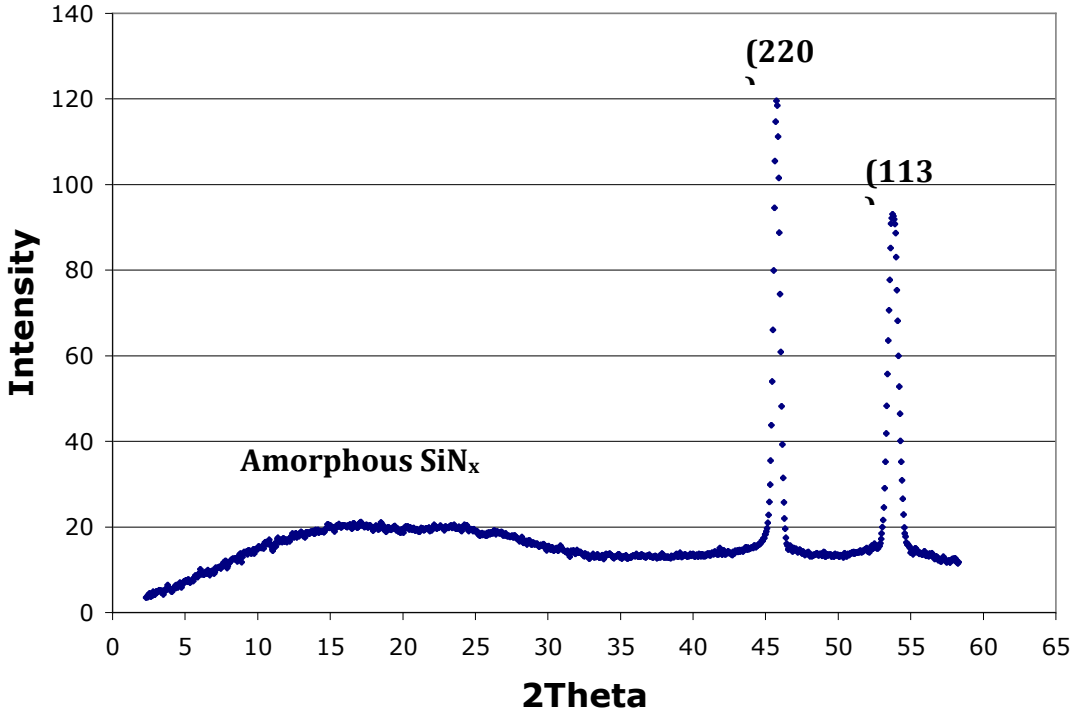

Figure 23: An x-ray diffraction pattern from 100nm of SiN_x on a bulk Si wafer. The broad, weak peak at small angles is from the amorphous SiN_x and the sharper peaks at high angles correspond to the (113) and (220) Bragg conditions in the Si substrate.

3.2.2 Nanomembrane characterization techniques

Using optical images, white-light interferometry, and Raman spectroscopy, I measure changes in the NM due to strain before and after SiN_x deposition. Optical images are taken to inspect for any physical changes to the NM, such as modification of etch holes and tears. Raman spectroscopy gives information about the strain state of the

NM, while white-light interferometry measures any topological changes, such as bending.

The handling, processing, and stress relaxation can visually change the NM window. Optical images are used to inspect for tearing in the membrane as well as any wrinkling. Figure 24 is a series of images taken after a 22nm Si NM covered with PR was transferred and bonded, after RIE was done to remove the PR, and after 125nm of SiN_x was deposited, respectively. It is evident that wrinkles form after the PR has been removed and are accentuated after the SiN_x deposition.

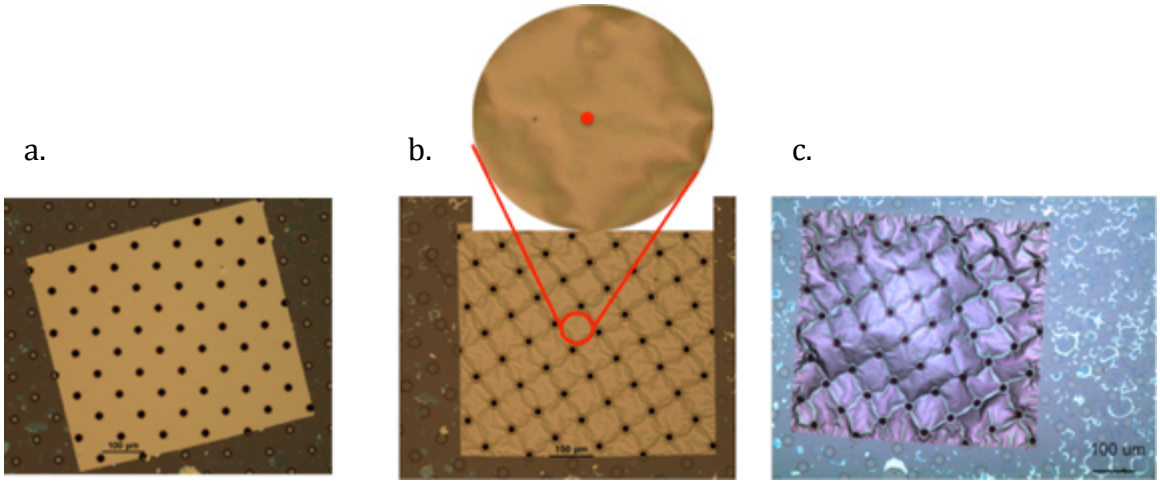

Figure 24: Optical micrographs of a 22nm Si NM after transfer (a), PR removal (b), and deposition of 125nm of SiN_x (c). The enlarged area is of an approximate area that Raman measurements would be taken and the red dot indicates an approximate spot size for the Raman laser.

White-light interferometry uses the interference of light reflected from an object to calculate the relative displacements in the out-of-plane direction. The beam from a light source is split, with part used as a reference and part incident on the sample. When the two beams are recombined, they form an interference pattern that can be used to create a topological map of the sample area.

The interferometry measurements were made with a Zygo New View microscope. Using a 10x objective, a series of overlapping images were taken and stitched together with the Zygo software (Figure 25a). Line profiles can be taken across the stitched image to give a profile of the NM (Figure 25b). The lateral resolution of this technique (~1μm) depends on the magnification of the objective used, while the vertical resolution (<0.1μm) depends on the optics.

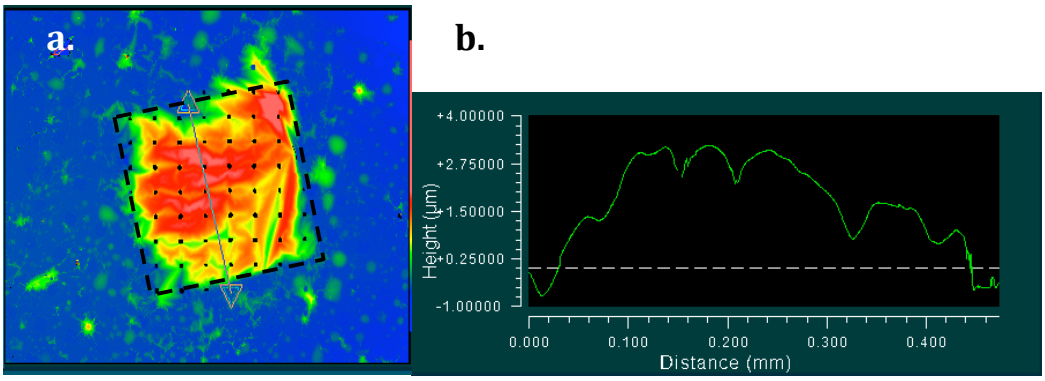

Figure 25: A topological map from white-light interferometry (a) and a line profile across that map (b). The map was obtained on a 22nm Si NM with 100nm of SiN_x deposited onto the backside.

The Raman process measures the inelastic scattering of optical phonons near the Brillouin zone center in a material. As shown in Figure 26, the incident laser light, with frequency ω_I, excites an electron into a higher energy level. A phonon is created with a frequency of ω_j while the energy of the electron decreases. When the electron recombines with a hole, a photon is created with a frequency of ω_s, which is the difference between ω_i and ω_j. This is seen as a peak shift (Figure 27), which can be related to film strain as

$$\Delta\omega = c\varepsilon_{Si} \qquad \textbf{Equation 23}$$

where *c* is calculated from the material's elastic deformation constants. Unstrained Si has a peak at 520.2 cm^{-1} and unstrained Ge has a peak is 300.7 cm^{-1}.[Parker, 1967] SiN_x is transparent at these wavelengths and does not have a Raman active mode within the range measured.[Ogura, 2008]

Raman spectroscopy is used to measure the strain in a material by measuring the shift in the peak. The magnitude of the peak shift relates to the magnitude of the strain and the direction of the peak shift relates to the sign of the strain. For a tensile strain, the peak shifts to lower wavenumbers and oppositely for compressive strain.

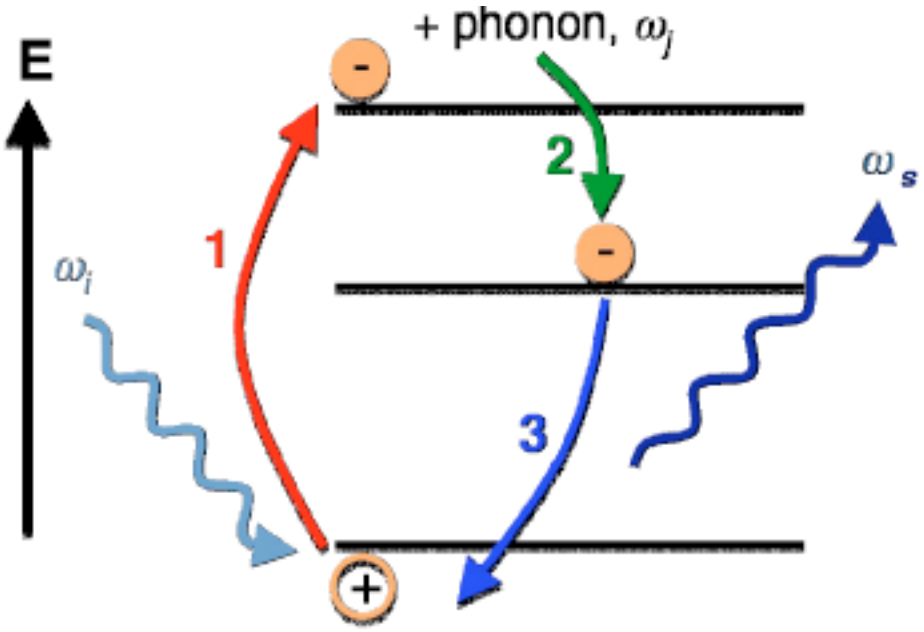

Figure 26: A diagram of the Raman process. The incident laser light, ω_i, creates a phonon whose energy can be detected as the difference between the incident frequency and the detected frequency ω_s. Image by D. Paskiewicz.

Raman spectroscopy was done using two systems: the LabRAM Aramis Horiba Jobin Yvon confocal Raman microscope and Thermo Fisher's micro Raman DXR. Depending on what was available and operational at the time as well as the nanomembrane material, either a 532nm or a 442nm laser was used. The penetration

depth of the 532nm laser is about 1000nm in Si and 24nm in Ge, while the 442nm laser's penetration depth in Si is about 290nm and 20nm in Ge. The greater the penetration depth, the more material is sampled, leading to a signal that is higher in intensity. Therefore, Si samples produced a signal about an order of magnitude higher than the Ge samples. In general, the 442nm laser is preferred for Si NMs because it has lower power and therefore produces less heating, while the 532nm laser is preferred for Ge NMs because it produces a higher-intensity signal.

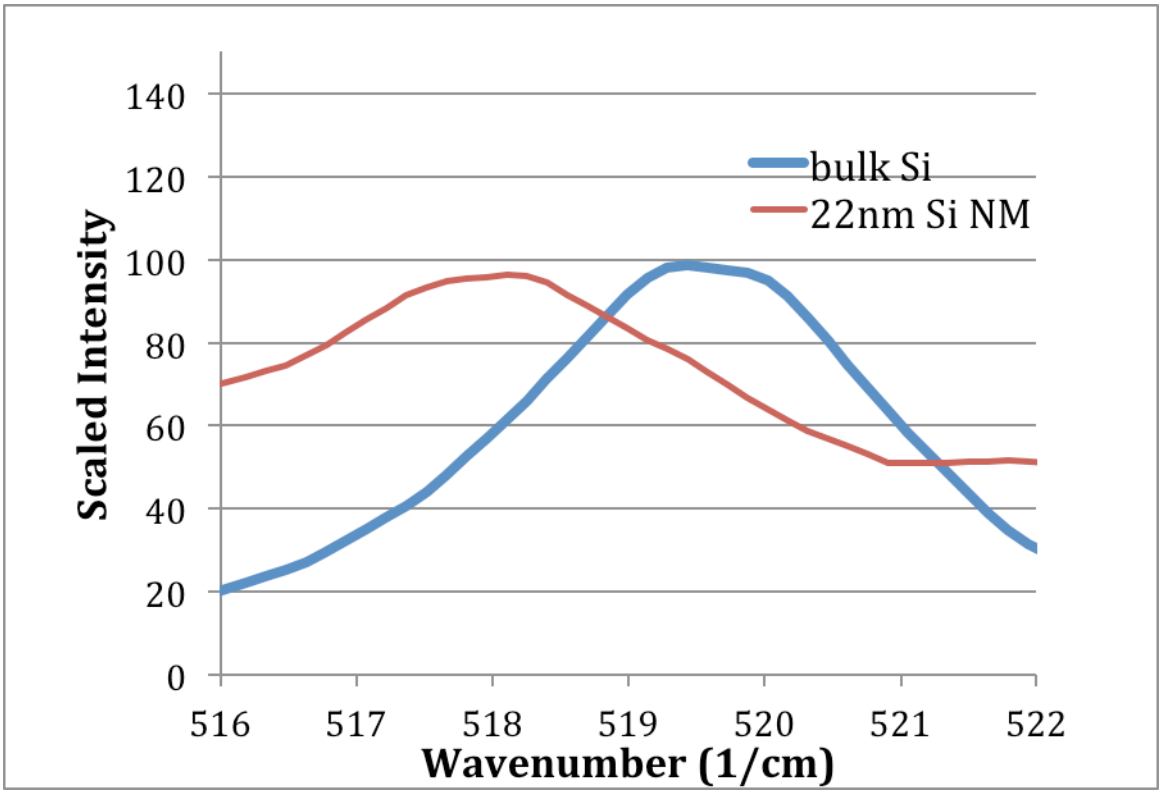

Figure 27: Spectra taken on bulk Si and a 22nm Si NM, each with 100nm of SiN_x. When the NM's spectral intensity is scaled by 16, the shift of the NM peak is clear.

The laser spot size and the size of the confocal apertures used determine the spatial resolution of the measurement while the grating determines the spectral resolution.

The magnification objectives determine the spot size of the laser on the sample. A 50x objective was used with the Horiba Raman, which resulted in a beam size of 1.4μm, while a 100x objective and a 25μm confocal aperture were used on the Thermo Raman, which resulted in a beam size of around 700nm. To make the strain calculations, I can assume that the NM is essentially flat in the measurement region and that any curvature due is effectively zero because the laser's spot size is small. The highest-resolution grating on each system was used to ensure good spectral resolution.

Three measurements were averaged anywhere from an approximately 10μm square area to a 300μm square area. After the Raman spectra were measured, a background subtraction and peak fitting were done with each instrument's software to determine the peak positions, and the difference in the peak position before and after SiN_x deposition was used to calculate the strain.

The lasers used in Raman spectroscopy can significantly heat small, thin samples like freestanding NMs when focused with a large microscope objective, which can lead to peak shifts that may be mistaken for strain. To minimize the heating on the sample, a short acquisition time is necessary. A short acquisition time, however, reduces the intensity of the signal. I varied the acquisition time until an appropriate time was found that is short enough to not heat the sample (no peak shift over time) while still providing a large enough signal-to-noise ratio. Both systems also provide a filtering feature that can attenuate the laser power, which was used in combination when varying the acquisition time.

3.3 Initial measurements on nanomembranes

3.3.1 Wrinkles and edge effects

After SiN_x is deposited onto the NM, wrinkles form as a consequence of stress relaxation. To explore the effect of wrinkles on the Horiba Raman signal, spectra were taken from the top of a peak and a neighboring valley. The measured strain is a sum of the bending and axial strain due to the transfer process and the bending and axial strain due to the SiN_x deposition. Because the error in the strain of both the peak and valley overlap, there is no strong indication that the wrinkles cause a difference in the strain that is measureable within the resolution of the instrument (but see below for a higher-resolution result). While the 442nm laser penetrates through both the Si and SiN_x, only a signal from Si is measured and any difference in the strain is averaged out through the thickness.

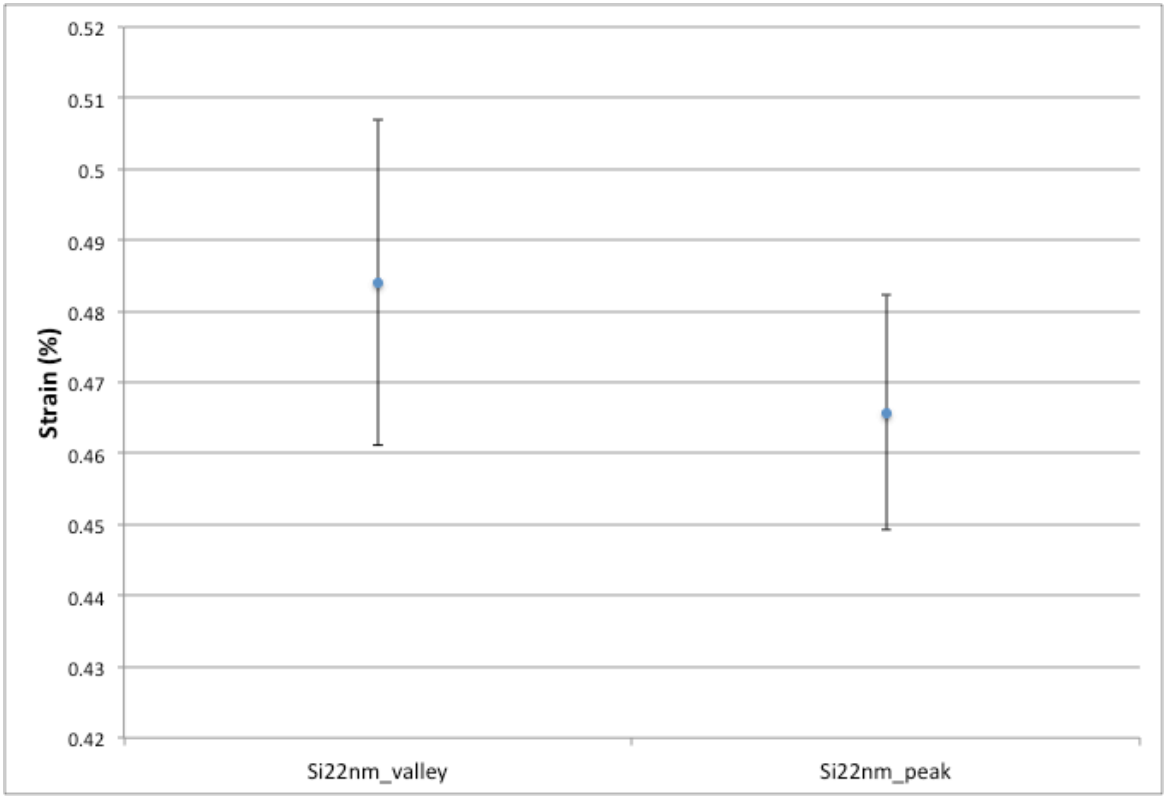

Figure 28: Strain determined from Raman spectra taken on a wrinkle's peak and valley. Within the error of the measurement, the strain does not appear to be affected by the curvature of the wrinkles as the centroids differ by 4%. Therefore we can use an approximation of only axial strain.

As I saw with local stressors (see Appendix A), unconstrained edges allow stress to relax while bonded edges allow strain to build up. There is a concern that locally created strain fields may propagate in lateral directions. With higher spectral resolution, Debbie Paskiewicz made a two-dimensional map near a bonded edge and etch hole with the 532nm laser on the Thermo Raman spectrometer with a spot size of 700nm, to explore how far laterally a strain gradient extends. Wrinkles were also present in the mapping region. After the spectra were compiled, the map was smoothed with an interpolation function in Mathematica. By mapping the Si peak shift on a 22nm Si NM with 100nm of SiN_x deposited, we determined that the strain gradients at the bonded edge and etch hole only extend about 700-1000nm, as shown in Figure 29b. At the bonded edge there is a fairly abrupt change from the strained, freestanding region to the unstrained, bonded NM.

The optical image (Figure 29a), shows wrinkles throughout the mapped area. The spectral sensitivity of the instrument used here is higher than that of the instrument used for data in **Figure 30** and is able to detect the change in strain due to the differences in curvature from one area to the next. At most, the variations in Raman peak shift are $\leq .8$ cm^{-1}, or less than 0.10% strain.

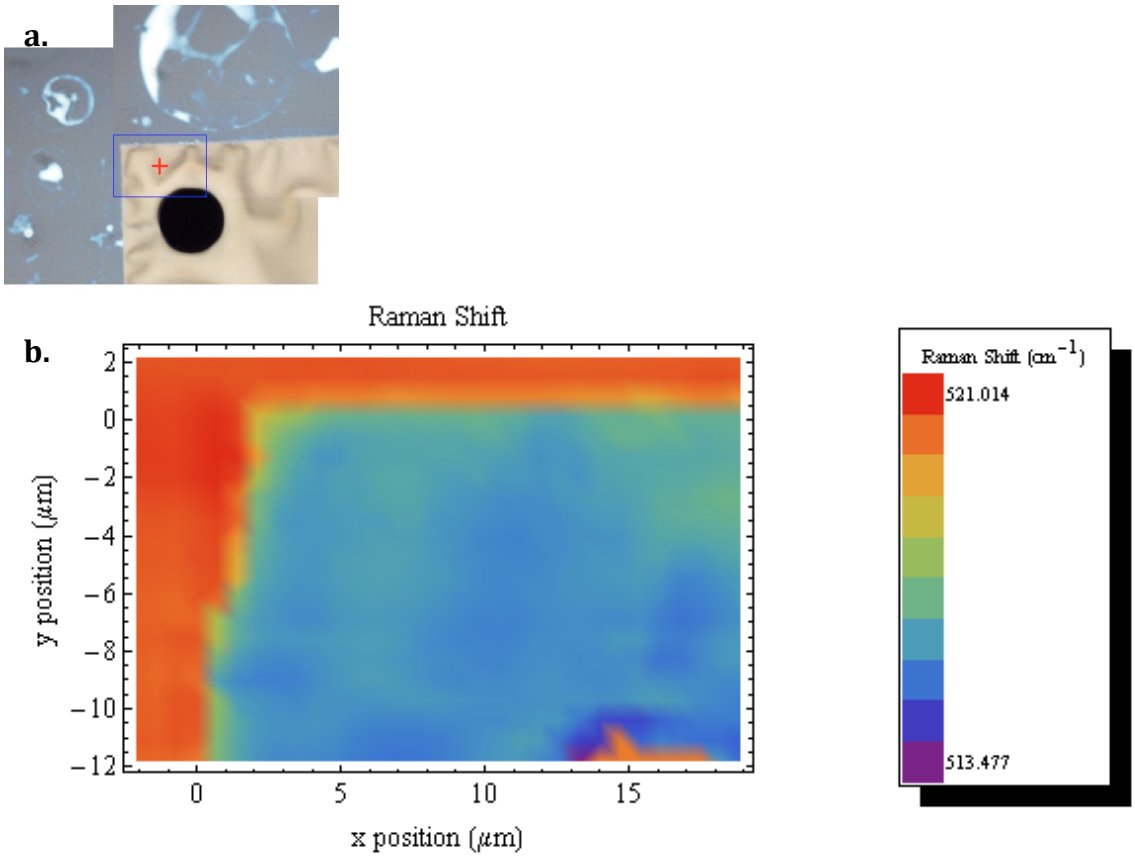

Figure 29: An optical image (a) of a 22nm Si NM with 100nm of SiN_x deposited on the reverse side in the region that was mapped with Raman spectroscopy. The Si peak shift is plotted (b) after an interpolation smoothing. Image by D. Paskiewicz.

3.3.2 Curvature and bowing in tethered NMs

White light interferometry was done on the bowed, tethered NMs before and after SiN_x deposition (Figure 30). The SiN_x imparts a tensile strain to the Si or Ge NM, causing it to elongate. The strain that is present in the Si or Ge NM is therefore related to the elongation in the bilayer. From the strain in the NMs, the elongation should be no more than 6μm, which is near the out-of-plane resolution for the optics used. The radius of curvature was calculated from these measurements but with the image processing and the resolution, the error was too large to be able to measure such a small change in NM length.

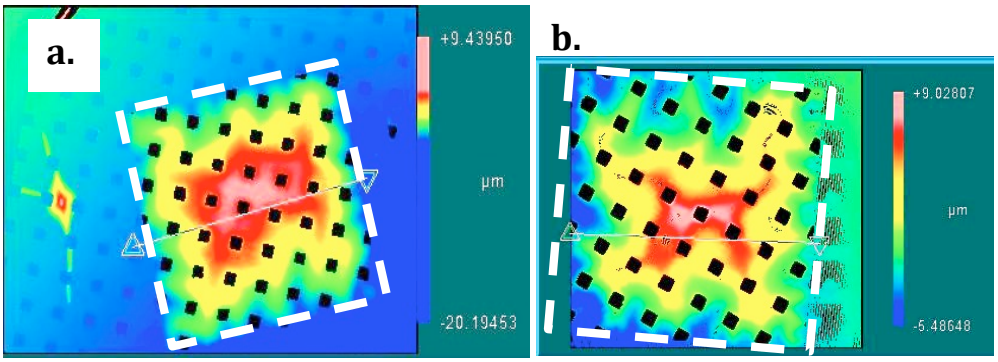

Figure 30: White light interferometry maps on the same 47nm Ge NM before (a) and after (b) 100 nm was SiN_x deposited.

3.4 Summary

Details for making a tethered Si or Ge NM were covered in this chapter. SiN_x was used to induce strain in the NM; it was first characterized on bulk Si. I have explained the measurement techniques that I used to characterize the SiN_x film properties and those of the Si NM or Ge NM substrates. Initial measurements on the nanomembrane wrinkles and bowing were also discussed.

3.5 References

Arghavani, R. et al. (2006). Reliable and Manufacturable method to induce a stress of >1GPa on a p-channel MOSFET in high volume manufacturing. *IEEE Electron Device Letters, 27*, p.362-365.

Cotler, T. et al. (1993). High quality plasma-enhanced chemical vapor deposited silicon nitride films. *Journal of the Electrochemical Society, 140*, p.2071-2075.

Freund, L. and Suresh, S. (2004). Thin Film Materials. Cambridge, UK: Cambridge University Press.

Gosálvez, M. A. et al. (2003). Surface morphology during anisotropic wet chemical etching of crystalline silicon. *New Journal of Physics, 5*, p.100.

Johlin, E. et al. (2012). Structural origins of intrinsic stress in amorphous silicon thin films. *Physical Review B, 85*, p.075202.

Kelly, M. (2007). *Elastic strain sharing in silicon/silicon germanium nanomembranes.* (Doctoral dissertation) University of Wisconsin, Madison, WI.

Martyniuk, M. et al. (2006). Stress in low-temperature plasma enhanced chemical vapour deposited silicon nitride thin films. *Smart Materials and Structures, 15*, p.S29- S38.

Ogura, A. et al. (2008). Evaluation of strain in Si-on-insulator substrate induced by Si_3N_4 capping film. *Japanese Journal of Applied Physics, 47*, p.1465-1468.

Ogura, A. et al. (2009). Evaluation and control of strain in Si induced by patterned SiN stressor. *Electrochemical and Solid-State Letters, 12*, p.H117-119.

Oliver, W. C. et al. (2004). Measurement of hardness and elastic modulus by instrumented indentation: Advances in understanding and refinements to methodology. *Journal of Materials Research, 19*, p.3-20.

Ong, P. et al. (2006). A new fabrication method for low stress PECVD- SiN_x layers. *Journal of Physics: Conference Series, 34*, p.764-69.

Paduschek, P. et al. (1983). Hydrogen-related mechanical stress in amorphous silicon and plasma-deposited silicon nitride. *Thin Solid Films, 110*, p.291-304.

Parker, J. H. et al. (1967). Raman scattering by silicon and germanium. *Physical Review, 155*, p.712-714.

Sánchez-Pérez, J. et al. (2011). Direct-bandgap light-emitting germanium in tensilely strained nanomembranes. *Proceedings of the National Academy of Sciences of the United States of America, 108*, p.18893-18898.

Stone, D. UW-Madison extended homepage. Elastic modulus calculated for a thin film on a silicon substrate [Data tables]. Retrieved from http://homepages.cae.wisc.edu/~stone/elasticity%20solutions.htm

Tencor. (1995). *Tencor FLX-2320 Thin film stress measurement user manual* (software version 4.2). Mountain View, CA: Tencor.

Toivola, Y. et al. (2003). Influence of deposition conditions on mechanical properties of low-pressure chemical vapor deposited low-stress silicon nitride films. *Journal of Applied Physics, 94*, p.6915-22.

IVK Nuclear and Radiation Physics' X-ray diffraction facilities. (2010). [Image representation of Bragg's Law]. Retrieved from http://fys.kuleuven.be/iks/nvsf/experimental-facilities/x-ray-diffraction-2013-bruker-d8-discover

Chapter 4

Results and conclusions

In this chapter, I compare overall system strain when SiN_x films are deposited on bulk and nanoscale substrates by plasma-enhanced chemical vapor deposition (PECVD). Film thickness and substrate curvature measurements were used to characterize the film uniformity and the stress in the SiN_x films deposited on bulk Si substrates, respectively. White-light interferometry and Raman spectroscopy measurements were performed on tethered NMs before and after SiN_x deposition to infer information about the stress in the film on ultra-thin substrates. Nanomembrane substrates of varying thicknesses as well as different elastic modulus (e.g., Si and Ge) were used. Results are compared and discussed.

4.1 Characterization of SiN_x on bulk Si

For SiN_x films deposited on a Si wafer, the microstructure and stress were measured. The thickness was measured on a bulk Si piece across a step produced by masking with Kapton tape that was removed after film deposition.

Of all the ways to deposit SiN_x, PECVD is a technique that is commonly available in local growth facilities and has a large number of deposition parameters to vary. Because of this, it can be challenging to reproduce. Thickness measurements made with AFM, for the thinner films, or profilometry, for the thicker films, were averaged over multiple depositions for the course of this project. Although, the resolution of the instruments should be able to resolve very thin films, as a multi-user instrument, the

profilometer's tip made it difficult to measure films around 30nm accurately so the AFM was used. The thickness for a given deposition time and nominally identical deposition conditions is known within an order of magnitude. Figure 31 shows that the average deposition rate is approximately 0.18nm/second.

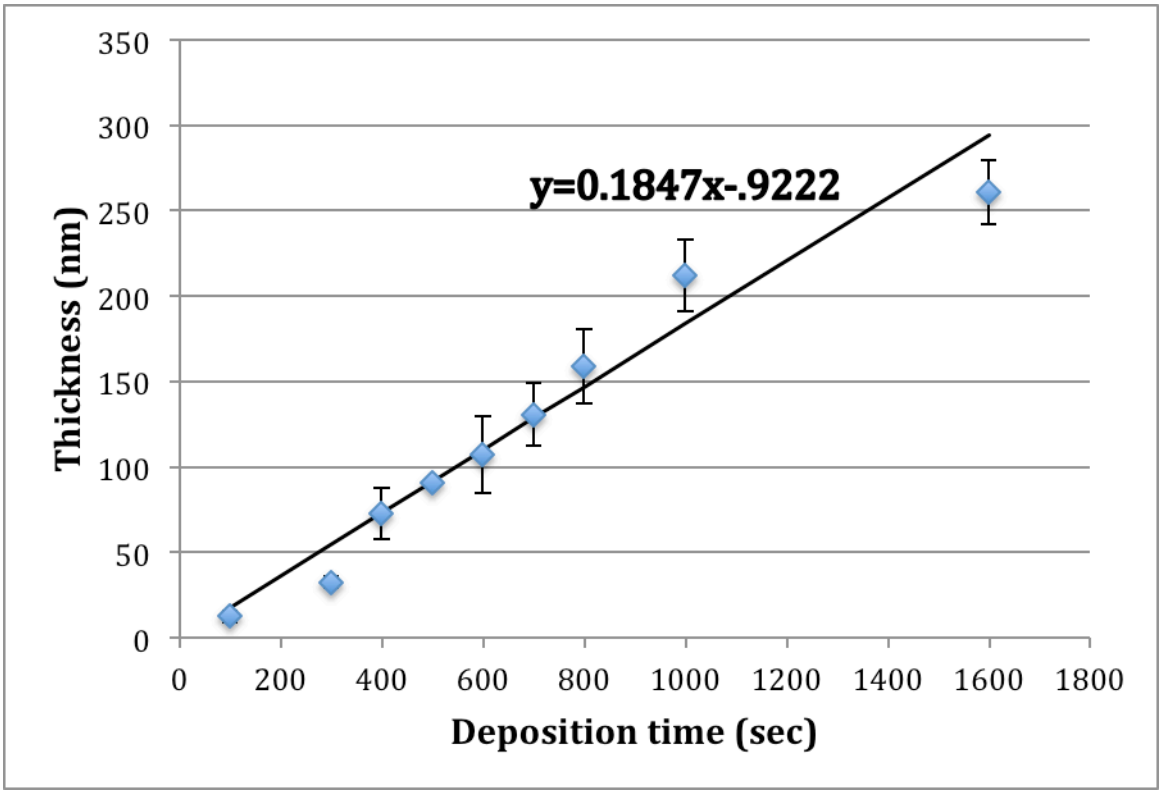

Figure 31: PECVD SiN_x thickness as a function of deposition time under the same deposition conditions. The line is a linear least squares fit going through zero. Points without noticeable error bars are single measurements and have the instrumental error only

SiN_x was deposited onto 3-inch Si wafers with the local PECVD system, the PT70, with thicknesses ranging from 32 to 260nm. Thinner films were deposited, but stress measurements were unreliable. The resulting wafer curvature is plotted in Figure 32. The slope of a linear least squares fit is directly proportional to the stress of the SiN_x film, $\sigma_{SiN,}$ using Stoney's equation, and gives a value of approximately -192MPa. While the SiN_x film stress values are plotted and compared in Figure 34, the data trend in Figure

32 suggests that the stress remains constant as a function of film thickness. For a PECVD film, compressive stress can build up from ion bombardment and surface changes that drive atoms into gaps and voids while tensile stress forms from H incorporation. Competing mechanisms can lead to a constant stress state similar to that discussed in Chapter 2.[Thompson, 1996] Literature values for PECVD deposited SiN_x range from -3 to +1.5GPa.[Ogura, 2009]

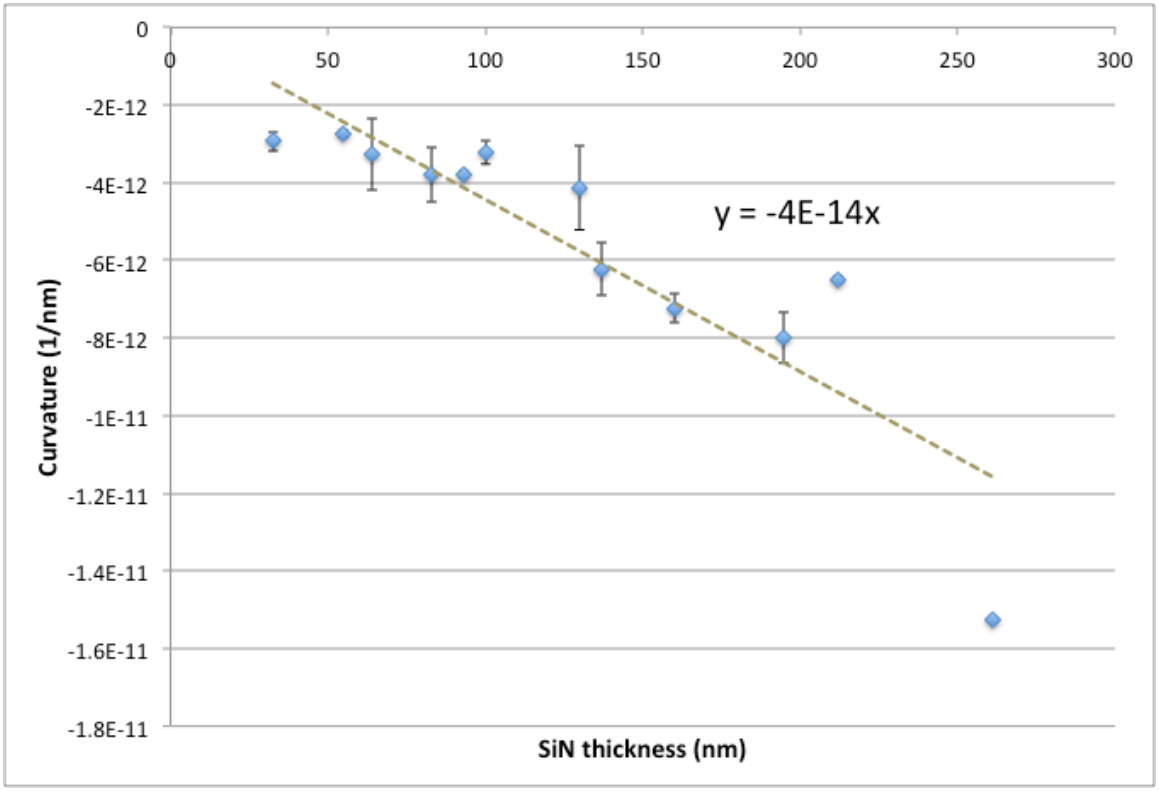

Figure 32: Wafer curvature as a function of deposited SiN_x film thickness. The dashed line is a linear least squares fit to the data forced to go through zero. The slope of the line gives the SiN_x stress from Stoney's equation. Error bars are calculated from the variation in curvatures on a wafer when measured at 0° and 90° azimuthal rotation. Points without noticeable error bars are measurements where the curvature was very symmetric across the wafer so the variation from measurements made at 0° and 90° was small. The instrumental error is unnoticeable on this scale as it is < 1%.

For thicknesses around 100nm ± 10nm, the film did not reflect well for the wavelengths used. The uncertainty in the curvature for films in that thickness range was

45% compared to 12% error for films that were outside this thickness range. Measurements suggested a large amount of asymmetric bending, and therefore the stress values calculated for 0° and 90° orientations on the same wafer were significantly different. I prepared instead a double-side polished wafer and measured the curvature on the reverse side. The extracted stress was now much more consistent in orthogonal directions on the wafer. The uncertainty reduced to 13% with the double side polished wafers.

4.2 Characterization of SiN_x on tethered-NM substrates

4.2.1 Dependence of Si NM strain on SiN_x thickness

A set of 53nm thick tethered Si NMs was fabricated and used as substrates for deposition of SiN_x with thicknesses between 90nm and 150nm, to investigate any possible dependence of the SiN_x film stress when deposited on extremely thin substrates. This thickness range was used because it was understood on a bulk substrate and therefore easier to interpret. The strain in the NM was calculated from the Raman shift (the difference in the shift before and after SiN_x deposition). The data are plotted in Figure 33 along with a linear least squares fit. The slope of this fit line gives the value of the SiN_x stress, $\sigma_{SiN} \sim -114$MPa, using Equation 11 in Chapter 2. The fit based on SiN_x stress found on bulk Si (see Figure 32) is also plotted for comparison.

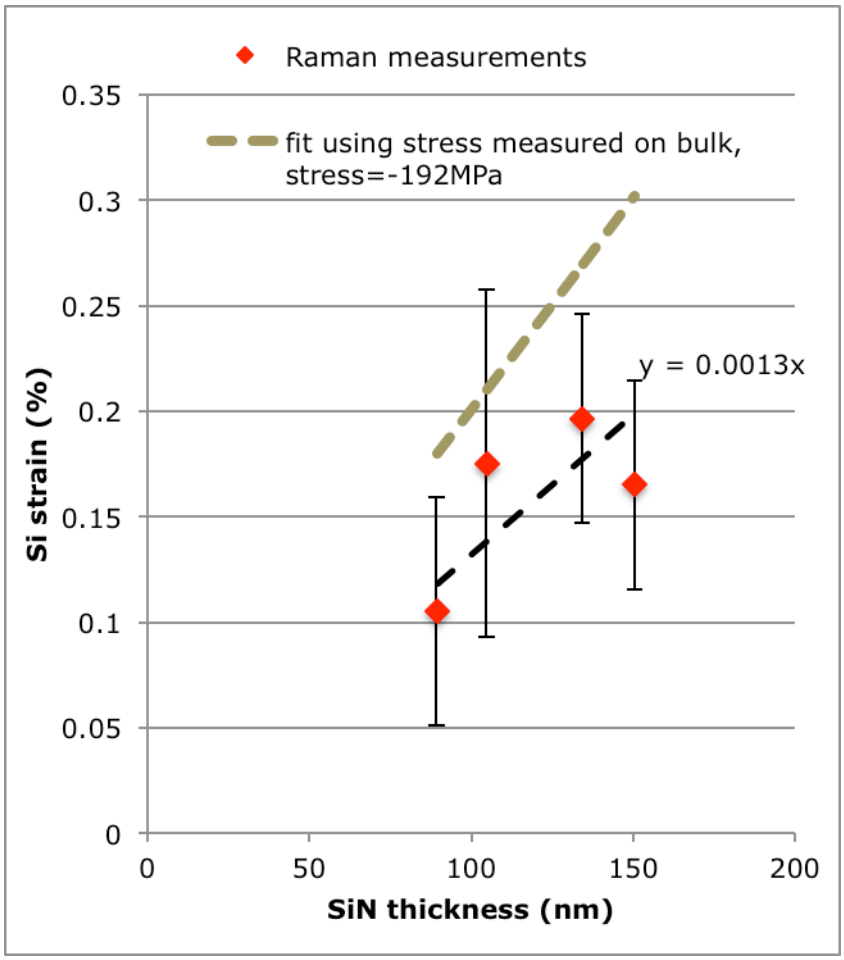

Figure 33: The strain in a 53nm thick Si NM produced by SiN_x deposited with different thicknesses, ranging from 90nm to 150nm. The dark dashed line is a linear least squares fit forced to be zero at the origin. Its slope gives a value of stress in the SiN_x of -114MPa. The heavier dashed curve above is calculated in the same way but using the bulk value of SiN_x stress, -192MPa.

I expected that the stress in the SiN_x film would change with thickness when deposited on a very thin substrate because the NM would continuously rob the deposited film of strain as it was shared (and thus potentially influence the growth mode). Unfortunately, the uncertainties are large for this data set, but if one believes the fit, then the stress in the SiN_x that is deposited onto the NM is the same order of magnitude as the stress for SiN_x deposited on bulk Si. The comparison is shown in Figure 34.

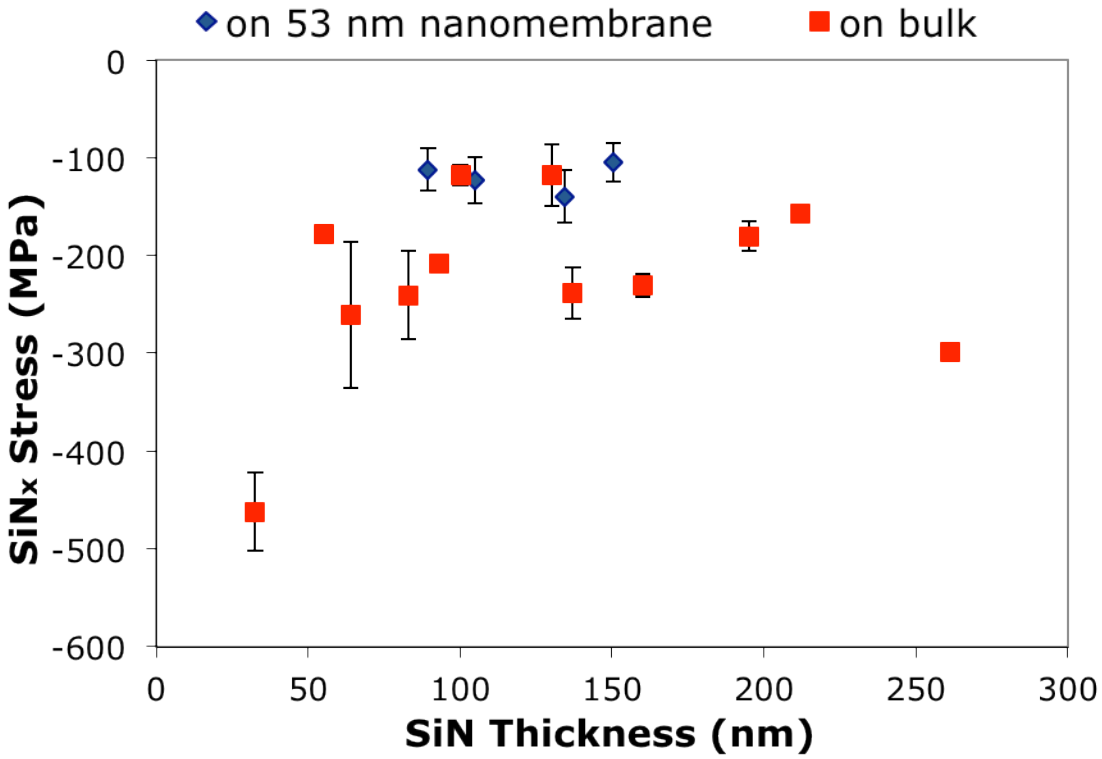

Figure 34: Stress in the SiN_x film as a function of the film thickness, for deposition on bulk Si and a 53nm thick SiNM. The values for a film deposited on a bulk Si substrate are similar to those deposited on a Si NM. The data points for bulk Si are obtained from the wafer curvature, see Figure 32. The data for the NM are obtained from the strain values in Figure 33. Compressive stress is plotted as a negative value.

It is unexpected that the stress in SiN_x films deposited on NMs should be the same for different thicknesses. As discussed earlier, we expected that the stress in the SiN_x should decrease for deposition on thinner NMs, as these accept more strain. As it must be true that the NM accepts strain (as is shown below and is known from [Kelly, 2007]), the SiN_x film stress nevertheless is constant, then there must exist a different cause than for growth on bulk Si. We know the NM is elongated during SiN_x deposition, which decreases the density of the film. For the film stress to remain constant there must be a mechanism during deposition that dynamically maintains the density of the film. We believe that ion bombardment, inherent in PECVD, which creates a continuing cascade of ions knocking atoms into gaps in the film, may maintain the density that the

film grown on bulk. Another way this can happen is if the surface atoms are driven into the films gaps also increasing the density. The extra volume created this way simply reflects a longer and wider film on the elongated membrane than on the equivalent bulk. I return to this point at the end of this chapter.

In Figure 32, I showed a linear fit to the curvature to give a constant stress value. When I plot the stress for growth on bulk directly, Figure 34, it becomes evident that the stress is more compressive for very thin and very thick SiN_x, similar to what is observed in the literature and shown in Figure 8 of Chapter 2. These values are interesting, especially for thinner films, but the thinner films are less reliable for bulk stress measurements needed for comparison. I therefore will continue to assume a constant stress in the bulk films for purposes here. These points do suggest, however, that efforts should be made to deposit both thinner and thicker films on NMs, where many interesting effects might be observable.

4.2.2 Dependence of NM strain on NM thickness

In this section I describe results of deposition of a 100nm thick film of SiN_x on Si NMs with thicknesses in the range of 9nm to 200nm. This value of SiN_x thickness was chosen because it is in the middle range of Si NM thicknesses. The NMs were characterized with Raman spectroscopy before and after the SiN_x deposition. The strains extracted from the Raman peak shifts are plotted in Figure 35 using Equation 23 in Chapter 3, $\Delta\omega = c\varepsilon_{Si}$. The strain measured before SiN_x was deposited is due to the transfer process along with any residual strain from the photoresist removal with a reactive ion etch. The strain measured after the SiN_x deposition is the result of the transfer strain plus the strain from SiN_x. All strain in the Si NMs is tensile.

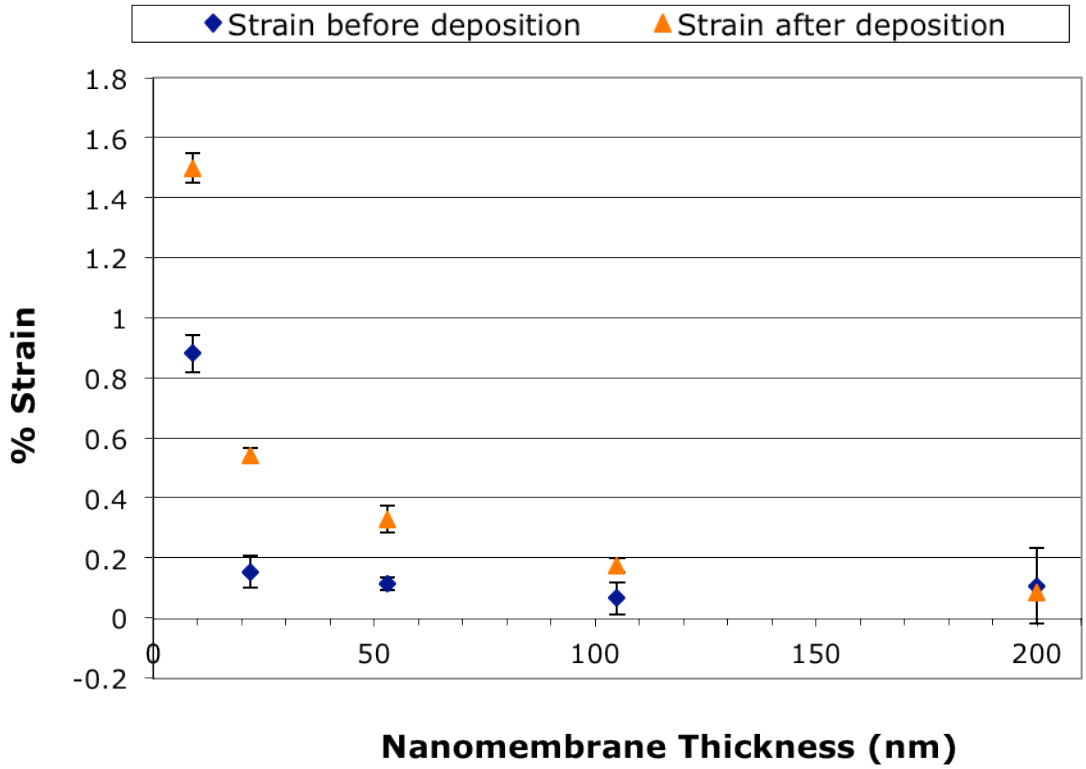

Figure 35: The strain measured in a Si NM as function of the NM thickness. The measurements were taken before and after 100nm of SiN_x was deposited. The data point for the thickest NM before deposition has a large error, leading to an uncertain value for the strain produced by the SiN_x for that NM thickness.

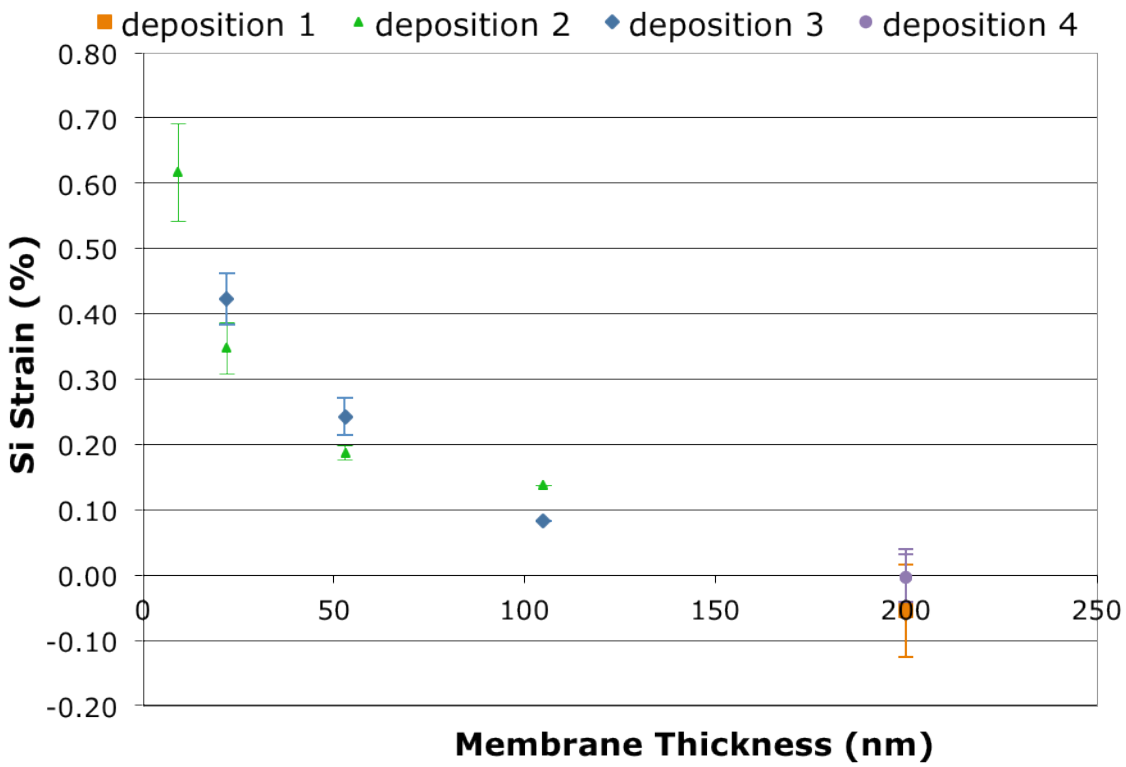

Figure 36: Strain in the Si NM purely due to SiN_x deposition. The difference in the strain before and after 100nm of SiN_x was deposited on Si NMs is plotted as a function of the NM thickness. Four different depositions were done to produce the data points.

The difference between the Si strain before and after SiN_x deposition represents the strain in the NM just from the SiN_x stress relaxation. Figure 36 shows these results, from four different sets of Si NMs. The four depositions are plotted separately in Figure 36 and averaged in Figure 38.

To demonstrate that this technique is valid and achievable on substrates with different elastic moduli, Ge NMs were used to perform similar experiments. From two different depositions, 60nm of SiN_x was deposited onto three Ge NMs that ranged in thickness from 47 to 150nm. Although the range of NM thicknesses was not as large as with the Si NMs, the data demonstrate a similar trend of increased NM strain from the

SiN_x deposition with thinner NMs (Figure 37), as expected from strain sharing arguments.[Kelly, 2007]

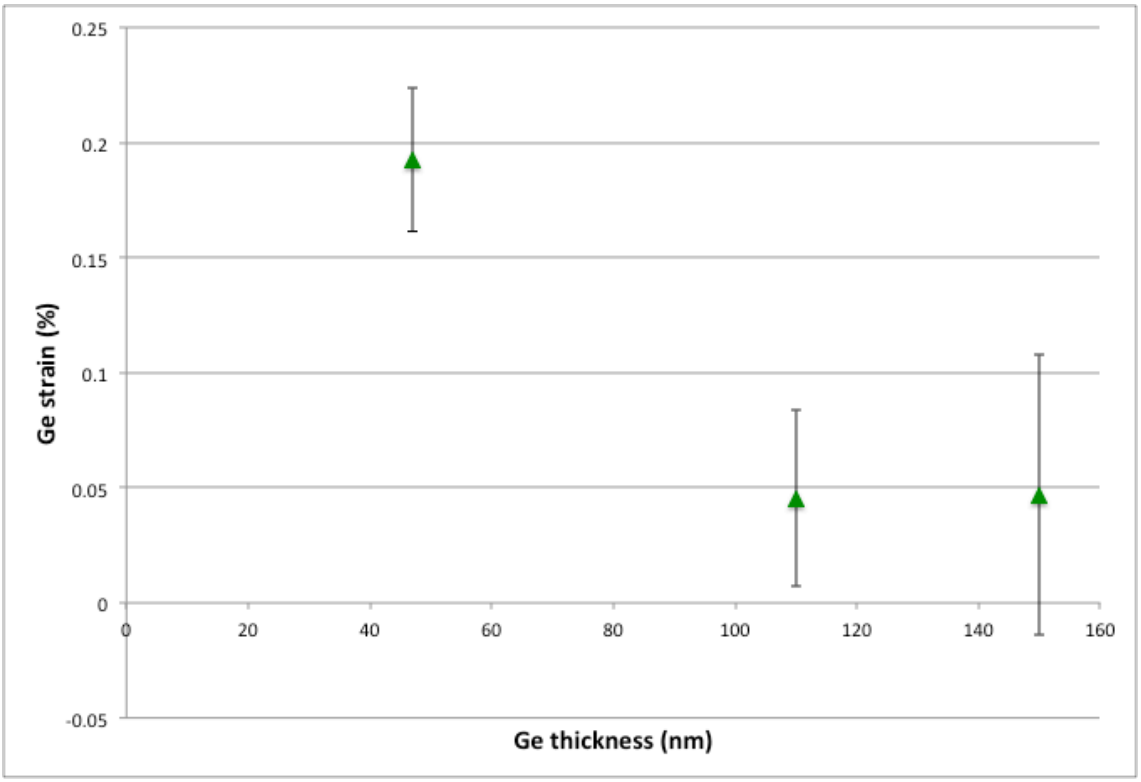

Figure 37: Ge NM strain due to a deposition of constant 60nm of SiN_x plotted as a function of Ge NM thickness. The strain is the difference between the strain before and after SiN_x deposition.

Because the magnitude of the SiN_x stress seems to be independent of the substrate thickness, I used the force-balance equation (Equation 11 in Chapter 2) to determine ε_{Si}. In Figure 38, I used the values for σ_{SiN} from the least squares fitting in Figure 32 (-192MPa) and Figure 33 (-114 MPa) and plotted them along with the strain values extracted from the Raman data. The resulting ε_{Si} fittings yield curves that match within a factor of two to the Raman data. This result is also obtained with the Ge NMs, as shown in Figure 40. For comparison to the case of constant mismatch strain, Equation 14 from Chapter 2 is plotted alongside, but is different by an order of magnitude as the NM

thickness decreases. In Figure 39, the Si NM strain and the SiN_x strain are plotted using the constant mismatch strain constraint where it becomes easy to see that a relatively constant SiN_x stress value would not properly fit my observations for the thinnest NMs.

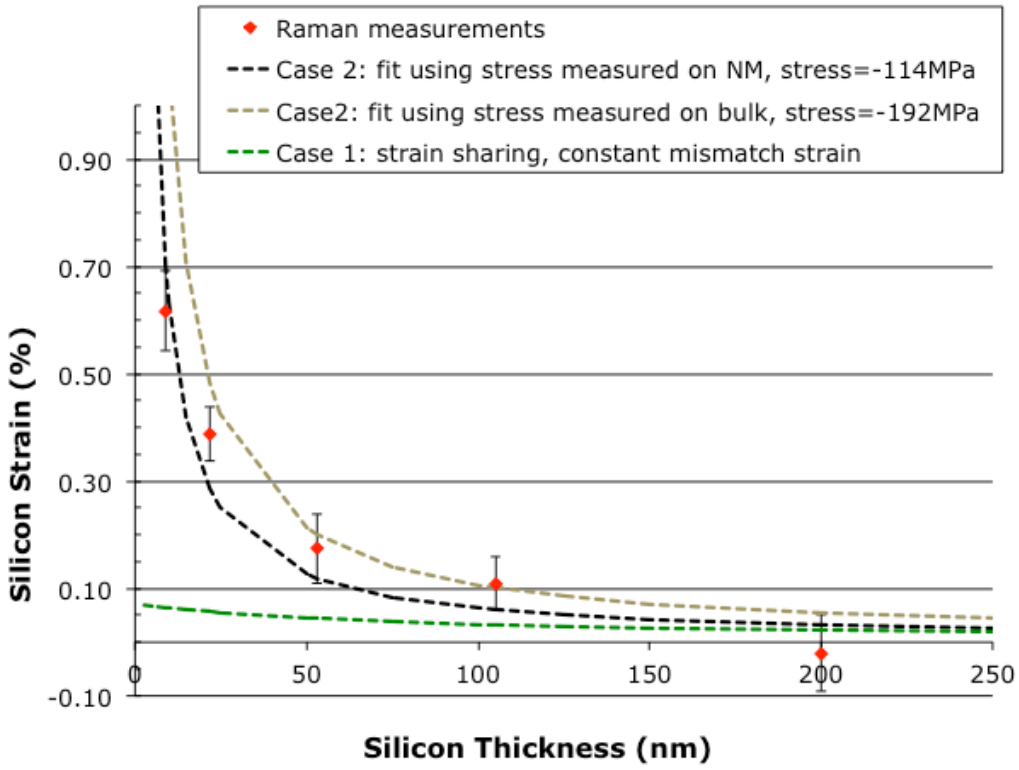

Figure 38: The Si NM strain due to stress relaxation in 100nm of SiN_x as a function of Si NM thickness. The upper (brown and black) dashed lines are the outputs of force blancing between substrate and film that assumes a constant stress in the SiN_x film, with values the same as on bulk and extracted for Si NMs. The lower curve represents constant mismatch strain and is an order of magnitude different from the Raman data on the thinnest NMs.

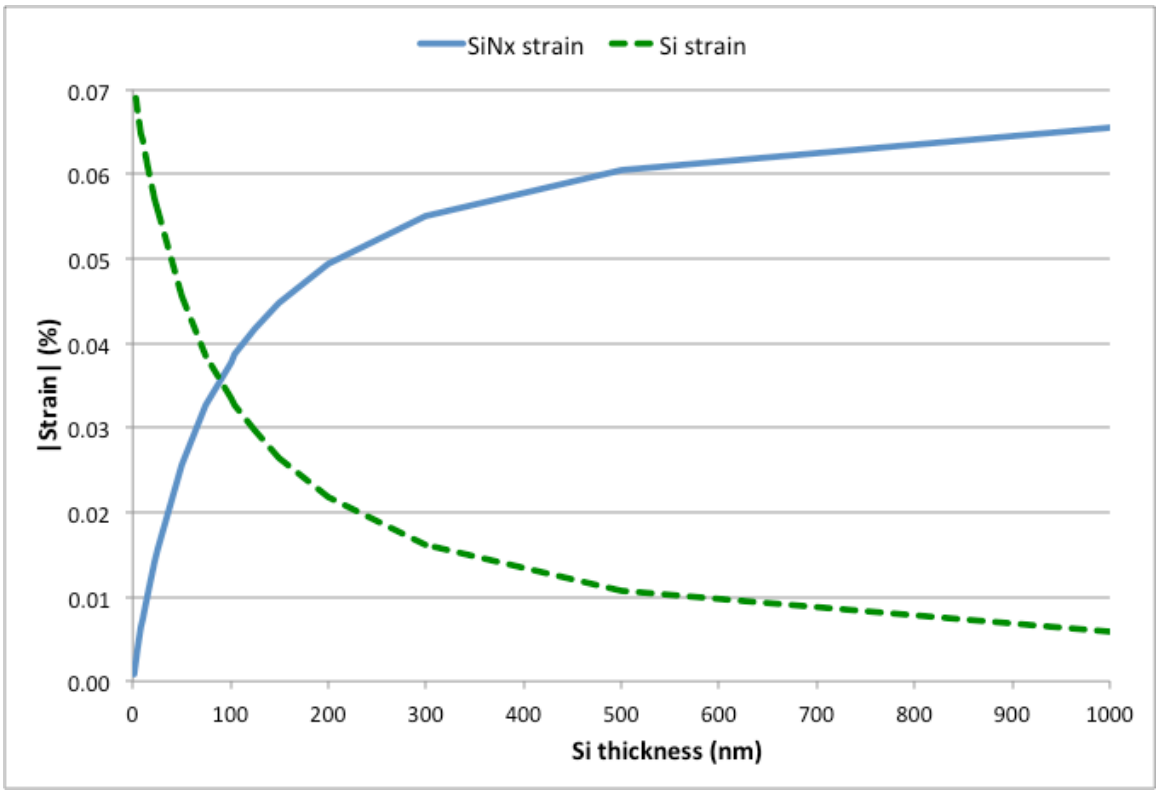

Figure 39: A plot of how the absolute value of the strain in the bilayer should behave if the mismatch strain was a constant value. The plot was made using Equation 13 and 14 in Chapter 2 and the value for the mismatch strain on a bulk substrate.

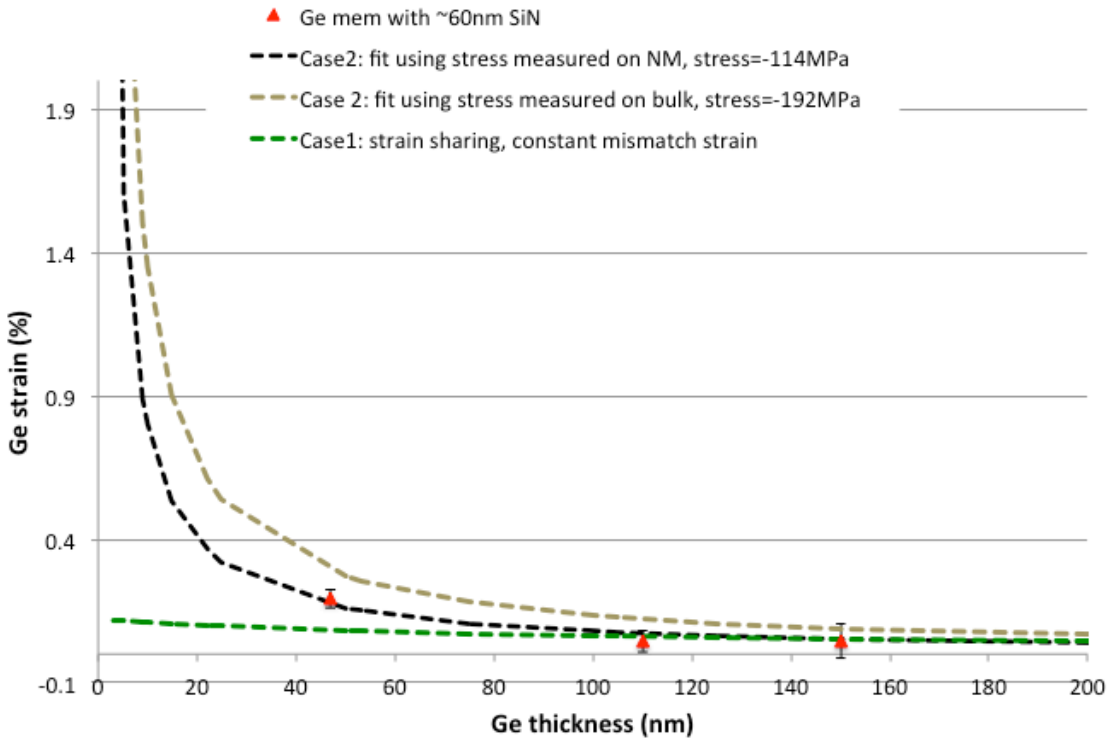

Figure 40: The Ge NM strain due to stress relaxation in 60nm of SiN_x as a function of Ge NM thickness. The upper (brown and black) dashed lines are the outputs of force balancing between substrate and film that assumes a constant stress in the SiN_x film, with values the same as on bulk and extracted for Si NMs. The lower curve represents constant mismatch strain.

In Chapter 2, I discussed the substrate's role during the film deposition, in particular for nanoscale substrates. The main idea was that a bilayer that has a thin film and a thick substrate would have a constant mismatch strain even as the substrate is thinned and the strain is redistributed between the film and substrate. The mismatch strain should be constant if the film properties are fixed and unchanging, the film is and remains adherent, and the stress relaxation is elastic. These conditions should be fulfilled for a film grown on a bulk substrate, and therefore the mismatch strain should be the same even as the substrate is thinned. The initial stress in the SiN_x film can be calculated from measurements on bulk using Stoney's equation (Equation 18 in Chapter 2) and the stress-strain relationship (Equation 3 in Chapter 2). For deposition on a NM substrate, I

speculate that a dynamic interaction with the substrate during deposition can exist and that therefore the mismatch strain can change. I can extract this changing mismatch strain using ε_{SiNx}, which is determined from the stress in the SiN_x film, and ε_{Si}, which is determined from Raman spectroscopy measurements on the front of the Si NM. The two mismatch strain values with increasing Si NM thickness are plotted in Figure 41. This implies that the dynamic response of the NM substrate does affect how much strain is in the bilayer system when compared to the same film deposited onto a much thicker substrate that could then be thinned.

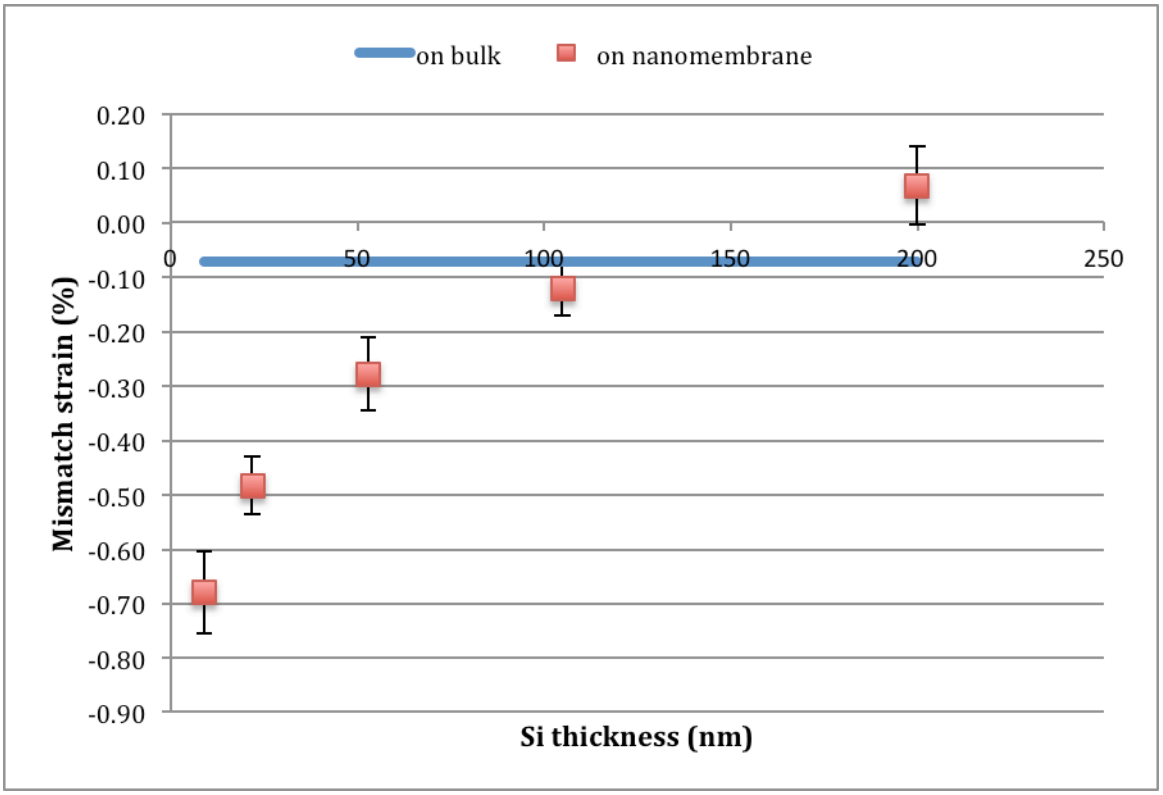

Figure 41: The mismatch strain for a 100nm thick SiN_x film in two cases: 1) assumption for a fixed film that has been grown on a bulk substrate that is then thinned and 2) for a 100nm film that has been grown directly on a Si NM of varying thicknesses that can respond to the stress dynamically. The mismatch strain in case 1) is calculated with Stoney's equation on the bulk substrate and is used at all substrate thicknesses based on the assumption that it will remain constant as the bulk substrate is thinned. The mismatch strain in the NM system is calculated using force balancing and Raman spectroscopy measurements. For the thinnest NM substrates, it is clear that the total strain in the bilayer system for case 2 is more than case 1.

4.3 Discussion of measurements

Despite the large body of literature on stress mechanisms in polycrystalline films, they are still poorly understood, and even less is understood about amorphous-film stress mechanisms. Stress in SiN_x may be due to H incorporation and ion bombardment during the deposition process, particularly in PECVD.[Ogura, 2009][Budhani, 1988][Paduschek, 1983] The competing stress mechanisms of H incorporation and ion bombardment may cause the film to reach a steady-state stress in the thickness range we are exploring. While this conclusion may not be surprising for films deposited on bulk substrates, it is not obvious why a similar trend in film stress on a NM substrate would occur. We know that the NM is expanding, and thus under tensile stress, implying it is robbing stress from the growing film, which would imply an ever lower stress in films deposited on ever thinner substrates. That is not what is found. Instead, on ultra-thin NMs, a constant SiN_x stress, σ_{SiN} is found. This result is surprising, because in prior work on epitaxial growth on Si nanomembranes [Roberts, 2006], strain sharing between film and substrate is found, leaving the film with lower stress. While strain sharing can explain the increase in NM strain as a function of decreasing NM thickness, as shown in Figure 38 and Figure 40, it is not observed as a decrease in the SiN_x stress. This is possible if the SiN_x stress continually builds up to a certain value independent of the substrate thickness or the amount of strain the substrate accepts.

In elastically relaxed, adherent bilayers, it would be expected that the strain in the system is conserved, or the mismatch strain would be constant, such that as one layer's stress is lessened, the other layer's strain would increase. If the SiN_x stress in my bilayer

always achieves a constant final stress and therefore strain while strain sharing, the total strain in the bilayer will be more than for the identical-thickness and composition film on a bulk substrate. There are stress mechanisms in the SiN_x that may be able to account for the film's constant final stress. In plasma processes, ion bombardment is a known cause for compressive stress. One could imagine as the SiN_x is deposited and the NM is elongating, the film's density would decrease as it too is elongated. Ion bombardment during continual deposition may compact the film to a desired equilibrium density. Another idea, proposed by Tello et al., is that as material is continually deposited onto a substrate surface, the surface potential changes and drives atoms into gaps or grain boundaries.[Tello, 2007] Perhaps, a similar surface potential change could be induced as the film is elongated, which may drive atoms into any gaps in the film caused by the elongation. So the competing mechanism of elongation, which causes the film to be less dense and less compressive, may be counteracted by continual ion bombardment and surface atom migration to increase the density of the film and establish a constant film stress.

Eventually, it would be ideal to study thinner amorphous films that experience stress dependence with film thickness, but for several reasons a constant-stress range is preferable to begin this project. First, this constant film-stress range is less complicated for a deposition technique that is known for its variability. Second, high spatial resolution, preferably in situ, would be ideal for exploring growing amorphous films but is not easily available.

4.4 Summary

Using a SiN_x film on a Si or Ge NM substrate, the thickness of each layer was vaired and the resulting strain in the NM was measured with Raman spectroscopy. Comparisons were made to a similar range of SiN_x thicknesses on bulk Si. Using a force balancing model, the final stress in the deposited SiN_x is found to be within the same order of magnitude independent of the substrate thickness.

Understanding thin film stress evolution and relaxation is a complicated picture with many theories. The results of this study have demonstrated that this measurement technique (tethered NMs as a strain gauge) has interesting results that have not been experimentally performed before. I have used NMs as a measurement tool to learn more about this process, and ended up learning that there is even more that is not understood yet. I have suggested some physical explanations for the our observations based on previous studies done on bulk substrates.

4.5 References

Budhani, R.C. et al. (1988). Kinetics of structural relaxation and hydrogen evolution from amorphous deposited silicon nitride. *Applied Physics Letters, 52*, p.284-286.

Kelly, M. (2007). *Elastic strain sharing in silicon/silicon germanium nanomembranes.* (Doctoral dissertation) University of Wisconsin, Madison, WI.

Ogura, A. et al. (2009). Evaluation and control of strain in Si induced by patterned SiN stressor. *Electrochemical and Solid-State Letters, 12*, p.H117-H119.

Paduschek, P. et al. (1983). Hydrogen-related mechanical stress in amorphous silicon and plasma-deposited silicon nitride. *Thin Solid Films, 110*, p.291-304.

Roberts, M. et al. (2006). Elastically relaxed free-standing strained-silicon nanomembranes. *Nature Materials, 5*, p.388-393.

Tello, J. et al. (2007). Kinetic model of stress evolution during coalescence and growth of polycrystalline thin films. *Physical Review Letters, 98*, p.216104.

Thompson, C. et al. (1996). Stress and strain growth in thin films. *Journal of Mechanics and Physics of Solids, 44*, p. 657-73.

Chapter 5

Summary and Outlook

5.1 Summary

In this dissertation, I have described a new platform for achieving and measuring strain in thin films. This was done by releasing nanomembranes (NM) from SOI and GOI and then bonding them over a frame made from bulk Si. A thin film of compressively stressed SiN_x, was deposited onto the backside, and the imparted strain was measured on the front of the NM. The SiN_x film was deposited with plasma-enhanced chemical vapor deposition and had an amorphous microstructure. Because the film is non-epitaxial, it can be deposited on virtually any substrate, and this was demonstrated by using both Si and Ge as NMs.

Measurements were made of the stress and the strain imparted by the SiN_x film on bulk substrates and on the NMs. The strain in the NM and stress in the thin film were compared on both substrates. The film stress is constant on the bulk substrate and appears to be so, from limited measurements, also on NM substrates. The two values of constant stress are very similar, a result that is surprising, as the total amount of strain in the NM system is more than on the bulk substrate. While there is still information to be gleaned from using an amorphous global stressor, this work would be best continued using of a different microstructure of thin film or a range of stress-dependent thicknesses.

In addition to this work, I have also spent much time studying the effects of local stressors on the electronic properties of the Si NM that are still attached to the underlying

oxide. The motivation for this work and experimental details are explained in the appendix that follows.

5.2 Outlook

While limited theoretical work has been done to learn how an ultra-thin substrate would react to an applied stressor, no study has yet deposited directly onto a nanometer-thin, freestanding region. I have shown that tethered, ultra-thin substrates can be used as an alternate way to achieve higher strains without the constraints of a rigid substrate. Previous work with nanomembranes has been limited to epitaxial stressors, which are restricted to certain materials and deposition processes. While the tethering limits this technique to the use of compressively stressed films, removing the frame by picking the freestanding area off with a compliant polymer stamp may allow tensile stressors to be used, although with smaller magnitudes.[Cavallo, 2010]

This work could be continued through the exploration of a several parameters: different stressor film microstructures, stress evolution after heat treatment, and further variations in the substrate compliancy based on elastic properties as well as etch hole sizes. Different deposition techniques (i.e. evaporation, sputtering) can induce stress through more ways than were discussed in this document and can also create a polycrystalline microstructure. Using the tethered NM approach to investigate stress mechanisms in polycrystalline films may be easier to do because the literature on polycrystalline films deposited on bulk substrates is more extensive and the film's crystal grains provide a spatially defined, well-understood (crystalline) area to measure film development. A measurement technique with both a moderate strain and high spatial resolution would be necessary.

With a dynamically reacting substrate such as tethered NM, heat treatment may change the film stress. Heating after deposition can enhance kinetic mechanisms of relaxation of the film.

I demonstrated that my results were applicable for substrates with different elastic properties, but the range of moduli values (142-180.5GPa) was small. To change the elastic properties further, other kinds of semiconductor alloy nanomembrane material, such as GaAs can be used.[Owen, 2009] For the existing materials, the compliancy of the Si and Ge NM can be changed by varying etch hole sizes such that they occupy a larger fraction of the NM surface area used in this work.

Furthermore, a growing area of research involves using nanometer-thin, freestanding areas to enhance the strain in materials that are notoriously difficult to strain.[Jain, 2012][Sánchez-Pérez, 2011] Recently, Jain et al. used 100μm-thick SiN_x pads to strain an attached area of 100nm-thick Ge. The whole structure was fabricated while supported by a very thick underlying Si/SiO_2 handle that was then undercut to release the Ge and part of the SiN_x pads. From stress relaxation in the SiN_x, the Ge was strained to almost 1% both uniaxially and biaxially. The technique described in this dissertation would offer a way to incorporate even more strain into a similar system if the SiN_x deposition parameters were adjusted to increase the amount of compressive stress that was directly imparted into freestanding Ge. This process is available to more materials that just Si and Ge as long as the substrate has the ability to be fabricated into a membrane and transferred through dry or wet processes.

5.3 References

Cavallo, F. et al. (2010). Semiconductors turn soft: inorganic nanomembranes. *Soft Matter, 6*, p.439-455.

Jain, J. et al. (2012). A micromachining-based technology for enhancing germanium light emission via tensile strain. *Nature Photonics, 6*, p.398-405.

Owen, D.L. et al. (2009). In-place bonding of GaAs/InGaAs/GaAs heterostructures to GaAs (001). *Semiconductor Science and Technology, 24*, p.035011.

Sánchez-Pérez, J. et al. (2011). Direct-bandgap light-emitting germanium in tensilely strained nanomembranes. *Proceedings of the National Academy of Sciences of the United States of America, 108*, p.18893-18898.

Appendix A

Band structure measurements on local and global stressors

Strain in semiconductors has been shown to improve electronic device performance by breaking the symmetry of the crystal to increase the carrier mobility.[Rim, 2003] Strain can also alter the material's band gap to be smaller, larger, or switch from a direct to indirect transition or vice versa[El Kurdi, 2010]. This strain is most commonly achieved through strain-graded buffer layers[Mooney, 1996], uniaxial stress [Lin, 2003], and biaxial stress [Roberts, 2006]. Uniaxial and biaxial stress in semiconductors can provide dislocation-free, strained material, and this is important to minimize strain relaxation and loss in the carrier mobility.

As an integral part of current MOSFET technology, local stressors are used to improve device performance. This section will introduce uniaxial and biaxial stress effects on the band structure and the measurement of those changes specifically for uniaxial strain in Si. About half of my time was spent patterning SiN_x to create periodically strained Si that is measured with x-ray photoemission electron microscopy. My initial sample measurements are inconclusive because the strain may be below the energy resolution of the instrument however the effects may become more obvious with higher strain or altered sample setups. While this section still uses SiN_x as a stressor

material, I have used electronic band structure differences to infer information about the strain instead of mechanical properties.

A.1 Band structure Definition

When many atoms are periodically arranged, the discrete electron energies align such that they can be plotted as bands in reciprocal space. These bands are the allowed energy levels for electrons in the material. In semiconductors the bands have a gap which separate the conduction band and valence band. Electrons in the conduction band are free to conduct electricity while in the valence band they are more tightly bound.

The primitive cell in reciprocal space is called the Brillouin zone. Points of symmetry are often highlighted as in Figure 42. At the center of the zone lies the Γ point. In Figure 43, the Si conduction band minimum lies at the Δ point and the valence band maximum is at the Γ point. Because the conduction band minimum and valence band maximum lie at two different points, the band gap is called indirect.

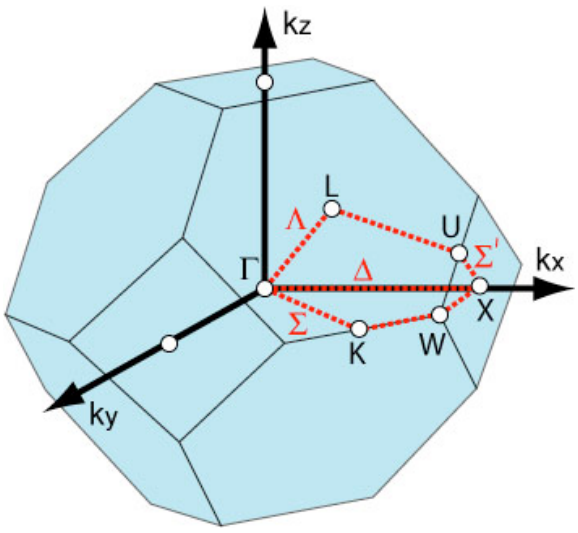

Figure 42: Diagram of the Brillouin zone of silicon with different orientations labeled. [Euaruksakul, 2009]

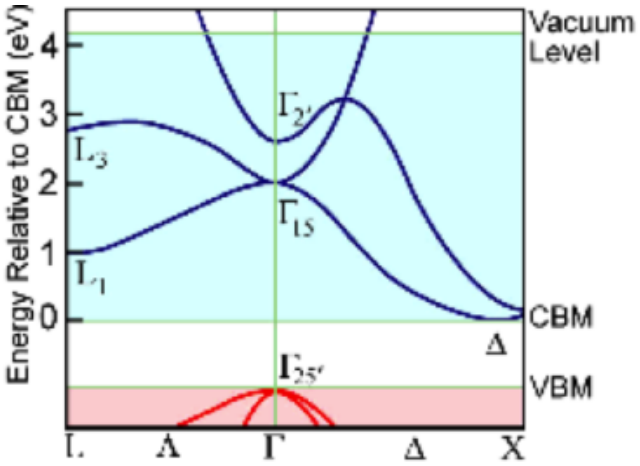

Figure 43: Energy band diagram of silicon. The blue band is the conduction band and the red band is the valence band. The white area highlights the band gap.[Euaruksakul Doctoral dissertation, 2009]

The material's electron arrangement is dependent on the symmetry of the system, which is influenced by the type of material and the orientation. Si (001) was used for these experiments and has a band structure that is six-fold symmetric at the conduction band minimum (CBM) Δ point.

A.2 Methods of biaxial strain

Biaxial strain is a two dimensional elongation or contraction of a material. One way to do this is to use mechanical bending (Figure 44).[El Kurdi, 2010] This method is common for Ge, which requires a large strain to change from an indirect to a direct band gap.[Sánchez-Pérez, 2011]

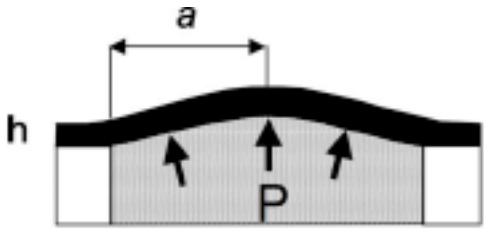

Figure 44: Schematic of thin Ge bulged with water pressure to produce strain. [El Kurdi, 2010]

Epitaxial mismatch is a popular method to induce biaxial strain and has been widely used in microelectronics processing.[Chu, 2009] By stacking layers of $Si_{1-x}Ge_x$ alloy upon each other with a greater percentage of Ge in each layer, the desired lattice constant is achieved. The stack of alloys is called a strain-graded buffer layer and an example image is presented in Figure 45. Each $Si_{1-x}Ge_x$ layer is grown past its critical thickness to relax the strain through dislocations. A dislocation can start at a stress concentrator or if there is some sort of defect already present to initiate it. Threading arms extend from the source of the dislocation to the next interface relaxing the stress along the way and scattering charge carriers. If enough dislocations form and pass into the device layer of silicon, the carriers will be scattered and can detract from the strain-induced mobility enhancement.

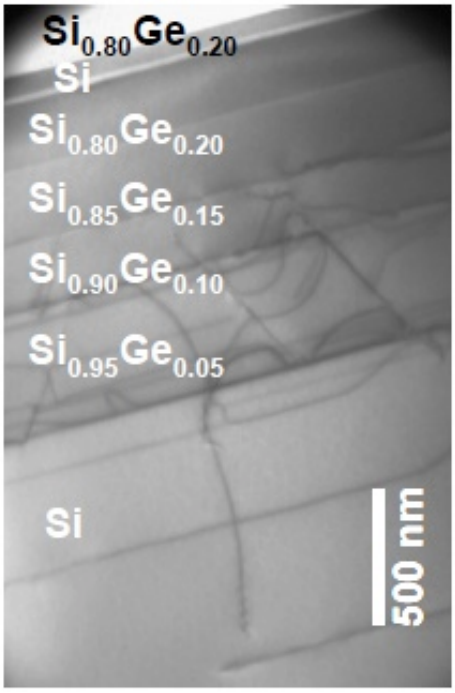

Figure 45: Transmission electron microscopy image of strain graded buffer layer. Each layer is labeled with the Si and Ge composition, and the dark lines are dislocations[Kelley, 2007]

Dislocation free, epitaxial growth on nanometer-thin sheets of single-crystal silicon, known as nanomembranes, is another way to create biaxial strain using epitaxial mismatch. By growing a pseudomorphic stressor layer of $Si_{1-x}Ge_x$ on silicon-on-insulator (SOI) under the critical thickness and releasing the Si from the underlying buried oxide layer, the mismatch strain in the $Si_{1-x}Ge_x$ is partially relaxed and shared with the Si.[Roberts, 2006] This was first demonstrated with Si by Roberts et al., where a trilayer was formed by adhering a second Si nanomembrane to balance the structure and prevent curling, as seen in Figure 46. By increasing the amount of Ge in the alloy layer, the lattice constant mismatch will increase leading to greater strain in the Si.

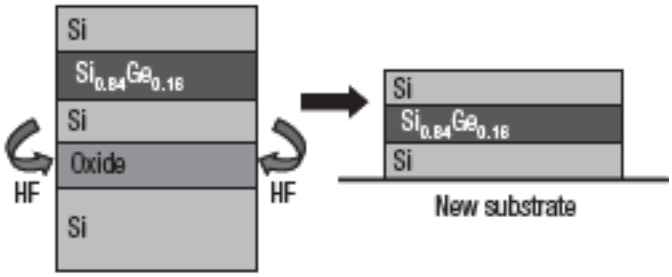

Figure 46: Schematic of Si nanomembrane trilayer with an epitaxially grown SiGe stressor before and after undercutting the oxide and transferring to a new substrate.[Roberts, 2006]

Biaxial strain can also be achieved with small, local stressors. Thin tethered nanoribbons of Si create an ideal structure to observe strain from nanostructures such as epitaxially grown Ge quantum dots.[Ritz, 2010] Ge quantum dots create small regions of biaxial strain in the Si under and in close proximity to the dot. Because of its nanoscale dimensions the strain field propagates through the nanoribbon, as in Figure 47. The thinness allows for local bending in the ribbons due to the relaxation of stress in the quantum dots. Finite element models were used to confirm the strain field gradient around the dots.[Kim-Lee, 2008]

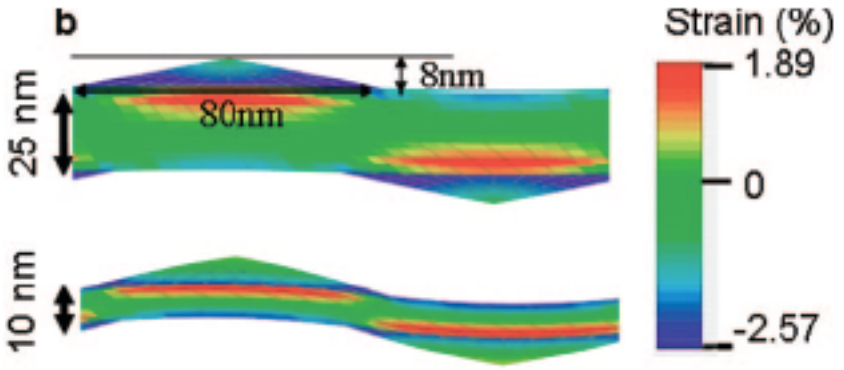

Figure 47: Finite element models of Ge QDs on two thicknesses of Si nanoribbon. The strain field from the QDs is mapped as a color gradient in the nanoribbon. [Huang, 2009]

A.3 Methods of uniaxial strain

Uniaxial strain leads to elongation or contraction of a material in one dimension and is the current method for improving carrier mobility in microelectronics. A one-dimensional strain can shift an indirect band gap to a direct band gap in material orientation that the biaxial strain cannot and provide a larger mobility enhancement in general than biaxial strain.[Sun, 2007] Stressor material is often deposited and patterned into stripes so that the long dimension remains essentially fixed while the short dimension is free to relax the stress.[Ogura, 2009] In this setup, a component of the strain is in the plane of the stress and a component of it is out of the plane providing a shear strain. For example, SiN_x capping layer on a MOSFET channel or a $Si_{1-x}Ge_x$ layer under the transistor gate are commonly found in microelectronics as uniaxial stressors. Another way to create uniaxial strain is with pure mechanical bending of beams, which can also provide a similar effect.[Chen, 2011]

It should be mentioned that not only electron mobility is increased, but hole mobility is also affected by strain. Hole mobility is difficult to predict due to valance band warping, which can rearrange the light hole and heavy hole bands. It has been

shown that when the band splitting due to strain is larger than kT, where k is Boltzmann's constant and T is the temperature, the interband hole scattering decreases [Sun, 2007]. This is most obvious with uniaxial strain leading to improved hole mobility.[Chu, 2009]

A.4 Measurement techniques

A.4.1 Strain effects on band structure

The strain components in three dimensions make up a second order tensor, which is simplified with crystalline symmetry, as described in Chapter 2. The strain tensor involves three kinds of strain: hydrostatic which changes the material's volume, shear strain that changes the lengths of the crystal lattice, and shear strain that changes the angles of the original crystal structure. For cubic crystals, the shear strain is what breaks the symmetry of the crystal and shifts and splits the maximums and minimums in the band structure. Hydrostatic strain acts in the plane and does not change the symmetry of the crystal. Therefore, hydrostatic strain can only shift the energy bands and not change the carrier mobility.

A.4.2 ARPES and XPEEM

The detection of energy band changes due to strain from nanostructures requires high energy and spatial resolution. Angle-resolved photoemission spectroscopy (ARPES) and x-ray photoemission electron microscopy (XPEEM) are two measurements that are sensitive to energy band changes. ARPES is a technique that can obtain momentum sensitive measurements of the valence band. The energy resolution is typically around

2meV and the spatial resolution is around 10μm. In comparison, XPEEM, a combination of x-ray absorption spectroscopy (XAS) and photoemission electron microscopy (PEEM) can spatially map the changes in the conduction band with an energy resolution of 10meV and a spatial resolution of around 30nm.

Both techniques involve an incident photon and an emitted electron, but the electron release process is different between the ARPES and XPEEM. With ARPES, the energy and the momentum of the electron are detected. To start a photon source excites an electron that then escapes from the material with an energy (E_e) that is calculated as

$$E_e = h\nu - \varphi - E_B \qquad \textbf{Equation 24}$$

where h is Plank's constant, ν is the frequency of the photon, ϕ is the work function of the material, and E_B is the binding energy. The escaped electron enters the detector, which has an acceptance angle with a finite range. The momentum of the detected electron, k, can be used to determine with the following relationship,

$$k = \frac{2\pi\sqrt{2mE_e}}{h} \qquad \textbf{Equation 25}$$

where m is the mass of electron.

In XPEEM, as in Figure 48, while scanning the photon energy, core electrons are excited into the conduction band. An electron from a higher-level de-excitation process is released as an Auger electron and begins a cascade of secondary electrons in the same process. The intensity of the secondary electrons is proportional to the density of states in the conduction band at the corresponding photon energy.[Ritz, 2009] All of the electrons released in this process amount to the total electron yield (TEY). The

derivative of the TEY with respect to the energy is the joint density of states of the 2p core level and the conduction band.

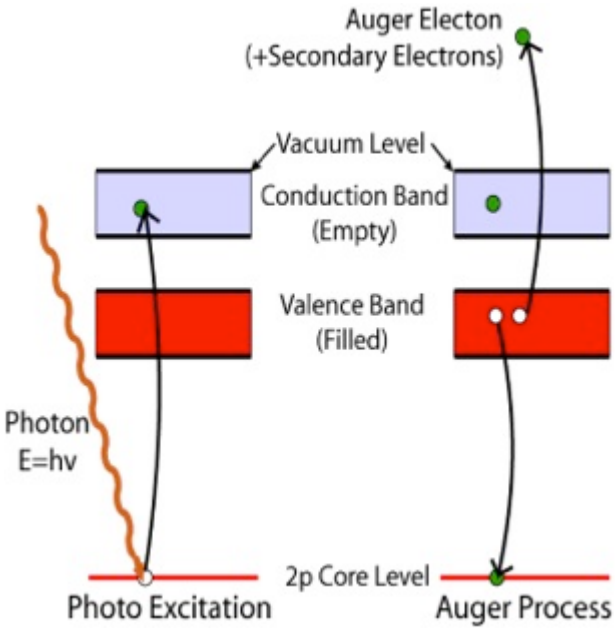

Figure 48: Diagram of how electron excitation happens in XPEEM.[Ritz, 2009]

A.4.3 Previous studies done on nanomembranes

When biaxial stress is applied to an in-plane direction, the out-of-plane direction changes length and the symmetry is broken into Δ_4 and Δ_2.[Euaruksakul, 2008] For compression in the plane, the out-of-plane direction, Δ_2, is elongated and the energy is raised as in Figure 49. Although this thesis will not cover it in detail, it should be noted that the symmetry is different in other orientations of Si and other semiconductor materials resulting in band structure behavior that may be different than described here.

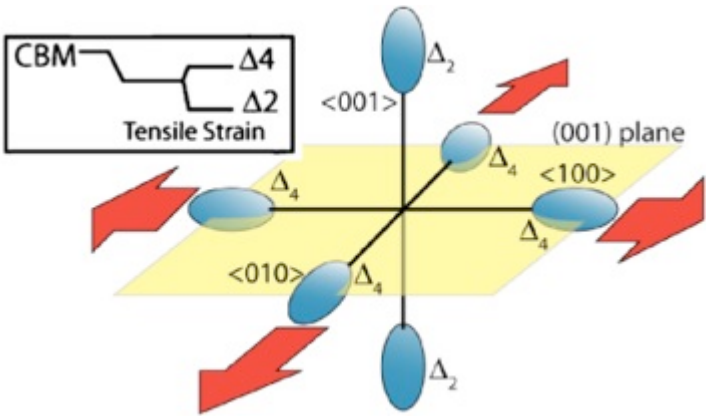

Figure 49: Schematic of the effect of in-plane biaxial strain on the Δ valley symmetry and resulting splitting that occurs in the conduction band.[Euaruksakul, 2008]

Previously, on large, biaxially strained Si nanomembranes, XAS recorded the shifting and splitting of conduction band peaks as the strain increased.[Euaruksakul, 2008] The magnitude of the shift was found to be proportional to the strain. Each peak was duplicated because of the spin-orbit coupling. With increasing strain, the Δ peak splits into Δ_2 and Δ_4, with Δ_2 shifting to lower energy and Δ_4 shifting to higher energy (Figure 51). With the Δ_4 shifting faster than Δ_2 in Figure 50, it appears that the Δ peak is converging with the L_1 peak when Si has 0.95% strain.[Euaruksakul, 2008]

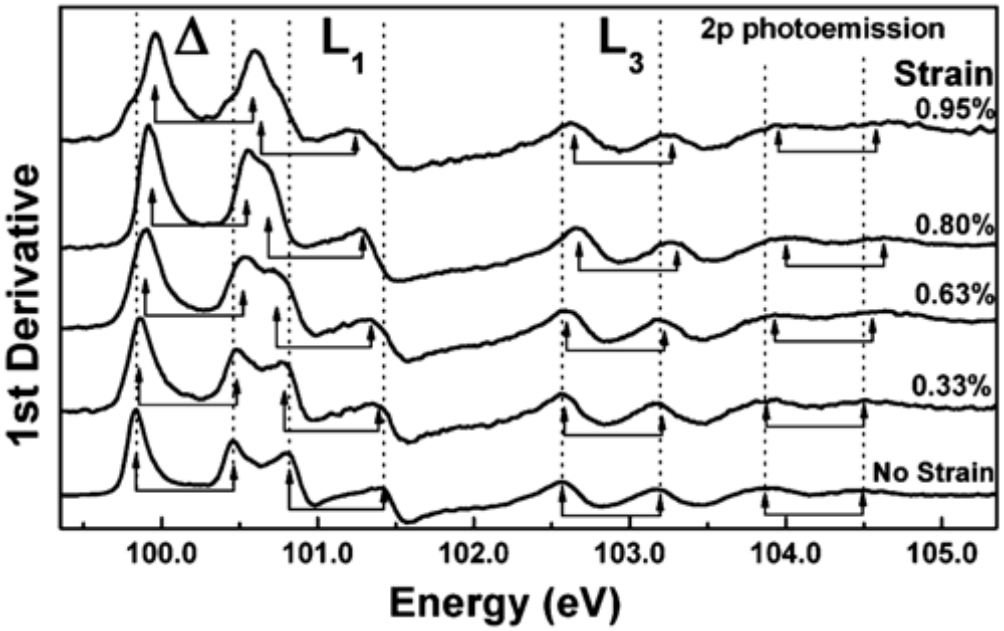

Figure 50: The first derivative of the XAS spectrum is plotted at various Si strain that range from 0.0 – 0.95%.[Euaruksakul, 2008]

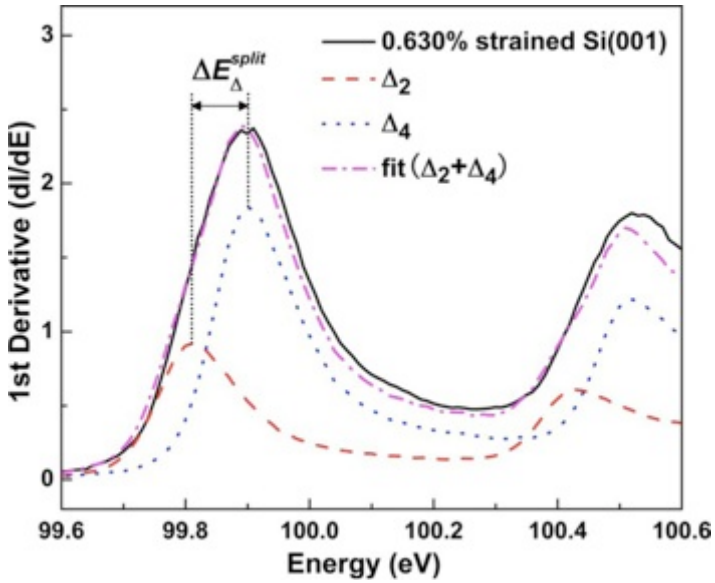

Figure 51: A closer view of the measured Δ peaks near 100eV with a model of the Δ_2 and the Δ_4 plotted in red and blue dashed lines, respectively. The summation of the two models is plotted in a dashed pink line and matches closely to measured value.[Euaruksakul, 2008]

A.5 SiN_x local stressors

A.5.1 Sample preparation

The work in this chapter uses SiN_x stripes as a uniaxial stressor. SiN_x is chosen as a stressor layer because it has been integrated into microelectronic fabrication and can produce large amounts of tensile and compressive strain by changing the growth parameters.[Saenger, 2008] The samples are fabricated at IBM and the SiN_x is deposited 100nm thick with –2.4 GPa of compressive stress onto SOI with 145nm Si template and 145nm buried oxide (Figure 52).[Saenger, 2008] The SiN_x is patterned into an array of SiN_x stripes ranging from 2mm x 2mm to 1um x 1um in dimension with the long edge oriented along the <110> direction.

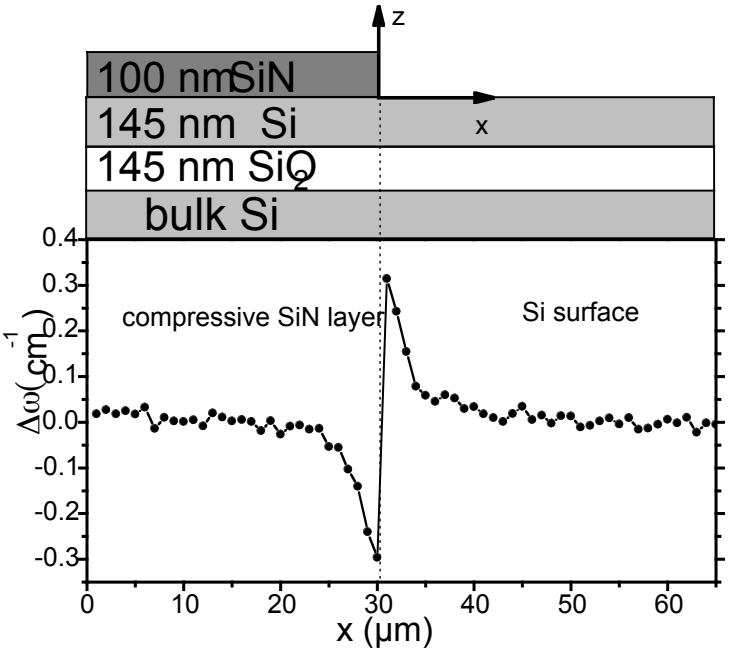

Figure 52: Raman spectrum taken on SOI with patterned SiN_x on top. Under most of the stripe, the Raman spectrum is not shifted. The free edge of the SiN_x stress is able to relax and strains the template layer of SOI. This strain can be seen as a shift in the Raman peak. Image by K. Saenger.

Under the SiN_x, Si stress is opposite in sign to the stress found in the SiN_x. Just beyond the edge of the stripe, the Si stress is in the same direction as the SiN_x. This is due to the stress relaxation near the edges of the stripe as in Figure 53. Using Raman, a wavenumber shift of $0.3cm^{-1}$ is measured near the edge of the SiN_x stripes (Figure 52), which corresponds to a strain of 0.04%[Saenger, 2008].

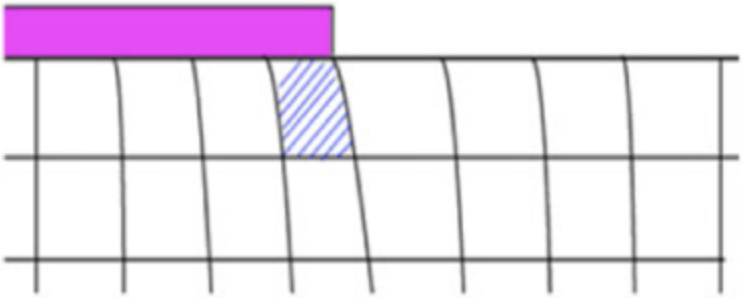

Figure 53: Diagram showing how the stress relaxation in the SiN_x can cause strain in the SOI template layer.[Ogura, 2008]

When using XPEEM, the sample must be relatively flat and conducting because a 20kV potential is applied between the sample and the microscope objective. Any sharp, high edges can focus the electric field and cause a spark, which can damage the sample. Grounding the sample prevents any distortions in the image that may be caused by an electric field that builds from charging. The sample is coated in Pt to provide a path to ground for charges and a normalization spectrum for data analysis. Pt is chosen because its spectral features do not overlap those of Si. When sputtered, the Pt film is smooth, continuous, and adheres well to the sample. The Pt conductive coating must be thin enough for the x-rays to penetrate through and the electrons to escape. Over the area of

interest, the Pt is thin (1nm), but for the normalization spectrum, the Pt needs to be thick (40nm) to block any Si signal.

A.5.2 Experimental measurements

XPEEM measurements required fine energy resolution, high beam flux, and good spatial resolution. A useful energy resolution of 10meV is obtained from highly monochromatic synchrotron light. Because the beamline used (VLS-PGM) at the Synchrotron Radiation Center (SRC) is sourced from an undulator magnet a high flux of x-rays will emit a strong signal in the XPEEM. Good spatial resolution comes from fine beam focus, which for the Elmitec PEEM III, is about 30nm. Measurements are surface sensitive because electron escape depth is only a few nanometers.

Electrons that are emitted from the sample are directed towards a multichannel plate (MCP), which enhances the signal. After the MCP, the electrons hit a phosphorous screen that fluoresces generating photons in the visible spectrum that are recorded with a CCD. An image was collected at each energy step and the intensity in each image is proportional to the density of states. Therefore each pixel has its own spectrum when scanned through the energy range, which can give localized spectral information.

Spectral normalization, done with a scan on the thick Pt, will remove any beamline features that occur in the data. Because of the masking during Pt deposition is done with a small piece of metal, the edge of the Pt is not sharp but a gradient due to some Pt getting under the edges of the mask. The sample's area of interest and the thick Pt cannot be viewed together under high magnification to allow for the normalization

scan to be taken simultaneously with the data. For this reason, a normalization scan is taken once a day and is used it to normalize the same day's data.

Measurements are taken near to and far from the SiN_x stripe edge (Figure 54) to compare strained and unstrained Si spectra in Figure 55. The derivative of the TEY as a function of energy enhances the absorption edges. The Δ and L_1 peaks are observed and appear to shift 50meV towards increasing energy. While this XPEEM system has been recorded to have a resolution of order of 10nm with the PGM beamline [Frazer, 2004] at the SRC, the actual working resolution is about 30nm. In this case, the shift we observe is too small to verify with our setup.

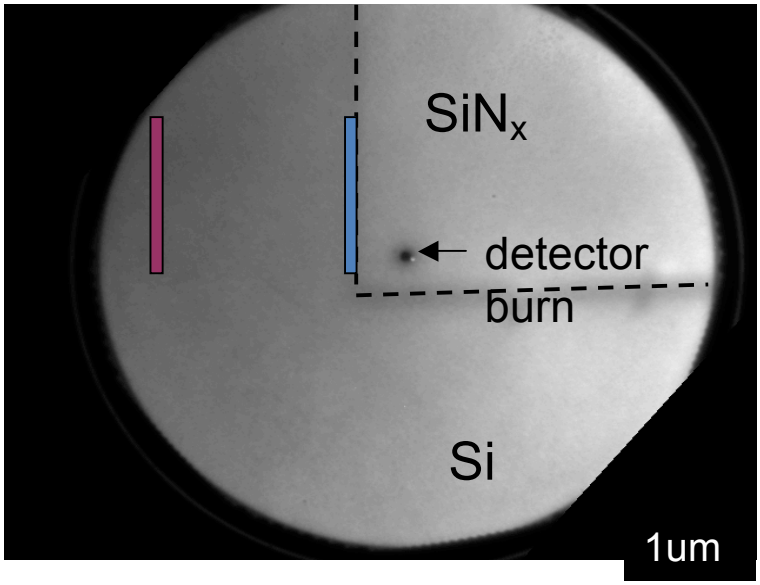

Figure 54: An XPEEM image of the edge of a SiN_x stripe on SOI. The blue (right) and purple (left) rectangles mark where the spectrum were taken.

To further enhance the observed strain, the SiN_x could be deposited with more stress. This may be possible by changing the deposition parameters. An increase by a factor of two should confirm if the shift seen in Figure 56 is real. Another way to increase the strain measured in the Si is to have a thinner initial Si template layer.

Previous work by Ogura et al. has shown that having a thinner Si template will allow more strain to be transferred from the SiN_x stressor when compared to bulk [Ogura, 2008]. Raman measurements were done on different substrates with the same thickness of SiN_x and the shift in the wavenumber was larger for SOI with both a thinner Si template and a buried SiO_2 layer. It was suggested that the reason for this was due to the smaller Young's modulus of the buried SiO_2, which made the Si template easier to strain than bulk Si.

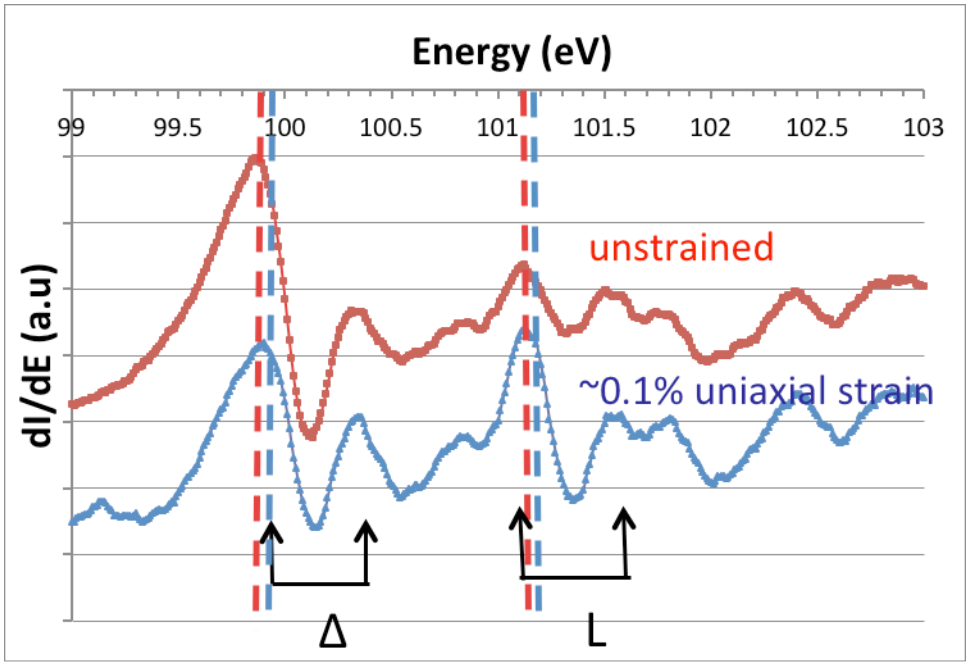

Figure 55: XPEEM spectra taken at the same spot as the Figure 54. The first derivative of the Δ and L_1 peaks is plotted and labeled with vertical lines marking the peak position of each spectrum.

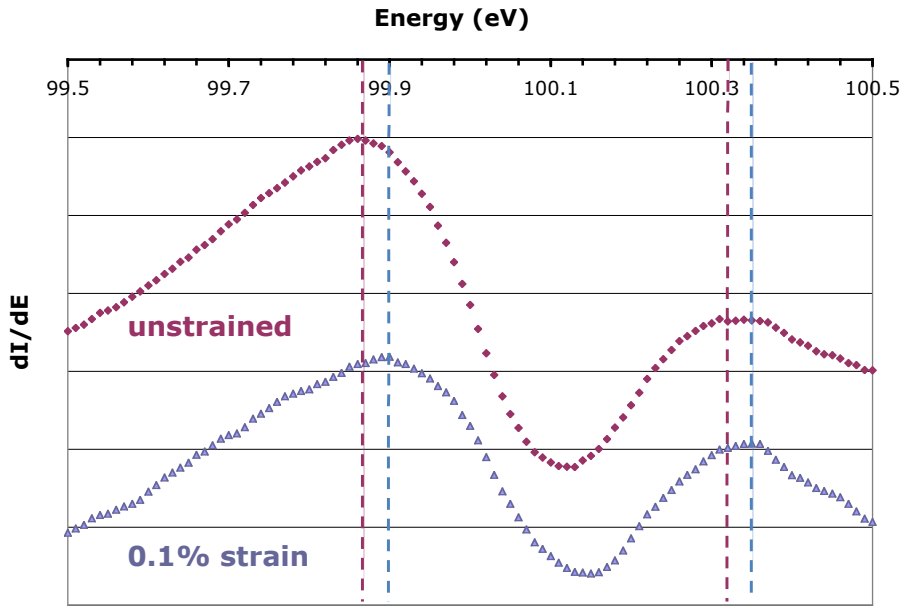

Figure 56: A closer view of the Δ peaks from an unstrained and strained Si area.

A.6 Summary

One way strain can alter a material's properties is to change the electronic band structure. I have overviewed methods to create and detect biaxial and uniaxial strain in semiconductors, with a focus on Si nanomembranes. SiN_x stripes were used as local stressor on Si nanomembranes to create uniaxial shear strain. Because the nanomembranes were attached to a rigid SiO_2 layer, the strain was only shared near the Si/SiN_x interface. Using XPEEM, the conduction band structure was explored, and although a shift appears, it is within the energy resolution of the measurement method. More strain would be needed to verify this through a higher stressed SiN_x or a thinner SiO_2 layer.

A.7 References

Chen, F. et al. (2011). Conduction band structure and electron mobility in uniaxially strained Si via externally applied strain in nanomembranes. *Journal of Physics D: Applied Physics, 44*, p.325107.

Chu, M. et al. (2009). Strain: A solution for higher carrier mobility in nanoscale MOSFETs. *Annual Review of Materials Science, 39*, p.203-29.

El Kurdi, M. et al. (2010). Band structure and optical gain of tensile-strain germanium based on 30 band k·p formalism. *Journal of Applied Physics, 107*, p.013710.

Euaruksakul, C. (2009). *Strain-band structure relationship in strained silicon nanomembranes.* (Doctoral dissertation) University of Wisconsin, Madison, WI.

Euaruksakul, C. et al. (2009). Relationship between strain and band structure in Si (001) and Si (110) nanomembranes. *Physical Review B, 80*, p.115323.

Euaruksakul, C. et al. (2008). Influence of strain on the conduction band structure of strained silicon nanomembranes. *Physical Review Letters, 101*, p.147403.

Frazer, B. et al. (2004). Spectromicroscope for the photoelectron imaging of nanostructures with x-rays (SPHINX): performance in biology, medicine, and geology. *Ultramicroscopy, 99*, p.87-94.

Huang, M. et al. (2009). Mechano-electronic superlattices in silicon nanoribbons. *ACS Nano, 3*, p.721-7.

Kelly, M. (2007). *Elastic strain sharing in silicon/silicon germanium nanomembranes.* (Doctoral dissertation) University of Wisconsin, Madison, WI.

Kim-Lee, H. et al. (2008). Engineering SiGe growth using mechanically responsive ultrathin substrates. *ECS transactions, 16*, p.299-305.

Lin, Y. et al. (2003). Thermoelectric properties of superlattice nanowires. *Physical Review B, 68*, p.075304.

Mooney, P. M. (1996). Strain relaxation and dislocations in SiGe/Si structures. *Materials Science and Engineering R-Reports, 17*, p.105-146.

Ogura, A. et al. (2009). Evaluation and control of strain in Si induced by patterned SiN stressor. *Electrochemical and Solid-State Letters, 12*, p.H117-119.

Ogura, A. et al. (2008). Evaluation of strain in Si-on-insulator substrate induced by Si_3N_4 capping film. *Japanese Journal of Applied Physics, 47*, p.1465-1468.

Rim, K. et al. (2003). Fabrication and mobility characteristics of ultra-thin strained-Si directly on insulator (SSDOI) MOSFETs. *IEEE IEDM Tech Digest*, p.49-52.

Ritz, C. et al. (2010). Ordering of nanostressors on free-standing silicon nanomembranes and nanoribbons. *New Journal of Physics, 12*, p.103011.

Ritz, C. (2009). *Local strain in silicon nanomembranes and its impacts on quantum dot growth.* (Doctoral dissertation) University of Wisconsin, Madison, WI.

Roberts, M. et al. (2006). Elastically relaxed free-standing strained-silicon nanomembranes. *Nature Materials, 5*, p.388-393.

Saenger, K. et al. (2008). Effects of patterned, stressed SiN overlayers on Si solid phase epitaxy. *Applied Physics Letters, 92*, p.124103.

Sánchez-Pérez, J. et al. (2011). Direct-bandgap light-emitting germanium in tensilely strained nanomembranes. *Proceedings of the National Academy of Sciences of the United States of America, 108*, p.18893-18898.